UNIVERSITY OF CALIFORNIA

SANTA CRUZ

A HIGH-RESOLUTION, REGIONAL-SCALE ANALYSIS OF STORMWATER RUNOFF IN THE SAN LORENZO RIVER BASIN FOR MANAGED AQUIFER RECHARGE DECISION MAKING

A thesis submitted in partial satisfaction
of the requirements for the degree of

MASTER OF SCIENCE

in

EARTH SCIENCES

by

Kyle Young

June 2016

The Thesis of Kyle Young
is approved:

_____
Professor Andrew Fisher, Chair

_____
Professor Michael Loik

_____
Professor Noah Finnegan

_____
Tyrus Miller
Vice Provost and Dean of Graduate Studies

TABLE OF CONTENTS

LIST OF FIGURES

LIST OF TABLES

GLOSSARY OF HYDROLOGIC TERMS

baseflow – water that is transmitted from groundwater aquifers to stream channels.

channelized runoff – runoff that has reached a stream channel; that component of streamflow that is equal to streamflow less baseflow.

Dunnian runoff – surface runoff that occurs when the soils are saturated at the land surface, also referred to as saturation excess runoff.

hillslope runoff – runoff that is transmitted through the landscape, but has not yet reached a stream. For the purpose of this study, hillslope runoff refers to the combination of interflow and surface runoff.

Hortonian runoff – surface runoff that occurs when the rate of precipitation (precipitation intensity) exceeds the soil's maximum rate of infiltration (infiltration capacity), also referred to as infiltration excess runoff.

interflow – the component of runoff that occurs in the subsurface, through the vadose zone.

runoff – the transmission of water through and on top of the landscape in response to precipitation.

streamflow – the combination of runoff and baseflow that reaches a stream channel. For the purpose of this study, simulated and observed streamflow will be referred to as *`runoff`* (in *`italic font`*) to align with PRMS variable nomenclature.

surface runoff – the component of runoff that occurs on top of the land surface, also referred to as overland flow. This can be subdivided into two separate processes: Hortonian (infiltration excess), and Dunnian (saturation excess) runoff.

ABSTRACT

A HIGH-RESOLUTION, REGIONAL-SCALE ANALYSIS OF STORMWATER RUNOFF IN THE SAN LORENZO RIVER BASIN FOR MANAGED AQUIFER RECHARGE DECISION MAKING

Kyle Young

Groundwater resources in the San Lorenzo River Basin (SLRB) are in a state of chronic overdraft, requiring well-informed mitigation measures. Distributed Stormwater Collection-Managed Aquifer Recharge (DSC-MAR) presents a cost-effective method of aquifer replenishment by collecting runoff and infiltrating it as recharge, but its successful implementation demands thorough knowledge of the distribution and availability of hillslope runoff. We apply a surface hydrology model to analyze the dynamics of hillslope runoff at high resolution (0.1 to 1.0 km^2) across the 350 km^2 SLRB watershed. We used a 3 m digital elevation model to create a detailed model grid, which we parameterized with high-resolution geologic, hydrologic, and land use data. To analyze hillslope runoff under a range of conditions, we developed a catalog of dry, normal, and wet climate scenarios from the historic record. Simulation results show high spatial variability of hillslope runoff, and indicate opportunities for runoff as potential supply for MAR during all climate scenarios. Additionally, our results reveal a consistent increase in the spatial and temporal variability of runoff under a wet climate scenario. The simulation's high-resolution output enables quantification of hillslope runoff at sub-watershed scales, commensurate with DSC-MAR catchments, demonstrating this method as a viable tool for MAR decision making and site planning.

DEDICATION AND ACKNOWLEDGMENTS

First and foremost, I would like to dedicate this project to my loving family – my wife, Sara, my daughter, Addison, and my son, Tristan – who remained supportive and patient despite the countless hours I spent 'in absentia' while conducting this work. This research would not have been possible without their love and encouragement, and their sacrifices through this endeavor were far greater than mine. Words cannot express how lucky I am to have such an amazing family. To that, I will just say to them: "Thank you!" and "I love you!"

I would also like to give thanks to my incredible coworkers on the "UCSC Hydro" Terrestrial Hydrology Team – Sarah Beganskas, Galen Gorski, Ryan Harmon, Elke Teo, and Walker Weir – a dynamite group of individuals who have been a true pleasure to collaborate with!

Lastly, I would like to thank Professor Andrew Fisher for being a team leader of rare caliber. Andy motivates those around him to achieve at the highest levels and it is an honor to receive his mentorship. My hope is that the impacts of this study will extend beyond the academic arena and to water resource management agencies for use in the siting and design of MAR projects. This "impact beyond academia" is what catalyzed my interest in this project, and I am incredibly grateful to Andy for believing in my abilities, and providing me with a meaningful, contributing role.

I. Introduction

A. Motivation

Groundwater is a vital resource for California's Central Coast hydrologic region. In the northern Central Coast, where the San Lorenzo River Basin (SLRB) is located, 89% of the region's water resource needs are supplied by groundwater (Figure I.1) (CA DWR, 2013). There is a similar reliance on groundwater in the SLRB, where groundwater meets over 50% of the water demands for the San Lorenzo Valley Water District, and nearly 100% for the Scotts Valley Water District (Johnson, 2015; Kennedy/Jenks Consultants, 2016). The importance of groundwater in the Central Coast is influenced by the absence of seasonal snow pack and the lack of significant imports from California's water transfer infrastructure (Figure I.2).

Groundwater also plays an important role in the ecological health of rivers and streams, providing a year-round, temperature-moderated water supply to riverine ecosystems (Brauman et al., 2007; Brunke & Gonser, 1997). Additionally, elevated groundwater levels and active groundwater recharge are important in coastal aquifers as they help prevent the degradation of aquifers due to saltwater intrusion (Werner & Simmons, 2009).

Given the Central Coast region's dependence on groundwater and groundwater's importance to ecosystem health, ensuring groundwater sustainability is a critical objective – one that has not yet been achieved. In recent decades aquifers in the SLRB have been subject to chronic overdraft, with several aquifers experiencing water table declines of over 150 feet since 1986 (Figure I.3) (Kennedy/Jenks

Consultants, 2015).

Groundwater overdraft is exacerbated by climate change and shifting land use. Regional precipitation records indicate that the climate has been trending towards increased variability and extremes. For example, within the nearby San Francisco Bay region, though average annual precipitation has been relatively static over the past 120 years, the region has seen an increasing frequency of large intensity storm events (Russo et al., 2013). This climatic pattern bears consequences for groundwater in that the occurrence of more frequent, large intensity storms tends to increase runoff and reduce recharge to aquifers (Russo et al., 2013; Woolhiser & Goodrich, 1988). Urbanization and other development in the SLRB also tend to reduce recharge to the region's groundwater aquifers. By increasing impervious area through the construction of roads, buildings, and other civil infrastructure, urbanization leads to increased runoff and reduced opportunities for infiltration and recharge (Tashie et al., 2016). The combined threats of increasing groundwater demand, climate change, and land development pose serious challenges to the SLRB's groundwater resources. Well-informed mitigation will be required to replenish the region's aquifers and ensure their sustainability.

B. Managed Aquifer Recharge (MAR)

Managed Aquifer Recharge (MAR) is the process of diverting excess surface water to an engineered well or basin where it can infiltrate into an underlying aquifer. MAR projects can include a range of technologies and methods that operate across a

spectrum of scales. At one end of the spectrum include minimally intrusive technologies such as low impact development (LID), in which highly pervious surfaces and/or infiltration structures are constructed, often amidst urban infrastructure. At the other end are regional spreading grounds, where complex engineering that includes large land areas are dedicated to water collection, treatment, and infiltration (LA DPW, 2016). While LID sites typically provide an infiltration benefit on the order of 1 - 10 acre-ft per year (ac-ft/yr), regional spreading grounds can facilitate recharge on the order of 10^4 - 10^5 ac-ft/yr (LA DPW, 2016; Newcomer et al., 2014). Distributed Stormwater Collection linked to MAR (DSC-MAR) is a cost-effective solution that avoids the infrastructural challenges associated with regional spreading grounds, while still providing relatively high yields (Arshad et al., 2014; Dillon et al., 2009). DSC-MAR involves the siting and construction of infiltration basins, drywells, or other infrastructure so that a fraction of natural runoff from hydrologic catchments can be routed to infiltrate and become recharge.

Figure I.4 shows an example of a DSC-MAR site in southern Santa Cruz County. At this site, stormwater is collected from a 172-ac catchment. The water passes first through a small settling basin, where suspended sediment is supposed to settle, and then is routed to a 4-ac infiltration basin. The infiltration basin is located above what appears to be a paleo-stream channel, having very sandy soils, whereas the surrounding area is characterized by finer and less transmissive soils. As a result, this catchment supplies considerable runoff for infiltration, even during relatively dry water years.

Successful DSC-MAR projects require three main features: an adequate water supply, good infiltration characteristics, and an underlying aquifer with space for supplemental storage. My research project focuses on the generation of storm runoff at a scale that is appropriate for DSC-MAR.

C. Study Objectives

As part of a larger research project to determine locations that are suitable for DSC-MAR, this study addresses the "supply" side of site selection. My primary goal is to provide a thorough evaluation of the spatial and temporal dynamics of runoff in the SLRB, exploring runoff generation during a range of climate conditions. This study is linked to a concurrent MAR suitability analysis that seeks to evaluate the suitability of locations throughout Santa Cruz and Monterey Counties for promoting infiltration and recharge (Figure I.5). The results of these studies will be combined as part of a regional analysis to find promising sites for DSC-MAR.

The three primary questions that my study seeks to answer are:

1. How much runoff is generated over the landscape throughout the SLRB?
2. What are the temporal and spatial dynamics of runoff and how are they affected by different climates?
3. What are the applications of these results to MAR site placement?

II. Runoff

A. Types of Runoff

Channelized streamflow originates from a variety of hydrologic reservoirs and processes, each of which yield different flow characteristics. For this reason, streamflow is commonly subdivided into categories, including runoff and baseflow. Runoff is those waters that are transmitted through and near the top of the landscape in response to precipitation, and can be further divided into a subsurface (interflow), and surface components (surface runoff) (Pumo et al., 2014).

Baseflow consists of waters supplied from groundwater aquifers adjacent to the stream channel. This component of streamflow relies on a gradient in potential energy ("head") between the waters in the channel and those of the surrounding aquifer. If this head gradient favors flow towards the stream, this process can deliver a significant supply of water to the stream channel (Pumo et al., 2014). Because baseflow depends on groundwater levels, it can be present in channels even in the absence of temporally proximate precipitation events, such as during seasonally dry periods or droughts.

Interflow (also referred to as "throughflow") is the passage of waters downslope through the vadose zone (Chorley, 1969). This type of runoff involves the transmission of waters not bound by capillary forces and requires soil moisture to be greater than field capacity. It is therefore associated with precipitation events (Pumo et al., 2014). Because interflow occurs above the water table, it flows faster than groundwater that contributes to baseflow. However, interflow is also subject to

tortuosity of pathways through the soil pores, viscous energy losses, and variations in soil capillary forces; as a result, it tends to be slower than surface runoff and contributes a more attenuated response (Chorley, 1969; Pumo et al., 2014). "Preferential flow" is a sub-category of interflow that occurs through large channels, conduits, or fractures in the vadose zone, all of which permit significantly faster flow rates than typically occur through the soil matrix (Nimmo, 2012). Although interflow is often thought to be a short-term response to individual storm events, when considered across a drainage basin it can provide significant contributions to streamflow (Pumo et al., 2014).

Surface runoff can be subdivided into two separate components: Hortonian (infiltration excess) runoff, and Dunnian (saturation excess) runoff (Beven, 2004; Dunne & Black, 1970; Horton, 1933). Hortonian runoff occurs when the rate of precipitation (precipitation intensity) exceeds the soil's maximum rate of infiltration (infiltration capacity) (Beven, 2004; Horton, 1933). All else being equal, the infiltration capacity of soils tends to decrease with smaller grain size, lower porosity, and higher soil moisture content. Thus the precipitation intensity at which Hortonian runoff can occur varies with soil moisture content, and can range considerably across a catchment and with time at a particular location. For impervious surfaces (such as pavement or hardpacked soils in developed regions), any precipitation that falls can contribute to Hortonian runoff, regardless of intensity.

Dunnian runoff occurs when the soils are saturated at the land surface – either due to an elevated water table or saturation in the upper soil layer – preventing

infiltration and causing additional precipitation to become runoff (Dunne & Black, 1970). Return flow is a special type of Dunnian flow in which waters that have already infiltrated flow downslope (as interflow) into saturated regions and subsequently exfiltrate to the surface (Hibbert & Troendle, 1988). Both Dunnian and Hortonian runoff experience fast travel times and therefore can produce a large magnitude, short time-scale response to precipitation, often dominating streamflow during storm events (Pumo et al., 2014).

B. Quantifying Runoff

Runoff in channels can be quantified by calculating the volumetric flow rate corresponding with different stream depths, and developing a correlation plot (rating curve) that associates streamflow with water level in the channel. Quantifying runoff over and through the landscape, which we'll refer to as "hillslope runoff," is significantly more difficult in practice.

Numerous studies have quantified hillslope runoff through direct measurement (Bartley et al., 2006; McGlynn & McDonnell, 2003; Sheridan et al., 2007; Wilcox et al., 1997). These studies involve engineered tools that route or trap hillslope runoff over small spatial scales and allow for *in-situ* measurement. Other studies have incorporated a mass balance approach by measuring precipitation, evapotranspiration, and changes in soil water content, and calculating hillslope runoff as the remaining term in the hydrologic mass balance equation (Domingo et al., 2001). Because of the robust instrumentation required by these empirical studies and

the relatively small spatial scales over which they operate, these methods are impractical for directly analyzing hillslope runoff across a watershed having an area of thousands of acres. More significantly, results of field studies depend on local characteristics and generally are not scalable due to heterogeneities in soil and vegetation across a watershed. Hydrologic modeling comprises an alternative to site-specific field studies for characterizing hillslope runoff, being based on a mass balance approach, but operating across a range of spatial and temporal scales.

Most watershed scale modeling studies of runoff examine basin-wide response to precipitation, integrated through simulation of channelized runoff and streamflow (Fang et al., 2015; Kirchner, 2009; LaFontaine et al., 2013; Pumo et al., 2014; Risley et al., 2011; Schumann et al., 2000). Studies on the impact of climate change or varying precipitation characteristics on basin hydrology also frequently evaluate streamflow at the basin scale (Woolhiser & Goodrich, 1988; Bae et al., 2008). Watershed studies that examine hillslope runoff, or recharge from hillslope runoff, typically evaluate and analyze basin-wide properties and system responses (Anbazhagan et al., 2005; Stone et al., 2001).

Cherkauer (2004) used the Precipitation Modeling System (PRMS) (Leavesley et al., 1983) to quantify recharge at the sub-watershed scale with an average spatial discretization of 37 km^2. Chang & Jung (2010) used PRMS to analyze the impact of climate change on runoff with an average grid cell size of 11 km^2. In this study, using PRMS and the historic climate record, we explored variations in hillslope runoff generated across a watershed area of 350 km^2, allowing for variations

in properties at a spatial scale ≤1 km^2. In the next sections, we present the field area where modeling was completed and introduce the formulation and application of PRMS to this problem.

III. Study Area

A. Location, Climate, and Land Use

The San Lorenzo River Basin (SLRB) is a 350 km^2, topographically defined watershed in Santa Cruz County on the central coast of California (Figure III.1). Elevation in the SLRB extends from sea level to ~1000 m-msl in the Santa Cruz Mountains (Figure III.3).

The climate in the San Lorenzo River Basin is strongly seasonal. The majority of the region's annual precipitation falls during October through May, with very little precipitation occurring during summer months (Figure III.6) (Kennedy/Jenks Consultants, 2013; PRISM, 2016). SLRB precipitation varies significantly by location, with the inland mountainous regions receiving substantially greater annual precipitation than the coastal regions (Figure III.4). Figure III.4a depicts notable variability of annual precipitation by location, with the inland mountainous regions (Ben Lomond and Felton) experiencing significantly greater precipitation than coastal locations (DeLaveaga and Santa Cruz) (CIMIS, 2015; PRISM, 2016; WRCC, 2015a-c). The moderating effect of the Pacific Ocean ensures a temperate climate year-round for the entire region, with no seasonal snowmelt and negligible snow occurring even at the highest elevations of the SLRB (Kennedy/Jenks Consultants, 2013).

The SLRB has a population of ~100,000 people, with most inhabitants residing in the city of Santa Cruz near the southern (coastal) boundary of the basin. Other population centers in the SLRB include Scotts Valley, Felton, Ben Lomond, and Boulder Creek (Figure III.2a). Development in the SLRB comprises mainly urban and suburban infrastructure in the region's two largest population centers of Santa Cruz and Scotts Valley (Figure III.2a), in addition to mining (Figure III.2b) and logging. The region's vegetation (Figure III.2b), as defined by the CALVEG (2014) vegetation and land use dataset, is largely wooded ("CON", "HDW", and "MIX"), interspersed with small regions of grass ("HEB") and shrubs ("SHB"), and punctuated by several large impervious areas ("URB") at the basin's city centers. Additional details on land use and vegetation in the region are depicted in Figure III.2a.

B. Hydrology

The defining waterbody in the SLRB is the San Lorenzo River, which starts in the northern headwaters of the basin and flows down the San Lorenzo River Valley, exiting the basin by entering the Pacific Ocean (Figure III.3). The SLRB watershed is defined as those lands that drain into the San Lorenzo River, and the watershed contains numerous contributing tributaries, including Kings, Bear, Newell, and Zayante Creeks (Figure III.2a) (Kennedy/Jenks Consultants, 2013). The region's only major water body, Loch Lomond Reservoir (Figure III.3), is located on Newell Creek and augments municipal water supplies for the San Lorenzo Valley Water District and the city of Santa Cruz, in addition to ensuring minimum ecological flows for

riverine habitat during periods of low flow in the San Lorenzo (Santa Cruz LAFCO, 2005). The San Lorenzo River has two gauging stations operated by the U.S. Geological Survey: one in Felton (station 11160500 at Big Trees, operating years: 1936-present) and another in Santa Cruz (station 11161000, operating years: 1952-1960, 1987-present) (Figure III.4b). Streamflow records are consistent with strongly seasonal precipitation in the basin; mean daily discharge typically peaks above 1,000 cfs in the winter (occasionally above 10,000 cfs), and flows in the summer are commonly ~10 cfs in Felton and ~1 cfs in Santa Cruz (Figure III.5). The observation that baseflow is commonly lower in Santa Cruz than in Felton indicates that the San Lorenzo River is a "losing" stream along this reach.

IV. Methods

A. Precipitation Runoff Modeling System (PRMS)

We used the Precipitation Runoff Modeling System (PRMS) (Leavesley et al., 1983; Markstrom et al., 2015) to simulate water routing through the SLRB. PRMS is a physically based, distributed parameter, continuous simulation watershed model. PRMS was selected for this modeling project because it is widely used, connects scalable hydrologic processes and their governing equations to physical characteristics, represents spatial variability in system properties, generates temporal hydrologic response at an appropriate scale, and the source code is publically available.

PRMS uses a series of linked equations to approximate a variety of hydrologic

processes, organized into modules (Knapp et al., 1991; Leavesley et al., 1983; Markstrom et al., 2015). The model domain is divided spatially into hydrologic response units (HRUs), and water is routed across and within the landscape in response to precipitation and other forcing. The fundamental equation used by PRMS requires water mass balance at each time step, and other governing equations require input associated with hydrologic properties and process rates, many of which are assigned independently to individual HRUs (Leavesley et al., 1983; Markstrom et al., 2015). The use of HRUs to represent spatially variable properties allows PRMS to simulate heterogeneity in both hydrologic inputs and system response, including precipitation, infiltration, soil moisture, and multiple forms of runoff. We ran PRMS using daily time-steps, the highest resolution available with the current model release, which should provide sufficient resolution for assessment of monthly runoff, including the influence of antecedent moisture on hydrologic routing (Markstrom et al., 2015).

The parameters assigned to each HRU delineate the geometry and flow characteristics of various water reservoirs and routing paths, governing how storage and flows are partitioned within HRUs, between HRUs, and between HRUs and stream channels (Figure IV.1a). For application of PRMS to the SLRB, we don't need to worry about snow/ice precipitation or snowpack storage, which greatly simplifies modeling (Figure IV.1b). PRMS considers storage and flow through a series of reservoirs, of which the soil is the most complex, comprising capillary, gravity, and preferential flow reservoirs (Figure IV.2, CPR, GVR and PFR, respectively).

Although the three main soil reservoirs could be interpreted from PRMS documentation as being arranged vertically (e.g., Markstrom et al., 2008; their Figure 19), they are conceived to coexist throughout each HRU (Figure IV.2). During each timestep, water is input to an HRU as precipitation and inflow from an adjacent HRU (if there is a connection or "cascade," as described later). Some of this water runs off immediately, depending on land use and soil characteristics, but remaining water can flow into each of the three soil reservoirs, either directly or as a flux between reservoirs. The function of the three soil reservoirs is described in greater detail later.

B. HRU Delineation and Property Assignment

HRUs represent the spatial discretization of simulation input and hydrologic calculation. The basis for HRU delineation was a digital elevation model (DEM) having 3 m spatial resolution (USGS, 2014a). A raster DEM with this resolution was freely available for most of the SLRB, but small gaps were patched with a 3 m DEM developed by the Association of Monterey Bay Area Governments (AMBAG, 2014), and (where necessary) with a 10 m DEM (USGS, 2014b) (Figure III.3). We used the composite 3 m DEM to construct HRUs having topographic drainage areas of 0.1 to 1.0 km^2.

HRUs were produced using standard methods, by calculating the elevation gradient vector at every raster cell in the DEM:

$$\vec{V} = \vec{\nabla} E(x,y) = \langle {}^{\partial E}\!/_{\partial x}, {}^{\partial E}\!/_{\partial y} \rangle \quad (1)$$

where E is the elevation, and $\vec{V}$ is the direction of steepest slope (inferred hydrologic

flow path) at each DEM location. The gradient vector was rounded to the nearest Primary InterCardinal direction (increment of 45-angular degrees) and flow accumulation was calculated at each raster cell as the aggregation of upslope raster cells along these vector paths. Raster cells whose flow accumulation exceeded a user-established stream definition threshold were combined to form a continuous stream network (Figure IV.3). These are not necessarily real streams that would be found on the landscape, but are virtual ("manufactured") streams as defined on the basis of the DEM.

We compared the manufactured stream network to the USGS streams database (USGS, 2014d) for accuracy and edited segments that misrepresented natural flow paths. These errors typically occurred in regions with relatively low topographic gradients, for which large variations in vegetation or infrastructure introduced artifacts in the DEM. The manufactured stream network, subdivided and ordered into individual stream segments, was used to delineate the HRUs as the catchment areas contributing to each segment in the network (Figure IV.3).

As part of the HRU delineation process, we assessed the presence of closed topographic depressions that would prohibit outflow. Initial DEM analysis resulted in a large number of depressions, most of which were found to be relatively shallow ($\leq$7.2 m) and caused by artifacts in the DEM, and were therefore ignored. We assessed the remaining 25 depressions based on the existence of waterbodies having no outlet, the soil infiltration capacity (IC), and the surface geology. Of 25 depressions, eight were interpreted to be true depressions, including three quarries

(Figure IV.3). These eight depressions were categorized as closed HRUs, or "swales," from which there is no surface runoff (Markstrom et al., 2015).

HRU sizes are controlled through the stream definition threshold, which describes the number of cells from which flow accumulates at any given point through the gradient vector calculations. We selected a stream definition threshold that would result in most HRUs having an area of 0.1 to 1.0 km^2, then split or combined initial HRUs as needed for those falling outside this target range, using a script in Python/ArcPy. The resulting map shows 865 HRUs for the SLRB (Figure IV.3), with the majority having an area of 0.2 to 0.6 km^2, and a mean area of 0.4 km^2 (Figure IV.4). These HRUs are large enough to minimize artifacts and "noise" from the 3 m DEM, but small enough to preserve considerable heterogeneity in properties, including variations in topography, soils, and vegetation (Molnar & Julien, 2000). Moreover, the majority of HRUs are smaller than the typical size range for targeted DSC-MAR catchment areas using stormwater collection (100 to 1000 acres, or 0.4 to 4.0 km^2), allowing a regional assessment of potential project sites to achieve larger programmatic goals for improving groundwater conditions. Additional information on HRU production is presented in the Appendix, "HRU Production Guide."

C. Cascades

Large, topographically delineated HRUs common to many PRMS models typically contain well-developed stream channels – sections of the watershed's stream network – to which they transfer outflow. As a modeling approximation, when the

outflows from an HRU are passed to these channels in PRMS (referred to as "channelized runoff"), these flows remain confined to the stream network and no longer interact with the HRU landscape. In contrast, small HRUs such as those in our study might not contain such channels, and the outflows from these HRUs can be transferred to downslope HRUs as "hillslope runoff" rather than being transmitted directly to the stream network.

Through this process of inter-HRU transfers, the connectivity of HRUs influences how much runoff an HRU will receive and produce. Accordingly, the Cascade Module in PRMS permits flow routing from upslope to downslope HRUs within each time step by allowing the user to select the HRU's dominant runoff method – whether channelized or hillslope – and to map corresponding HRU-to-HRU and HRU-to-stream connections as "cascade links" (Markstrom et al., 2015). By aggregating flow between HRUs, the cascade process allows us to determine the total runoff available as outflow from each HRU.

To assess the dominant modes of runoff across the simulated landscape, we checked for the existence of a USGS-delineated ("blue line") stream channel in each HRU, pruning the manufactured stream network if there was no blue line stream (Figure IV.5) (USGS, 2014d). Manufactured stream segments whose distance from a blue line stream exceeded a prescribed tolerance of 50 m (between stream centroids) were deleted. HRUs containing a blue line stream were classified as "channelized runoff-dominated," whereas others were classified as "hillslope runoff-dominated." To determine the cascade links between HRUs and streams, we identified the flow

order between segments in the edited stream network. Because every HRU contains a manufactured stream segment (developed as part of HRU production), these flow connections denote HRU-to-HRU cascade links for HRUs that are "hillslope runoff-dominated," and HRU-to-stream cascade links for HRUs that are "channelized runoff-dominated" (Figure IV.6).

D. PRMS Parameters

Each HRU in PRMS is uniquely defined through the assignment of >60 parameters (Table IV.1, identified in **bold font**). Parameter values determine the behavior of water storage and transfers between reservoirs within each HRUs, between HRUs, and from HRUs to stream segments (Figures IV.1 and IV.2). These parameters are spatially variable and either temporally static or vary by month-of-the-year. Some parameter values were specified on a continuous scale, while others were assigned based on soil and/or vegetation type, as discussed below.

Basic topographic and geospatial parameters, such as HRU area and slope, were calculated using the DEM as the average value across each HRU. More complex parameter values were calculated from combinations of input data. As one example, the parameter **soil_moist_max**, the maximum soil water volume available for transpiration, is a function of available water capacity (AWC) and rooting depth (R) (Markstrom et al., 2015):

$$\textbf{soil\_moist\_max} = AWC \times R \tag{2}$$

As another example, the parameter **sat_threshold**, the maximum soil water volume

available for gravity drainage and/or interflow, is a function of soil porosity (n), field capacity (FC), and thickness (d) (Markstrom et al., 2015):

$$\textbf{sat\_threshold} = (n - FC) \times d \tag{3}$$

Many of the soil and vegetation parameters assigned to each HRU were derived from the USDA Soil Survey Geographic Database (SSURGO) dataset (Soil Survey Staff, 2014) or the USDA's CALVEG (Classification and Assessment with Landsat of Visible Ecological Groupings) dataset (CALVEG, 2014). These datasets were organized by common characteristics and grouped into spatial polygons. Because SSURGO data is also organized into distinct soil layers with depth, we calculated input data values for each spatial polygon using weighted averages through all layers (Soil Survey Staff, 2014). For example, infiltration capacity (IC) for each soil polygon was calculated as an effective conductivity using the harmonic mean of the soil layer saturated conductivities:

$$IC = \frac{\sum_{i}^{n} d_i}{\sum_{i}^{n} \left(d_i / K_i \right)} \tag{4}$$

where d_i is the thickness of each soil layer, K_i is the saturated conductivity of each soil layer, and n is the number of soil layers. A minimum and maximum effective conductivity was calculated using minimum and maximum conductivity values for each soil layer (as reported in the SSURGO database), respectively, and IC was taken as the geometric mean of these values (Table IV.2). Additionally, AWC, percentage sand, and percentage clay were determined for each polygon as depth-weighted

averages (Table IV.2).

From the average values of percentage sand/clay, we assigned PRMS soil types of sand, loam, or clay to each soil polygon (USGS, 2014c). Similarly, we assigned PRMS vegetation types (bare, grasses, shrubs, "trees" or deciduous, coniferous) to each vegetation polygon based on CALVEG vegetation categories (CALVEG, 2014). Input data that were not represented in SSURGO and CALVEG datasets were determined from a survey of published literature and assigned to each soil or vegetation polygon according to these PRMS soil/vegetation types (Table IV.2).

The soil and vegetation input data (defined for polygons that do not correspond to HRUs) were assigned to each HRU using area weighted or area-and-density weighted functions (Equations 5 and 6, respectively):

$$X_{HRU} = \frac{\sum_{i}^{n} x_i A_i}{\sum_{i}^{n} A_i} \tag{5}$$

$$X_{HRU} = \frac{\sum_{i}^{n} x_i A_i D_i}{\sum_{i}^{n} A_i D_i} \tag{6}$$

where X_{HRU} is the HRU value, x_i is the soil or vegetation polygon value, A_i is the area of the soil or vegetation polygon, D_i is the vegetation density, and n is the number of soil or vegetation polygons within the HRU. The application of these weighting functions is depicted in Figure IV.7a and shown with the following examples:

Example #1 (Figure IV.7b): $$\textbf{soil\_moist\_max}_{\text{HRU}} = \frac{\sum_{i_s}^{n_s} AWC_i A_i}{\sum_{i_s}^{n_s} A_i} \times \frac{\sum_{i_v}^{n_v} R_i A_i}{\sum_{i_v}^{n_v} A_i} \quad (7)$$

where AWC_i is the available water content for each soil polygon; R_i is the rooting depth for each vegetation polygon; and n_s and n_v are the number of soil and vegetation polygons (respectively) within the HRU.

Example #2 (Figure IV.7c): $$\textbf{wrain\_intcp}_{\text{HRU}} = \frac{\sum_{i_v}^{n_v} s_i A_i D_i}{\sum_{i_v}^{n_v} A_i D_i} \quad (8)$$

where s_i is the canopy storage for each vegetation polygon.

Additional steps were taken to calculate the potential evapotranspiration (PET) coefficient (**hamon_coef**), imperviousness fraction (**hru_percent_imperv**), and the linear soil zone routing coefficients (**fast_coef_lin**, **slow_coef_lin**, and **ssr2gw_rate**). **hamon_coef** was given a different coefficient value for every month of the year, which we scaled proportionately to the mean monthly PET from 1991 to 2001 (Figure IV.8), as measured at the DeLaveaga climate station (Figure III.4b) (Station #104, CIMIS, 2016). **hru_percent_imperv** was calculated by assigning a binary "1.0" or "0.0" imperviousness fraction to each vegetation polygon according to its CALVEG (2014) land use type, and then applying the area weighting function (Equation 5) to determine the total HRU fractional area that is impervious (Viger et al., 2010).

For the linear soil zone routing coefficients, we partitioned the range of IC

values for all soil polygons (Equation 4) into five quantiles and assigned a corresponding IC "index" of 0 through 4 to each soil polygon based on its IC quantile. This assignment of IC indices approximates a log-2 scaling of *IC* (inches/day), where:

$$ICindex \approx \log_2(IC) - 2.3 \quad (9)$$

We applied the area-weighting function (Equation 5) to calculate a single *ICindex* for each HRU and scaled the PRMS default coefficient for each parameter by the *ICindex*. Because the IC values span more than two orders of magnitude, this $\log_2$ scaling allows us to preserve the variability of IC data across the basin, and prevents the highest IC values from overwhelming lower IC values in the area-weighted averaging functions.

E. PRMS Variables

Whereas PRMS parameters are spatially variable but temporally static (or vary by month-of-the-year), PRMS variables (identified in *italic font*) vary in space and change with time. The principal PRMS variables include *tmax* (maximum daily temperature), *tmin* (minimum daily temperature), *precip* (total daily precipitation), and *runoff* (daily streamflow at each gauging station) (Table IV.1). The first three – *tmax*, *tmin*, and *precip* – serve as daily climate inputs (energy, water), whereas *runoff*[1], is used to calibrate and validate the simulation.

Parameter-elevation Relationship on Independent Slopes Model (PRISM) climate data from WY1982 to WY2014 was used as simulation input (PRISM

[1] To align terminology with the PRMS variable "*runoff*", which refers to observed streamflow (baseflow + interflow + surface runoff), this study will also use the term "*runoff*" (in *italic font*) to denote simulation "streamflow" (primarily for calibration and validation purposes).

Climate Group, 2016). PRISM uses data collected from monitoring stations throughout the contiguous United States to produce daily precipitation and temperature data that is spatially continuous and interpolated on an 800 m, rectangular grid (PRISM Climate Group, 2016). We validated the data for our study region by plotting PRISM precipitation at grid cells that correlate with local precipitation stations at Santa Cruz and Ben Lomond (Figure IV.9) (PRISM Climate Group, 2016; WRCC, 2015a; WRCC, 2015c). Although the daily data (Figure IV.9b) displays occasional mismatch between PRISM and station data, plots of the daily precipitation differences (Figures IV.9c-d, showing station-minus-PRISM precipitation) reveal nearly symmetrical, equal and opposite precipitation differences between neighboring days. This effect is likely caused by the different times at which data sources divide daily precipitation events (e.g., 12:00-to-12:00 versus 00:00-to-00:00 or 09:00-to-09:00), resulting in an arbitrary separation of events across multiple "days." Different climate stations use different data intervals to define days, and it is not possible to reassign or shift data between these intervals. An assessment of cumulative annual precipitation (Figure IV.9a) suggests that the PRISM data provides a reasonably accurate representation of input to the system, particularly when considering monthly basin response.

Values for *tmax*, *tmin*, and *precip* were assigned to each HRU from the 800 m PRISM data using the area-weighting function in Equation 5 (Figure IV.10). Values were assigned for every day from WY1982 to WY2014, providing a 33-year (12,053-day) chronology of daily climate data as input to the model.

F. Calibration and Validation

The model was run for a 33-year period using the PRISM climate input values from WY1982 to WY2014 and commencing on October 1, 1981. Thus the simulation period commences with the start of a water year, at the end of the region's seasonal dry period. To facilitate model calibration and validation, we divided the study region into three subbasins (Figure IV.11) and selected the downstream, Santa Cruz gauging station as our primary data reference (USGS, 2015b). This location encompasses runoff from two subbasins and maximizes the contributing watershed area for the calibration process. We segregated model output into three distinct time periods (Table IV.3): a six-year model start-up and stabilization period (WY1982 to WY1987), a 14-year calibration period (WY1988 to WY2001), and a 13-year validation period (WY2001 to WY2014).

For the model's initial conditions we set storage in the soil reservoirs to minimums and the groundwater reservoir to 10.0 inches (Table IV.1). The time period used for calibration begins with the first year of available data from the Santa Cruz gauging station (USGS, 2015b). The model was calibrated by comparing simulated and observed *runoff*[2] for monthly and annual time periods, with the goal of the study being to provide accurate hillslope runoff volumes on monthly timescales. Calibration to the daily hydrograph was not attempted for several reasons. Daily time discretization for climate input (the highest resolution available) will artificially reduce the magnitude of most precipitation events, because precipitation

[2] USGS gauge data reports total streamflow, comprising both runoff and baseflow components. For this reason, calibration and validation were conducted using the combination of baseflow, interflow, and surface runoff outputs from the model.

tends to be most intense for minutes or hours at a time. The problem is compounded for longer duration events, which are more likely to span adjacent days and thus be subdivided into smaller events. This process reduces daily precipitation and soil moisture saturation, thereby favoring infiltration and subsurface flows (interflow, gravity drainage, and baseflow) over more rapid Dunnian surface runoff. The delineation of relatively small HRUs may also tend to favor infiltration and subsurface flows over surface runoff, due to increased soilzone routing options. Consequently, this representation is conservative from the perspective of assessing surface runoff resources available for stormwater collection for managed recharge (a primary goal of this study), and will tend to underpredict peak event *runoff* observed in stream channels. As a practical matter, calibrating for daily channel flow would require running the model with timesteps of hours or less, and high-resolution input data from across the basin are not available at this resolution. In addition, although older versions of PRMS had an option for using smaller time steps to assess event response (Leavesley et al., 1983), the latest release is limited to daily (or longer) time steps (Markstrom et al., 2015).

We conducted sensitivity tests to determine the primary tuning parameters for monthly and annual calibration (Table IV.4). To calibrate the model, we sequentially adjusted these parameters (individually and in combination) and evaluated monthly and annual *runoff* results until the model produced an acceptable match to gauge data, with a mixture of under- and over-prediction of observations. We also looked at the general shape of daily hydrographs to assess if baseflow recession was adequately

represented. Calibration was evaluated at the Santa Cruz gauging station using the following metrics:

1) Cross-plots of simulated versus observed *runoff*, constructed for both monthly and annual data.

2) Normalized root mean square deviation (NRMSD) metrics between simulated and monthly *runoff* values, calculated as:

$$\mathrm{NRMSD} = \frac{\sqrt{\left(\sum_{i}^{n}(x_i - o_i)^2 / n\right)}}{(o_{\max} - o_{\min})} \tag{10}$$

where x_i is simulated *runoff*, and o_i is observed *runoff*, n is the number of data points in the sample, and $o_{\max}$ and $o_{\min}$ are the maximum and minimum observed *runoff* values in the sample. For the monthly calibration, NRMSD was calculated for each month of the water year and then averaged over the rainy season months to determine a final NRMSD value. As discussed later, the most useful monthly NRMSD calculation is for the rainy season in our study area (November through April), when most precipitation occurs, so that results are not biased by simulations of the dry season.

3) A mass balance comparison to verify that multi-year simulated *runoff* matched observed, and that soil and groundwater reservoir levels did not systematically accumulate or lose water mass over the long term. We were particularly concerned with the potential for chronic accumulation of water in the simulated groundwater reservoir, which would tend to increase baseflow over time.

Once model calibration was complete, we conducted a validation exercise during the subsequent 13-year period, using the same metrics to assess the fit of simulation outputs to observed `runoff`. We also examined simulated and observed daily hydrographs (`runoff` time series) to assess the general pattern and timing of event response, for both calibration and validation. However, as described earlier, daily hydrographs were not used for quantitative calibration.

G. Climate Scenario Model Run

To analyze the temporal and spatial dynamics of hillslope runoff under a variety of climate regimes, we created a catalog of "dry," "normal," and "wet" climate scenarios using the historic record. To do this, we used PRISM data for the entire SLRB (Figure IV.12) to calculate the non-exceedance probabilities, p, of annual precipitation from WY1982 to WY2014 as:

$$p = \frac{m}{n+1} \tag{11}$$

where m is the rank based on total annual precipitation (from largest to smallest), and n is the total number of years examined. We selected water years nearest the 20th, 50th, and 80th non-exceedance probabilities to represent "dry", "normal", and "wet" climate groups, respectively, using five years for each of the dry and wet groups, and seven years for the normal group (Figure IV.12). In aggregate, these water years span ~80% of the PRISM period of record in terms of total annual precipitation, from 10% to 90% of non-exceedance probability. We randomized the order of the water years

within each of the three climate groups to create three climate scenarios – "dry," "normal," and "wet" (Table IV.5). We ran PRMS for a single simulation that represented these conditions in sequence, using associated PRISM (climate) values as inputs. We inserted two model stabilization periods using "normal" climate conditions, one at the start and one between wet and dry climate conditions (Table IV.5). By using the historic record to create these climate scenarios, we preserved the complex array of natural precipitation characteristics – intensity, duration, persistence, and spatial distribution – to the extent available in the observational record. This selection of input data should result in a wide and representative range of the precipitation and temperature characteristics that are typical of each climate scenario.

We analyzed model-generated outputs, including *precipitation*, *hillslope runoff* (Equation 12), and hillslope runoff-precipitation ratio (*RPR*) (Equation 13), for temporal and spatial dynamics and trends.

$$hillslope\ runoff = interflow + surface\ runoff \tag{12}$$

$$RPR = \frac{hillslope\ runoff}{precipitation} \tag{13}$$

interflow and *surface runoff* were aggregated to quantify *hillslope runoff* for this study. This was done in recognition of the complex interplay between the two hydrologic processes and the difficulty of accurately fixing their ratios in the calibration process, making their segregation relatively arbitrary. Additionally, combining the two components was deemed appropriate for this study's goals, as

DSC-MAR sites will likely result in the collection of both runoff and shallow interflow. This is due to the design of MAR infiltration basins as recessions in the landscape, having sloped sides and relatively level basin floors (Bouwer, 2002; Dillon et al., 2009). These geometries encourage the transition of interflow to return flow (a type of Dunnian runoff) by promoting interflow slowdown, saturation, and exit to the land surface in the concave regions between basin walls and floor (Dunne & Black, 1970; Chorley, 1969). Moreover, the absence of a dominant slope on basin floors promotes the stagnation of horizontal flow velocities, for both runoff and shallow interflow, in favor of ponding and downward movement – a factor additionally assisted by the high infiltration capacity characteristic of MAR sites (Bouwer, 2002; Chorley, 1969).

The baseflow component of runoff was not included in the analysis of hillslope runoff, as this component is routed directly into stream channels and thus is typically not available to use as a water supply for DSC-MAR. The definition of RPR presented above can result in values >1, in contrast to the traditional runoff coefficient (RC). An RPR can be >1 because it includes runoff that originated higher up in the basin, not just runoff resulting from precipitation falling on a particular area of interest. The distinction between RPR and RC is discussed later when results of the simulation are presented. To analyze the variability of hillslope runoff, we use mean annual and mean monthly data drawn from the HRU population for spatial variability, and full basin data drawn from the (rainy season) monthly population for temporal variability. For discussion purposes, we refer to the range between the 25th and 75

percentiles of these hydrologic data as the interquartile range.

V. Results

A. Calibration and Validation

1. Calibration parameters

Results from the calibration are shown in Figures V.1 to V.4, with NRMSDs given in Table IV.3. Given the SLRB's strong seasonal precipitation and the study goal of analyzing hillslope runoff, the most important NRMSD metric is based on the six-month rainy period (November through April) when the majority of precipitation occurs (Table IV.3).

The primary parameters adjusted for the annual calibration were **gwflow_coef**, and **gwsink_coef**. For monthly *runoff*, the primary parameters used in the calibration include the horizontal routing (interflow) coefficients (**slowcoef_lin**, **slowcoef_sq**), the vertical routing (gravity drainage) coefficients (**ssr2gw_rate**, **ssr2gw_exp**), and the maximum soilzone volumes (**soil_moist_max**, **sat_threshold**). The horizontal routing coefficients were minimized to match the observed hydrograph response, which exhibits minimal *runoff* during small precipitation events and a significant, rapid response with a steep recession during medium to large events (Figure III.5). The vertical routing coefficients were then tuned in combination with the soilzone volumes to improve the monthly calibration. Due to the strong seasonality of precipitation, stabilization routinely occurred after the first simulation year and test runs indicated that the simulation results were unaffected by the initial

conditions (soil and groundwater content) after stabilization, precluding the need to calibrate on initial conditions.

2. Calibration and validation

A list of calibration parameters, including calibration ranges and final values, is given in Table IV.4. With the exception of the two largest monthly events during the calibration timeframe (January 1997 and February 1998), the simulation did a reasonable job of matching observed monthly *runoff* (Figure V.1a). During these two months of extreme precipitation, however, the crossplot (Figure V.1a) shows a clear inability of the model to represent channel runoff. Because this phenomenon persisted despite parameter adjustments, it is likely due to the model's inability to simulate hydrologic processes that are common during the most extreme events, e.g., Hortonian runoff due to high precipitation intensities at sub-daily timescales. Once again, the fundamental problem is with the input climatological data, which virtually always underrepresents event intensity. To avoid calibrating to these extremes at the cost of the remaining 166 months, we removed these outlier months and their associated years (Figures V.1a-b) and updated the calibration.

The updated calibration (Figures V.1c-d) yielded a small improvement in NRMSDs (Table IV.3) and an improvement in the multi-year mass balance, for which the total difference between simulated and observed *runoff* was reduced from 18.3 inches to 7 inches over 14 years. The histogram of monthly differences between simulated and observed *runoff* also shows a good overall match of the data, with a

modest bias towards underrepresentation of runoff during lower flow periods (Figure V.2). The updated calibration improved the timing and response of simulated *runoff* at monthly timescales, as depicted in Figure V.3 (USGS, 2015b). Presented at finer temporal resolutions, the simulation hydrographs show a good approximation of most observed *runoff* data at the Santa Cruz gauging station. However, the simulation underestimates most mean daily discharges >1,500 cfs, likely because of input data limitations, the use of daily time steps, and fine discretization of the model domain, as discussed earlier (Figure V.4) (USGS, 2015b).

Model validation was conducted by analyzing the results of monthly and annual *runoff* from WY2002 to WY2014, using the final calibration values identified in Table IV.4. The annual NRMSD was lower for the validation period than for the calibration period, whereas monthly NRMSDs were somewhat higher (Table IV.3). Both annual and monthly *runoff* values clustered around the one-to-one line when comparing simulated to observed values (Figures V.5a-b). There was a systematic underestimation of the three largest monthly events and a notable misrepresentation of two months having intermediate precipitation totals, December 2002 and January 2003 (shown as triangles in Figure V.5a). There was a significant precipitation event that spanned these two months, generating simulated runoff mainly during the second month, but greater observed runoff during the first month. This result illustrates an additional challenge in discretization of PRMS output by month – a small offset in the timing of event response can lead to a significant apparent error. One might attempt to "calibrate" around an error such as this, but it

would likely lead to unrepresentative parameter selection. If these two monthly data points are omitted from the validation, the NRMSD is significantly improved (Table IV.3 and Figure V.6).

B. Climate Scenarios

1. Precipitation

Mean annual precipitation across the basin ranges from 30.2 inches under the dry scenario to 59.2 inches under the wet scenario. Hyetographs for the climate scenarios (Figure V.7) show similar seasonal precipitation patterns, with the majority of precipitation occurring between November and April and little-to-no precipitation during the months of June through September. Additionally, each scenario exhibits a similar range of precipitation magnitudes, with the dry scenario producing nearly commensurate maximum monthly intensities (20.7 inches per month) as the normal and wet scenarios (21.5 inches and 26.9 inches, respectively). All of the climate scenarios include months of heavy rainfall, but they are rarer and less persistent during the dry scenario. In contrast, months of elevated precipitation are more frequent and persistent in the normal and wet scenarios.

There is greater temporal and spatial variability of precipitation with the wetter climate scenario compared to the normal and dry scenarios (Figures V.8, V.9 and V.10). Histograms of monthly, rainy-season precipitation for all HRUs show a clear increase in precipitation for December, January, and February from dry to wet climate scenarios (Figure V.8), with an interesting trade-off between November and

March. March precipitation is greatest under the dry and wet scenarios, but is lower under the normal scenario. November precipitation shows the opposite pattern, being greatest under the normal scenario and lower under both dry and wet scenarios. The implications of these shifts are discussed later.

2. Full basin response

To align the results with the project goal of determining runoff availability for MAR, hillslope runoff was quantified as the surface runoff plus interflow (Equation 12) exiting the HRU, which includes the amount of runoff generated by the HRU plus runoff received from upslope regions via cascades. For the basin response, hillslope runoff (as above) was summed for all HRUs and normalized over the entire basin area.

The mean monthly hillslope runoff for dry, normal, and wet climate scenarios is 0.5 inches, 0.9 inches, and 1.7 inches (Figure V.11), equating to total annual runoff volumes for SLRB of approximately 43,000, 78,000, and 147,000 acre-ft/year. The maximum monthly hillslope runoff for dry, normal, and wet climate scenarios is 7.0 inches, 7.2 inches, and 11.7 inches. Comparing the hydrographs to the hyetographs, the temporal pattern of hillslope runoff roughly follows that of precipitation (Figure V.11). For each climate scenario, significantly less hillslope runoff is produced for months having ≤4 inches of precipitation (Figures V.11 and V.19a). Thereafter, monthly runoff increases with precipitation, though there is no strong correlation between monthly RPR and precipitation values within each climate scenario (Figure

V.19).

Unlike the runoff coefficient (RC), which accounts only for the runoff generated within a region (as a fraction of precipitation), the RPR metric includes runoff that flows from upslope areas. As a result, RPR can be greater than 1.0. The monthly RPR time series generally emulates the monthly hyetographs for each climate scenario, but there are anomalously high RPR values when precipitation during one month leads to considerable runoff during the subsequent month. We filtered out RPR values >0.5 that occurred during a month of negligible precipitation (<0.01 inches) to minimize these artifacts (Figure V.15). The mean monthly basin RPR is 0.12, 0.21, and 0.37; whereas the maximum monthly basin RPR is 1.1, 2.8, and 8.8 for dry, normal, and wet climate scenarios, respectively. This trend of increasing mean monthly and maximum monthly RPR values with wetter climates can also be seen in the Box and Whisker Plots of basin monthly RPR (Figure V.17).

The variability of basin hillslope runoff (Figure V.13) is considerably less than that for precipitation (Figure V.9). The interquartile ranges for precipitation are 4.6 inches, 6.6 inches, and 9.4 inches (Figure V.9), whereas those for hillslope runoff are 0.8 inches, 2.3 inches, and 4.5 inches (for dry, normal, and wet climate scenarios, respectively) (Figure V.13). The relatively low temporal variability of hillslope runoff is also revealed in the stacked histograms (Figure V.12), showing bin sizes of hillslope magnitudes that are very similar for each month of the rainy season.

Basin monthly hillslope runoff shows a positive trend in temporal variability with wetter climate scenarios, having interquartile ranges of 0.9 inches, 2.3 inches,

and 4.5 inches for dry, normal, and wet climate scenarios, respectively (Figure V.13). The temporal variability in monthly RPR also increases under wetter climate scenarios, having interquartile ranges of 0.19, 0.21, and 0.30 for dry, normal, and wet scenarios (Figure V.17).

3. Spatial distribution of hillslope runoff

Much like precipitation, there are consistent spatial patterns of hillslope runoff and RPR across the SLRB for each climate scenario (Figure V.20). The spatial variability of annual hillslope runoff (Figure V.14) is approximately two to three times larger than that of precipitation (Figure V.10), with the former having interquartile ranges of 3.9 inches, 4.9 inches, and 8.4 inches, for dry, normal, and wet climate scenarios, respectively. This relatively large spatial variability for runoff is also apparent in the stacked histograms of runoff and RPR (Figures V.12 and V.16), in which there is a wide range of runoff responses for each month.

The spatial variability of annual hillslope runoff across SLRB (Figure V.14) increases with wetter climates, from 8.2 inches for the dry scenario, to 14.7 and 25.4 inches normal, and wet climate scenarios, respectively. Similarly, the spatial variability of the annual RPR is also greater with progressively wetter climate scenarios, having interquartile ranges of 0.27, 0.37, and 0.43 (dry, normal, and wet; Figure V.18). Thus the regions that produce disproportionately more runoff as a fraction of precipitation are even more important under a wetter climate scenario than under a drier climate scenario.

VI. Discussion

A. Calibration and Validation

1. Calibration parameters

The primary adjustments made during calibration were to those parameters that characterize the soilzone (Figure IV.2). Water is delivered to and transferred between the three soilzone reservoirs: preferential flow, capillary, and gravity (PFR, CPR, and GVR, respectively). Soilzone parameters define the storage capacity and basis for routing water between these reservoirs. Before interpreting calibration of soilzone parameters, I briefly review how water is routed within this part of PRMS (Figure IV.2).

Water is delivered to the soil layer as precipitation throughfall and/or Hortonian runoff from upslope HRUs. The model first apportions some of this water as Hortonian runoff. The remaining water is allowed to infiltrate into the soilzone, where it is initially divided between the PFR and the CPR. The PFR is the fraction of the soilzone containing preferential flow channels. Water in the PFR is allowed to exit either as (fast) interflow or as Dunnian runoff once the PFR becomes saturated. The CPR extends to the vegetation rooting depth and accounts for that fraction of soil moisture between the wilting point and field capacity, where water is bound in the soil matrix by capillary forces and available for evaporation and transpiration (upper capillary zone) or transpiration only (lower capillary zone). In addition to infiltration, the CPR also receives input as interflow and/or cascading Dunnian runoff. When the water content in the CPR reaches field capacity, any additional water is passed onto

the GVR, which extends to the full soil depth and comprises the fraction of soil water between field capacity and porosity. Water in the GVR is not bound in the soil matrix and can exit as (slow) interflow or as gravity drainage to the groundwater reservoir. When saturated, additional input to the GVR is delivered to the PFR. Finally, when the PFR becomes saturated, any additional water becomes Dunnian runoff (or "saturation excess overland flow").

The dynamics of these inter-reservoir transfers are complex, and the parameters that define the soilzone are strongly interconnected, often requiring more than one soilzone parameter to be calibrated in sequence to achieve a desired response. Additionally, the ratio of Dunnian runoff to interflow can be modified significantly while still assuring monthly and annual mass balance in the calibration process, which could lead to non-unique solutions with similar calibration performance.

Santa Cruz gauging station data (Figure III.5, Figure V.4) shows a subdued response during small precipitation events, but a significant, "flashy" response during larger events that occur in rapid recession. To match the subdued response during small precipitation events we minimized several routing coefficients (**fastcoef_lin**, **fastcoef_sq, slowcoef_lin**, **slowcoef_sq**). Larger values for these coefficients resulted in excessive basin runoff response to small events. We also found it necessary to reduce the **pref_flow_den** parameter to avoid an immediate runoff response from the PFR (via fast interflow). Considered in aggregate, these calibration settings suggest that the SLRBs hydrologic response includes relatively little runoff until the soil

becomes saturated, consistent with good drainage and high soil storage capacity. Once the soil becomes saturated, there can be a large, rapid (Dunnian) runoff response. The relatively modest generation of interflow could result from spatial variability, including soils with relatively low conductivities. Interflow passing downslope within the basin would be limited by areas with the least transmissive properties. It might also be that lateral interflow is overwhelmed by preferential flow in the vertical direction via macropores such as deep root channels.

To match simulated to observed monthly *runoff*, we adjusted the vertical routing coefficients (**ssr2gw_rate**, **ssr2gw_exp**) and the maximum soilzone volumes (**soil_moist_max**, **sat_threshold**). The linear vertical routing coefficients, **ssr2gw_rate**, were calibrated to the lower end of the calibration working range, whereas the vertical routing exponents, **ssr2gw_exp**, were calibrated to the upper end of the range (Table IV.4). This is consistent with relatively efficient routing of GVR water to groundwater.

CPR and GVR soil reservoir water parameters were also modified during calibration (Table IV.4). Final values for the maximum water volume in the CPR for each HRU, **soil_moist_max**, were in the range of 0.11-20.95 inches, with a basin average of 10.0 inches. The maximum water volume in the GVR for each HRU, **sat_threshold**, included a similar range (Table IV.4), with a basinwide average of 1.5 inches. Higher values of **soil_moist_max** allow for more ET from the CPR, limiting the short-term runoff response to small precipitation events. Lower values of **sat_threshold** tend to reduce the extent of slow interflow within the GVR, resulting

in a more rapid Dunnian response shortly after the GVR receives inflow.

These parameters represent geometric characteristics of the soil reservoirs and were derived from regional input data, including: vegetation rooting depths and available water content for **soil_moist_max**; and soil thickness, porosity, and field capacity for **sat_threshold**. Adjustments made during calibration suggest that these parameters might also account for soil and hydrologic characteristics not represented in available field data. In adjusting these parameters during calibration, we multiplied original values by a fixed ratio, shifting the averages as needed to match the observed *runoff* response, while preserving the spatial variability given by the data.

A CPR that holds more water than the GVR normally requires a rooting depth greater than soil depth. For example, given an AWC of 0.1 and a water holding capacity (n - FC) of 0.2, the basin average calibrated values for **soil_moist_max** and **sat_threshold** (Table IV.4) correspond to a rooting depth of 100 inches and a soil depth of 7.5 inches, respectively. The important role of deep roots in arid and semi-arid regions suggests that values used are reasonable for this application (e.g., Devitt & Smith, 2002; Seyfried et al., 2005). Additionally, rooting depths of 100 inches have been noted in the literature (e.g., Canadell et al., 1996), and may be justified in the SLRB because of local zones of deep soils and/or fractured bedrock interspersed amidst a predominantly shallow soil layer (Seyfried et al., 2005). Soil and rooting heterogeneities in both horizontal and vertical directions can significantly affect patterns of infiltration and runoff (Loik et al., 2004). Consequently, deep, localized features such as these may provide significant reservoirs for water to become deep

recharge or be bound in the soil matrix for transpiration. As these deep zones become more saturated during large precipitation events, the surrounding shallow soils would become saturated as well, generating Dunnian runoff.

Dunnian runoff in PRMS is generated after the saturation of shallow soils. Because shallow soils play a dominant role in determining the generation of Dunnian runoff, we applied a harmonic mean rule for soil thickness when calculating **sat_threshold** (Tables IV.1 and IV.4). SLRB data indicates soil depths of 9 to 1575 inches, with a harmonic mean of 30 inches, and the calibrated thickness was ~7.5 inches.

Evapotranspiration (ET) is facilitated through three primary processes in the model, the first two of which are heavily influenced by the region's vegetation:

1) Capture of precipitation by the vegetation canopy (Figure III.2b) and subsequent evaporation. The volume of precipitation susceptible to this process is determined by the parameters **wrain_intcp** (Figure IV.7c) and **srain_intcp**, and is significant in the SLRB given the region's dense vegetation.

2) Infiltration of throughfall into the CPR soilzone (Figure IV.2), where it is bound in the soil matrix and subsequently transpired. This soil reservoir, determined by **soil_moist_max**, correlates with the vegetation rooting depth and also constitutes a significant volume, as discussed previously.

3) Evaporation from the Upper CPR (Figure IV.2), which constitutes a relatively small volume (**soil_rechr_max**, Table IV.1) due to shallow evaporation depths in soils (Heitman et al., 2008).

Due to the lack of PET data in the region we did not calibrate the model to directly match ET or PET, and instead represented the temporal variability, month-to-month, of PET by scaling the model's PET coefficient (**hamon_coef**) proportionately to the mean monthly PET at the SLRB's nearest CIMIS station. Consequently, because our calibration focus was on monthly and annual runoff vice ET, water lost from the system due to ET and the groundwater sink (determined by the parameter **gwsink_coef**) may be interchangeable. Nonetheless, the simulation mass balance indicates that only about 35-percent of precipitation in the model makes it to the stream channels. Given the simulation assumption of a multi-year steady state (multi-year change in storage ~ 0), this demonstrates that the combined impacts of ET (governed by the processes discussed above) and the groundwater sink (e.g. anthropogenic withdrawals, flows to deep aquifers and/or directly to the ocean, etc.) are significant in the SLRB.

2. Calibration and validation patterns

Although the final monthly calibration and validation statistics are good for the simulations overall (NRMSD = 0.137 and 0.212, respectively), and should be sufficient for the intended purpose of these simulations (planning for development of DSC-MAR systems) there remain systematic differences between simulated and observed runoff. In particular, comparisons of simulated and observed monthly runoff (Figures V.1 and V.5) show a tendency for simulations to: (a) overestimate runoff under moderate precipitation conditions (2–5 inches/month), and (b) underestimate

runoff under high precipitation conditions (8-12 inches/month).

This pattern proved difficult to resolve during calibration and validation, as modifications to parameters that tend to reduce the first effect also exacerbate the second, and vice versa. The under-representation of runoff during wet months is likely to have resulted in part from how precipitation was applied by the model because of the temporal discretization of data. Daily precipitation data and simulation time steps have two related impacts on intensity: reduced intensity of precipitation for periods lasting less than 24 hours, and reduced intensity for events >24 hours that span multiple days. For example, consider a relatively heavy precipitation event lasting 30 continuous hours, with the heaviest precipitation (a "cloudburst") occurring during one hour within a single calendar day. Daily simulation time steps will reduce the mean storm intensity of the full event, dividing it between two or three days, and the highest simulated intensity of precipitation during these days will be much lower than observed during the cloudburst. As a result of both of these effects, more water will be infiltrated in the simulation than occurred in the natural system, and much of that infiltrated water will be routed along paths that delay delivery to the channel (e.g., slow interflow from the GVR, Dunnian runoff from the PFR, see Figure IV.2). This behavior is nonlinear, disproportionately influencing the wettest time periods, and influences both monthly and annual water balances as peak flows are reduced and delayed and more water leaves the landscape as ET or groundwater recharge.

Given this behavior during high precipitation periods, calibration in an attempt to match annual water hydrographs may contribute to the over-representation

of runoff during moderate precipitation periods. Additionally, there could be a contribution related to the fine spatial scale of the HRUs used to define the model domain. Creation of many small, heterogeneous HRUs gives the simulated landscape more routing options than it would otherwise have with larger HRUs. With many small HRUs, inflows are routed to subsurface flow or ET in some HRUs, while becoming rapid Dunnian runoff in others. However, if small HRUs were combined into one homogenous HRU, the runoff response would be dampened for small-to-moderate precipitation events during which the GVR doesn't become saturated and Dunnian runoff is prevented. Conversely, for large precipitation events during which saturation occurs in the larger HRU, Dunnian runoff would be triggered from the entire domain, yielding a response of greater magnitude than would be produced by numerous, small HRUs. In summary, the use of smaller HRUs (which provides insights into local differences in runoff by representing heterogeneous soil and vegetation conditions) could cause the full basin to increase simulated runoff for moderate precipitation events, while decreasing runoff magnitudes and creating runoff time delays for larger events. These are the two main forms of unresolved misfit apparent during both calibration and validation simulations (Figures V.1 and V.5).

It is worth considering whether these explanations might apply to the two highest precipitation months of the simulations (Figure V.1a, January 1997 and February 1998), which were omitted from analysis during the final stages of calibration (Figure V.1c). Simulated *runoff* during these months was not only below

that observed, it was also less than *runoff* simulated during other months when total precipitation was lower. We suspect that this model response resulted from under-representation of Hortonian runoff. For pervious soils with high infiltration capacities (as in much of the SLRB, where sand-rich soils have mapped infiltration capacity values >20 ft/day; Table IV.2), Hortonian runoff can only occur when the precipitation intensity is extremely high. Precipitation intensities necessary to produce Hortonian runoff on high-IC soils do not typically persist over 24-hour periods. Thus representation of these events would be required at time scales of hours (or perhaps minutes).

As soil moisture content increases, infiltration capacity decreases, and the rainfall intensity required to exceed IC and produce Hortonian runoff decreases as well. Based on this relationship, PRMS estimates Hortonian runoff from pervious areas using a contributing area approximation, in which Hortonian runoff in each HRU is calculated as originating from a fractional area that increases with soil moisture content. This approach is not capable of simulating runoff produced by short duration, torrential precipitation that exceeds the infiltration capacity. Hortonian runoff that is not generated by the model can infiltrate into the CPR where it will be lost to ET. As a result, calibration of soil routing parameters to match these extreme events either will not be possible, or will result in a gross over-prediction of runoff during lower precipitation events. This was the conundrum that led us to avoid trying to calibrate the model to match runoff during the highest precipitation periods.

In summary, we are satisfied with the annual and monthly calibration and

validation results for the SLRB, and believe that the resulting PRMS simulation provides a reasonable representation of water routing across the landscape for most of the period of record. We are less concerned with forcing PRMS to match runoff observations during extremely wet periods for several reasons. First, calibrating to match runoff observations during wet extremes tends to cause difficulties in matching observations during normal to dry periods (in part because of limitations in model resolution, as discussed earlier). Second, underestimating runoff during the wettest periods will make simulations more conservative from the perspective of assessing water supply options for MAR. Finally, we are most interested in assessing the relative contributions to runoff from different parts of the basin. For that purpose, in the next section we explore runoff generation under dry, normal, and wet precipitation conditions, using data from the observational record to drive the model.

B. Climate Scenarios

1. Precipitation

By using the historic record in the construction of climate scenarios, we were able to preserve the diversity of precipitation characteristics that are vital to runoff response, including distribution, intensity, duration, and persistence (Figures V.7 and V.20a). One such characteristic is the occurrence of months having substantial precipitation, even during the dry climate scenario. We also see the persistence of precipitation, where months with significant precipitation often occur adjacent to each other (especially during the wet climate scenario).

The distribution of monthly precipitation across the HRUs shows some interesting patterns (Figure V.8). As expected, there is more precipitation during some of the wettest months (December, January, and February) during the wetter scenarios. However, we were surprised to see that there is not a monotonic pattern for the months of November (wettest under the normal scenario) and March (driest under the normal scenario). These shifts are relatively well defined for the period of record, but it is not clear if they have persisted over longer time periods.

The patterns for mean annual precipitation show a striking consistency in spatial distribution (Figure V.20a). All three climate scenarios show the most precipitation in the mountainous regions along the northeastern and southwestern edges of the SLRB (Figure V.20a and Figure III.3). However, there is also a precipitation "low" in the high elevation northwest region, as well as a precipitation "high" in the valley just inland/east of the western mountains. These may result from the typical pattern(s) of storm tracks across the SLRB and provide good justification for modeling precipitation at high resolution.

2. Full basin response

The climate scenario hyetographs and hydrographs (Figure V.11) reveal several interesting relationships between precipitation and runoff in the study region. First, there are numerous months in all three scenarios for which zero, or nearly zero, hillslope runoff is generated despite moderate monthly precipitation. During such months, streamflow would be limited to baseflow (or releases from Loch Lomond

Reservoir). The soil moisture content remains below field capacity for these months, with all water bound in the CPR soil matrix and available only for ET.

Second, significant hillslope runoff tends to occur only if there has been precipitation during that month and the preceding month. Rarely does a month produce significant runoff when the preceding month receives only negligible precipitation, mainly because the CPR must be full (at field capacity for the soil) before interflow and/or surface runoff can be produced by the GVR. Finally, we see that (when considering the basin as a whole) there is runoff generated during some months in the dry climate scenario, suggesting that there may be DSC-MAR opportunities even during dry years. As in the normal and wet scenarios, significant runoff months in the dry scenario (though infrequent) are also preceded by moderate precipitation months. In combination, these patterns help to emphasize the importance of antecedent soil moisture on runoff generation in the SLRB.

A second primary observation is that the runoff response of the basin is smoothed and attenuated relative to the variability seen in precipitation input. The landscape contains numerous reservoirs where water is sequentially stored and released – including canopy storage, soil reservoirs, and the surface of impervious hardscapes. As a result, the landscape dampens the basin wide response to precipitation.

The temporal variability of basin runoff also increases with wetter climate (Figure V.13), mainly because of increases in the largest monthly runoff events under the wet climate scenario, while the smallest runoff events are similar in magnitude for

all scenarios. A more interesting trend is revealed by the relative change in basin monthly runoff with changes in monthly precipitation. Although there is a nearly linear relationship (with a slope of 0.5) between mean monthly hillslope runoff and precipitation for all climate scenarios, mean monthly runoff constitutes a larger fraction of precipitation for the wet climate scenario than for dry (Table VI.1, Figure V.17). Figure V.17 also illustrates an increase in the temporal variability of basin RPR for wetter climates, indicating that the trend of increasing RPR values with wetter climates is expressed the most during the largest events. In summary, disproportionately more runoff is produced as a fraction of precipitation for the wet climate scenario than for the dry climate scenario. By comparison, within each climate scenario there is no discernible trend in a cross-plot of basin monthly RPR versus monthly precipitation, implying that runoff remains relatively constant as a fraction of precipitation for each individual climate scenario (Figure V.19b). This finding will be particularly useful for assessing the potential to collect stormwater runoff for MAR projects.

3. Spatial distribution of hillslope runoff

By HRU, the spatial distribution of hillslope runoff and RPR spans a wide range, with the largest magnitudes of hillslope runoff and RPR being 418 inches and 6.95, respectively – occurring during the wet climate scenario and for the same HRU (Figures V.20b/c). High values such as these result, in part, from use of the PRMS cascade module. The cascade module enables hillslope runoff to be transferred from

upslope to downslope HRUs before reaching a stream channel. Some of the upslope runoff aggregates directly with the runoff generated by the downslope HRU; the rest increases the downslope HRU's soil moisture content, contributing to additional runoff generation (Figure IV.2). With the use of cascades, if a downslope HRU has an area that is smaller than that of upslope/contributing HRUs, a "funneling effect" occurs in that the volume of cascading runoff is applied over a smaller area, resulting in a larger RPR. Additionally, cascading flows increase the soil moisture content of downslope HRUs, boosting their production of runoff. Regions such as these should be focal points for assessment of hillslope runoff as potential supply for MAR.

The spatial variability of runoff (Figure V.20b) is significantly greater than that of precipitation (Figure V.20a), illustrating the importance of soil, vegetation, and land use characteristics. Different physical features – depending on land use, vegetation, topography, soils, and other characteristics – have different effects on runoff response. In combination, these features contribute to the runoff response, lending to spatially variable runoff behaviors. In short, heterogeneity and variations in the landscape can diversify, magnify, and punctuate spatial sensitivities to precipitation, yielding a highly varied response.

Figure V.20d shows three important SLRB-wide datasets used by PRMS: percent sand in soil, percent impervious area, and vegetation coverage density. Each landscape feature shows considerable spatial variability, and each appears to correlate (roughly) with patterns of runoff generation. Although a multivariate analysis would be required to quantify these correlations, PRMS appears to simulate greater runoff

from parts of the landscape having less sandy soils, more impervious area, and less vegetation density. That the simulations display such a spatially complex sensitivity to precipitation helps to justify the use of high-resolution input data and relatively small HRUs. Additionally, these results illustrate the functionality and utility of the model – specifically its ability to produce high-resolution output that can support the broader project goal of analyzing hillslope runoff at the sub-watershed scale for development of MAR projects.

The distribution of hillslope runoff indicates an increase in spatial variability under a wet climate scenario (Figure V.20b). Similar to the temporal trends discussed in section VI.B.2, this is also an expected outcome, caused by a few regions that produce proportionately greater runoff during the wet climate scenario, while other parts of the SLRB generate little-to-no runoff under all climate scenarios. This observation is also apparent in an aggregate analysis of all HRUs in the SLRB (Figure V.14). Moreover, there is an increase in the spatial variability of RPR across the basin during the wet climate scenario (Figures V.20c and V.18). Thus, areas that generate the most runoff are also most responsive to differences in precipitation patterns, producing more runoff as a fraction of precipitation during the wet climate scenario.

Given the high spatial resolution of hillslope runoff provided by the simulation (Figures V.20b/c), these results can be used as a preliminary MAR planning and estimation tool. Because our results account for upslope contributions to runoff (via cascades), the values for each HRU in Figure V.20b represent hillslope runoff derived from a cascading series of HRUs. These "cascading HRU series" can

be viewed as individual catchment areas for potential DSC-MAR sites. Consequently, resource managers could use Figure V.20b to assess locations that meet runoff targets for MAR. For example, using a conservative estimate of 100-acre catchments, if a basin goal is to infiltrate 1000 acre-ft/year, 10 project locations might be selected, with each located in an HRU that delivers an annual average of 100 acre-ft/100 acres.

As another MAR planning tool, we used the simulation of hillslope runoff, by HRU, to calculate the cumulative areal distribution of mean annual precipitation (Figure VI.1) and hillslope runoff (Figure VI.2). For each climate scenario, Figure VI.1 depicts how much of the study region receives at least a particular amount annual precipitation. Similarly, Figure VI.2 depicts how much of the study region delivers at least a specified amount of annual runoff under a dry, normal, or wet climate scenario. For example, consider the same goal of generating 100 ac-ft/yr of runoff per 100 ac of drainage area. Under a dry climate scenario, about 15% of the SLRB meets this objective, equivalent to ~50 km^2. In contrast, about 30% of the SLRB meets this target under the normal climate scenario, and 60% meets this target under the wet climate scenario. In aggregate, this suggests that there is a lot of opportunity within the SLRB to collect stormwater runoff for MAR. Additional work is needed to assess many additional factors, include the interest of landowners and agencies, availability of space in underlying aquifers, engineering requirements, and water rights and permits.

VII. Conclusions and Future Work

A. Conclusions

This study demonstrates a method for modeling hydrologic basin response at sub-watershed scales to assess the spatial and temporal dynamics of hillslope runoff as potential supply for MAR. To assess hillslope runoff over a range of climate conditions while preserving the region's characteristic precipitation patterns and qualities, we used the historic record to build three climate scenarios based on annual precipitation – dry, normal, and wet. By using a fine scale representation of topographically defined grid cells (HRUs), and leveraging numerous high-resolution data sets, we produced simulation outputs at spatial resolutions of 0.1 to 1.0 km^2. Because PRMS is discretized to use daily time steps, and there is little climate data available across the SLRB at higher temporal resolution, we calibrated the model on the basis of monthly and annual timescales. The results show opportunities for hillslope runoff as potential supply for MAR during all climate scenarios. The results also indicate that a larger fraction of basin precipitation becomes hillslope runoff during wetter climates, that this trend is accentuated for the largest monthly events, and that both the spatial and temporal variability of runoff increase under a wetter climate.

For all climate scenarios, the simulation shows that hillslope runoff has a smaller temporal variability and a larger spatial variability than does the precipitation input. This results from the landscape's ability to dampen and prolong the temporal response to precipitation in some areas by absorbing and releasing waters, while

delivering runoff quickly in other areas, due to landscape heterogeneities. That our simulation can produce such a spatially diverse response is, at least in part, a consequence of high-resolution input data and relatively small HRUs.

This study's high-resolution results support our project goal of analyzing hillslope runoff at the sub-watershed scale, and can be used to determine locations throughout SLRB that yield ample supply for MAR (Figure V.20b). Such locations (as HRUs) can be further evaluated for potential project sites by combining results of runoff simulations with a concurrent MAR site suitability analysis, which analyzes soils and geology to determine where water can successfully infiltrate and become recharge. Plotted as cumulative areal distribution curves (Figures VI.1 and VI.2) runoff model results can also be used for MAR planning and assessment for the entire basin.

These results will enable resource managers, planners, engineers and stakeholders to assess the feasibility of DSC-MAR objectives in the SLRB based on hillslope runoff supply under various climates. Additionally, when combined with an analysis of MAR soils and geologies, these results should help with screening and placement of future field projects.

B. Future Work

There are tremendous opportunities for additional analyses related to this study. We felt it necessary to conduct a manual calibration in this study, informed by careful review of the hydrographs, to prevent an undesired, non-unique match of the

monthly and annual mass balance. Given that were able to produce a reasonable match to monthly hydrographs during both calibration and validation periods, the climate scenario simulation should be indicative of the actual SLRB runoff response. However, there is potential to optimize model calibration using a more sophisticated procedure. With 865 HRUs, it is prohibitive to manually calibrate parameters by individual HRU. Using automation, the primary calibration parameters (identified in section V.A.1) could be adjusted independently for all (or selected) HRUs. Automation provides no guarantee that the calibration would be improved, and because of limitations in input data (both spatial and temporal), there is also the potential that refined calibration would result in unrealistic parameters or reveal other problems. Still, it would be worth attempting to improve the response of the model.

The next step in this study is to overlay PRMS simulation results with those from a concurrent MAR suitability study. The MAR suitability study provides a spatially continuous assessment of soil and groundwater conditions for infiltration and recharge. Identifying how much of the study region might be viable for DSC-MAR requires a joint analysis that considers where there is ample supply (through this study), and where that supply can successfully recharge aquifers. The latter analysis includes only about 25% of the SLRB area because of limitations in the availability of subsurface data, but it will still prove useful when combined with PRMS results.

As mentioned in section VI.B.3, the hillslope runoff values in this study indicate what is delivered at the HRU outlet point, and contributions from upslope

HRUs (via cascades) are focused along the manufactured stream(s) within any given HRU. As a result, it would be interesting to combine our high-resolution runoff results with a contributing area analysis conducted at the extreme high resolution of the DEM raster. This process would involve siting potential DSC-MAR infiltration basins, each approximately 1-5 acres in size, and determining the contributing area to each basing using the gradient and flow accumulation calculations in section IV.B. Then, by rerunning our simulation without cascades, we could calculate runoff coefficients for each HRU, RC_i, and apply these values to the HRU precipitation value, P_i, to determine hillslope runoff for each HRU over the simulation. Finally, for each potential DSC-MAR infiltration basin, we would determine the area of each HRU, A_i, that overlaps with the infiltration basin's contributing area to calculate the total runoff volume to each DSC-MAR site as:

$$hillslope\ runoff_{MAR} = \sum_{i}^{n} RC_i \times P_i \times A_i \tag{14}$$

This analysis could be conducted by randomly placing DSC-MAR infiltration basins across the study region as a survey of available supply for DSC-MAR sites throughout SLRB. Alternatively, we could selectively pick locations that have been pre-screened for both hillslope runoff supply and MAR suitability (as previously discussed) to enable a higher fidelity assessment of viable DSC-MAR sites and their volumetric potential.

It would also be valuable to assess SLRB's pre-development runoff response. This would require adjusting the model's vegetation and land-use parameter inputs to

reflect conditions that existed prior to anthropogenic influence. Though data is limited for historic vegetation conditions, we can approximate these conditions by setting the vegetation polygons of human-modified areas (e.g. urban, agriculture, non-savannah grasslands) to match the vegetation characteristics of their surrounding polygons. We would, additionally, set the percent impervious parameter to 0.0 throughout the entire region. This analysis would quantify and compare the basin's pre- and post-development runoff responses, including the impact on naturally occurring recharge. It would also enable an assessment of how much recharge to "target" via MAR in order to counter the effects of past and future land development on runoff and recharge.

Lastly, it would be useful to conduct a multivariate statistical analysis, such as a Principal Component Analysis (PCA), between several input parameters and hillslope runoff. This analysis could reveal the relative influence of parameters and parameter combinations on hillslope runoff and help reduce the list of required data input to the model. It may also serve as a first step in devising a more tractable, simple correlation-based approach at conducting hillslope runoff analyses for MAR decision making.

VIII. Figures

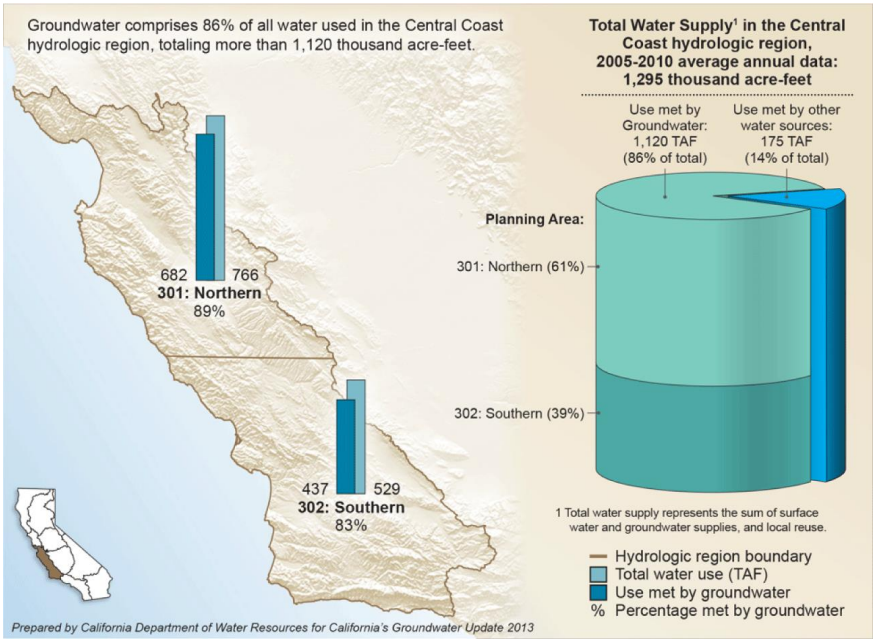

Figure I.1

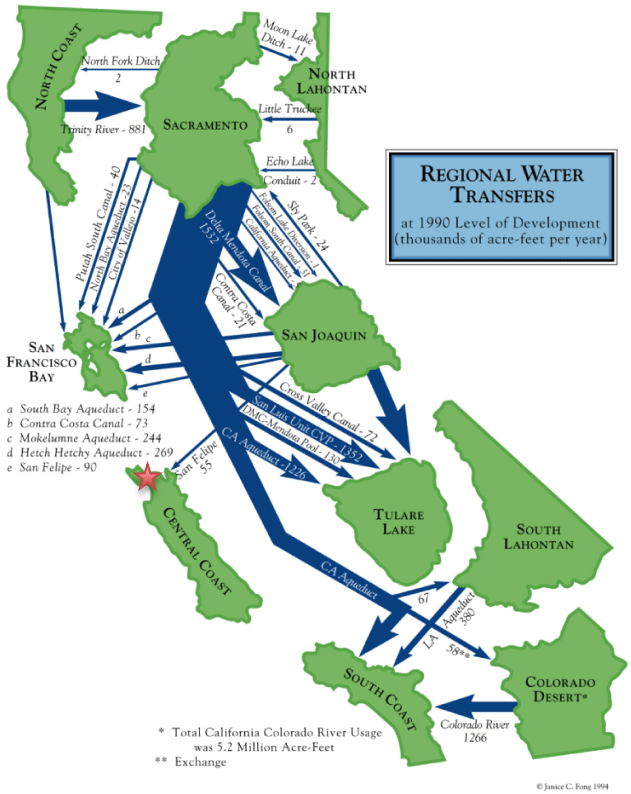

Figure I.2

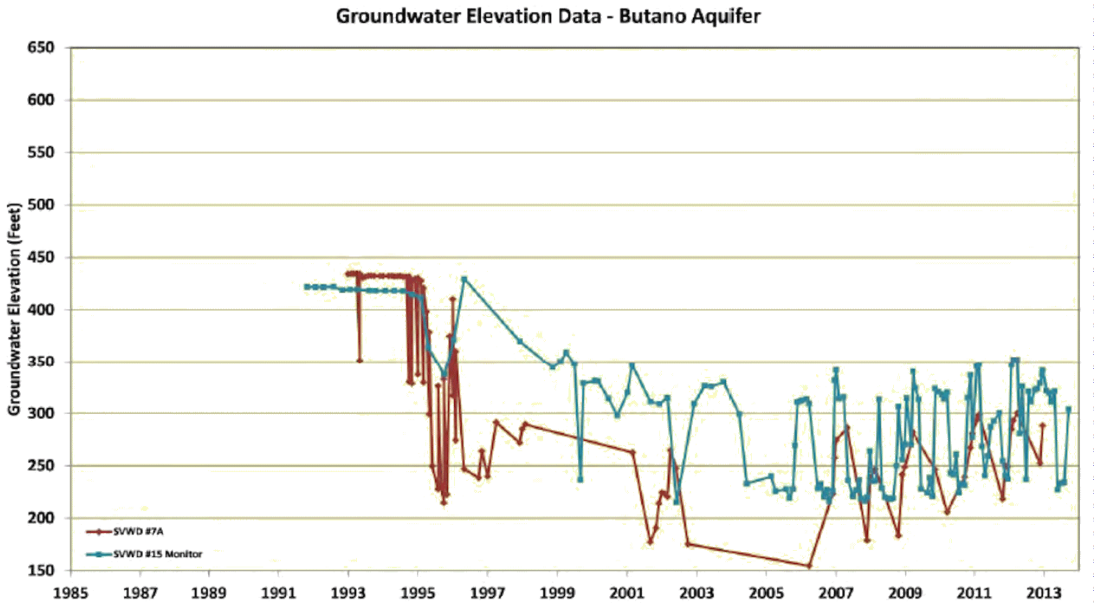

Figure I.3a

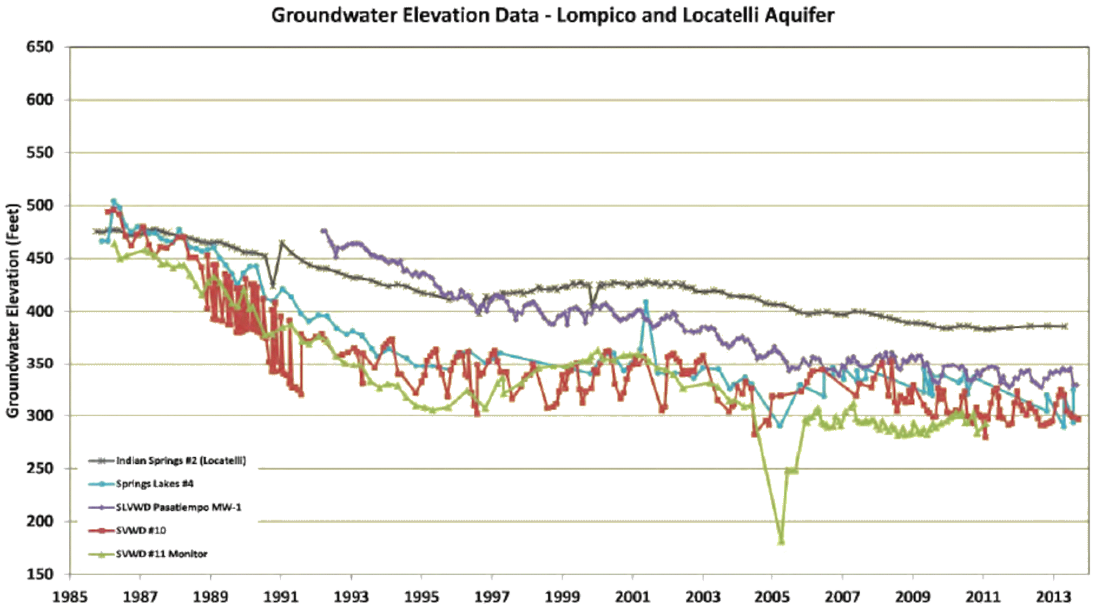

Figure I.3b

Figure I.4a

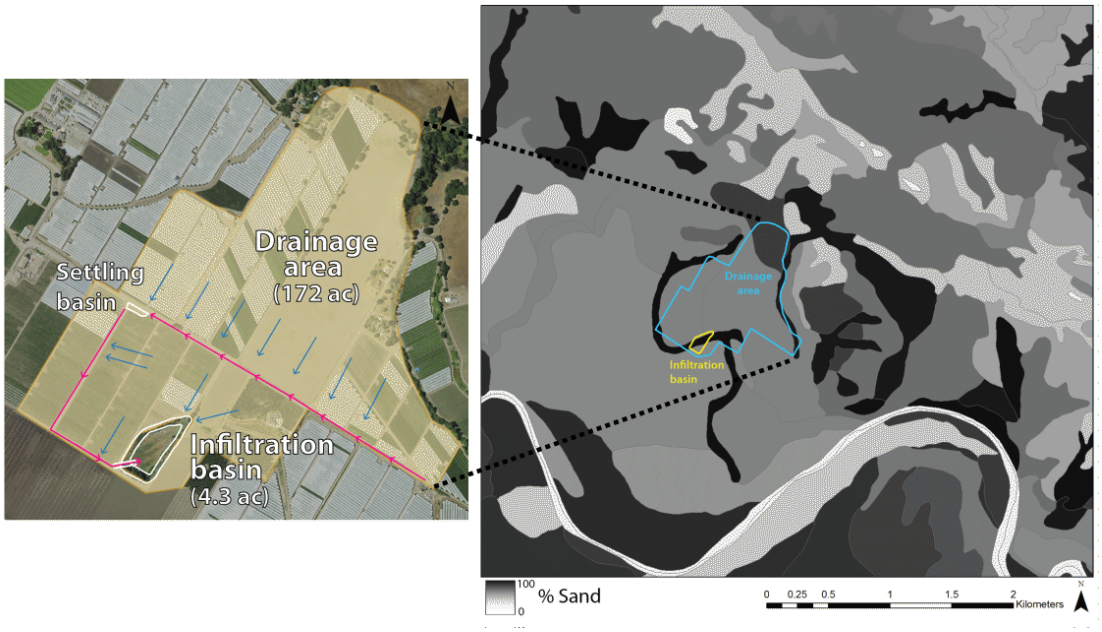

Figure I.4b

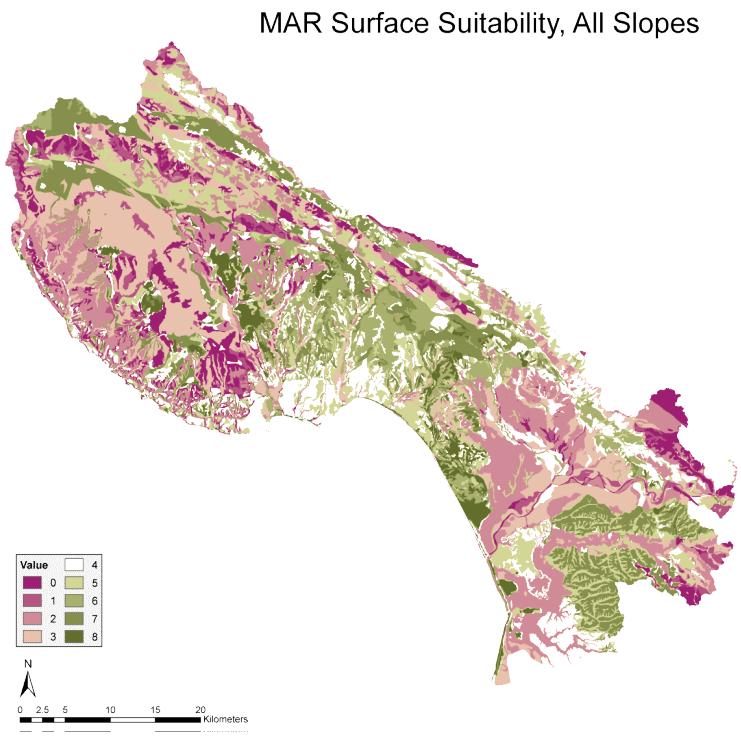

Figure I.5a

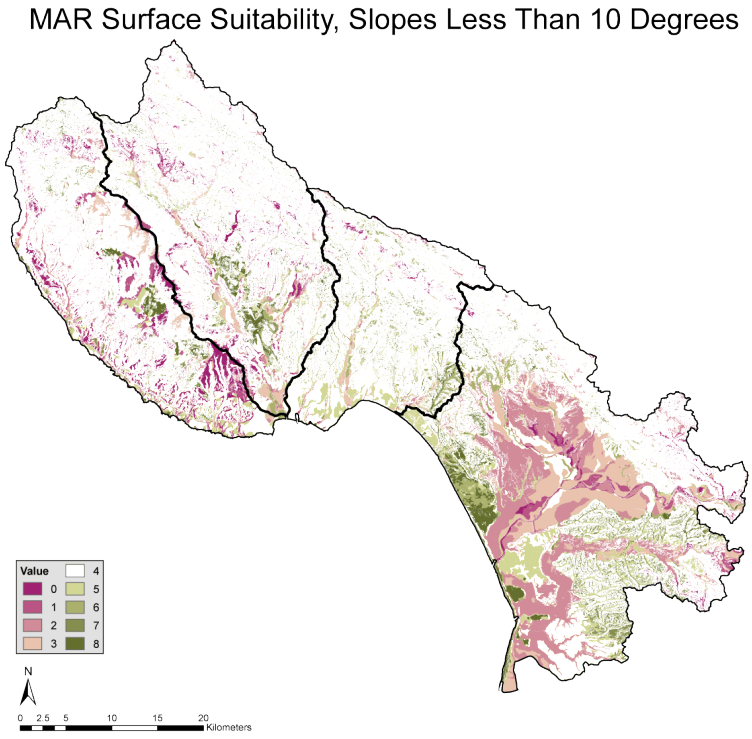

Figure I.5b

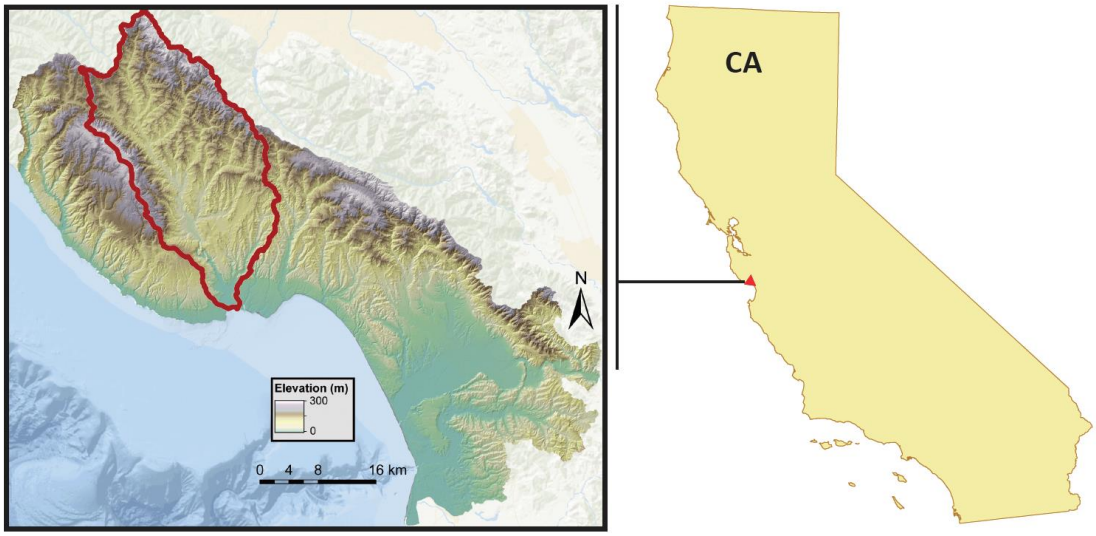

Figure III.1

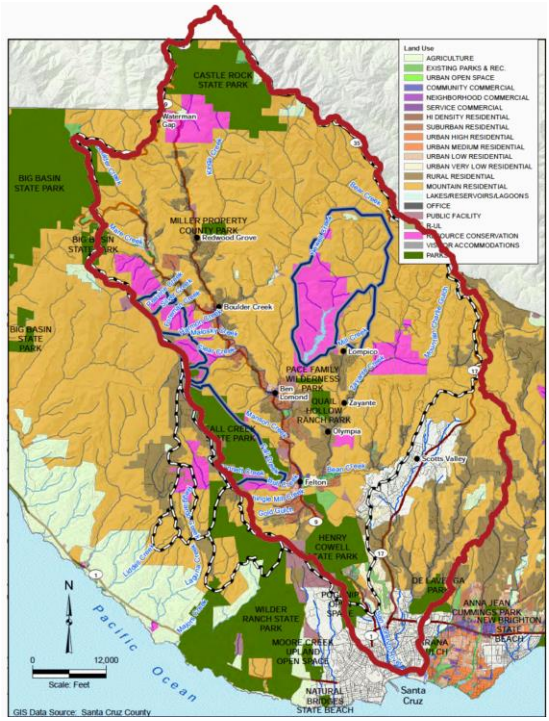

Figure III.2a

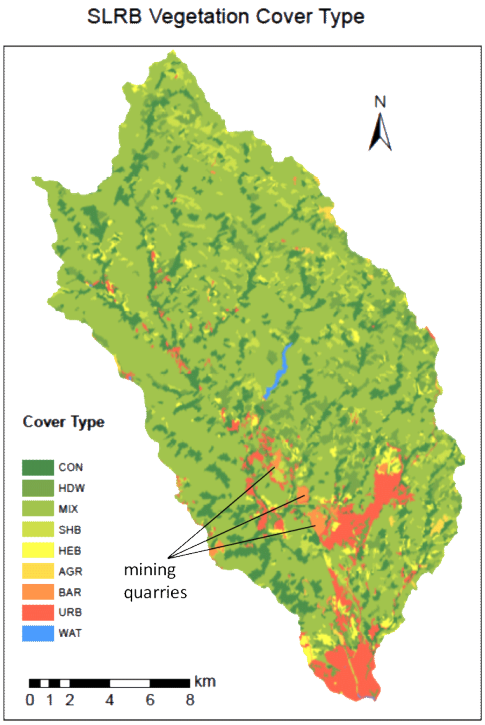

Figure III.2b

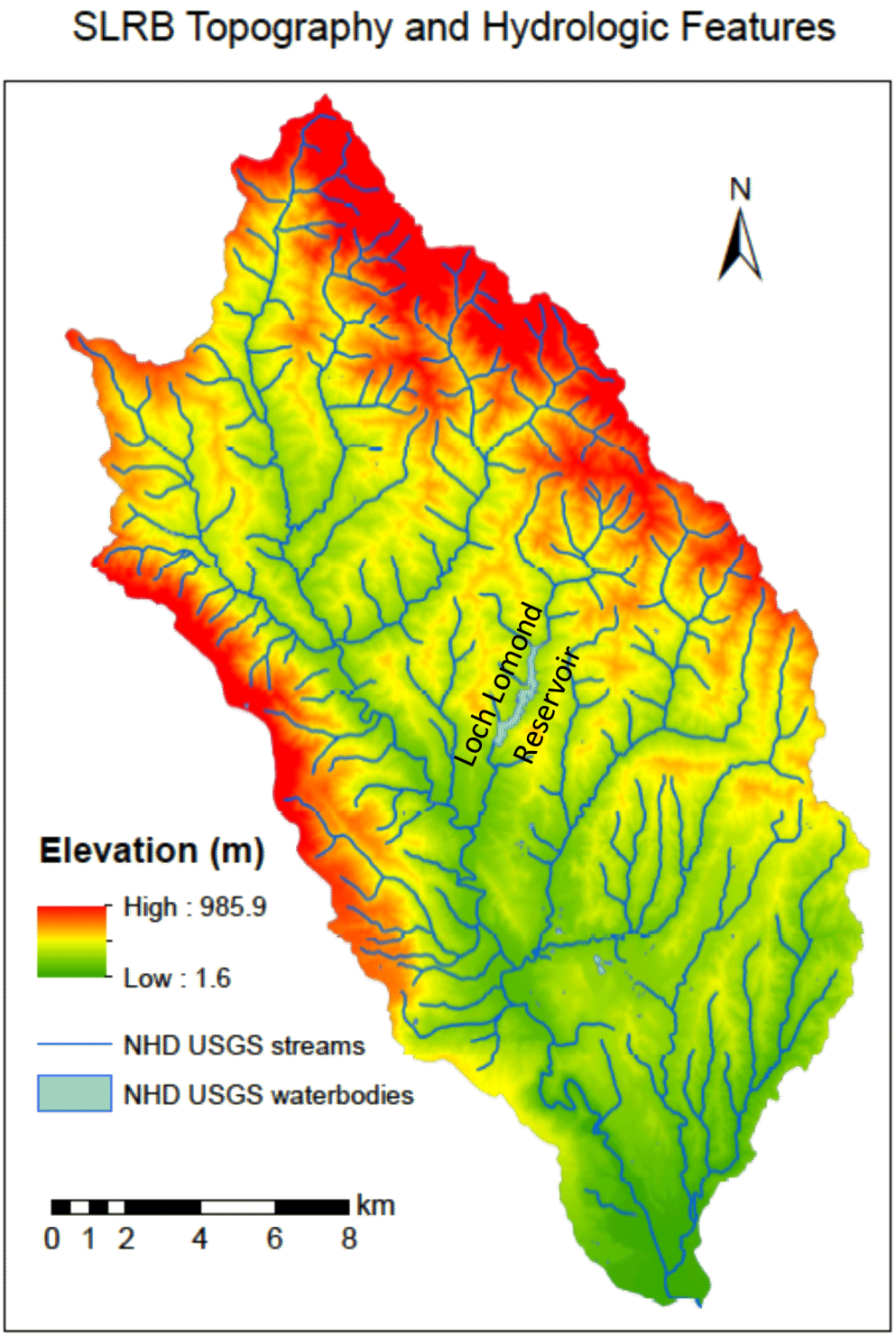
SLRB Topography and Hydrologic Features
N
Loch Lomond Reservoir
Elevation (m)
High : 985.9
Low : 1.6
NHD USGS streams
NHD USGS waterbodies
km
0 1 2 4 6 8

Figure III.3

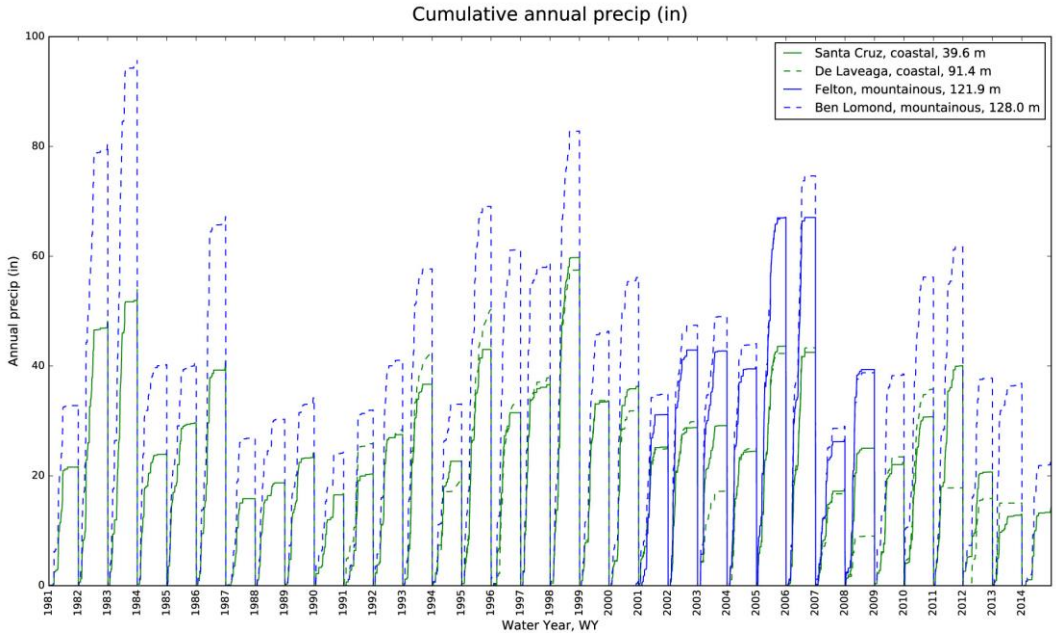

Figure III.4a

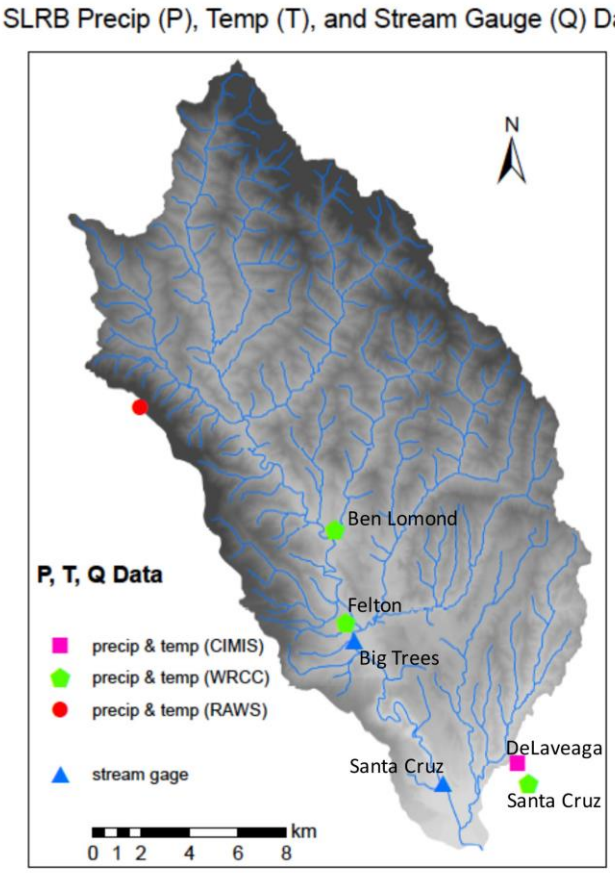

Figure III.4b

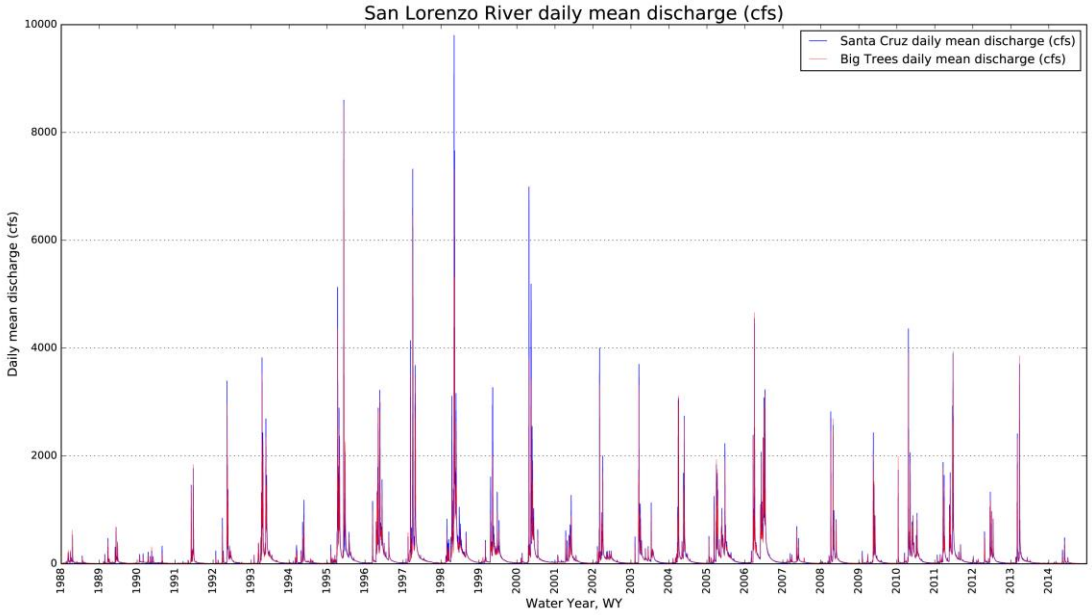

Figure III.5a

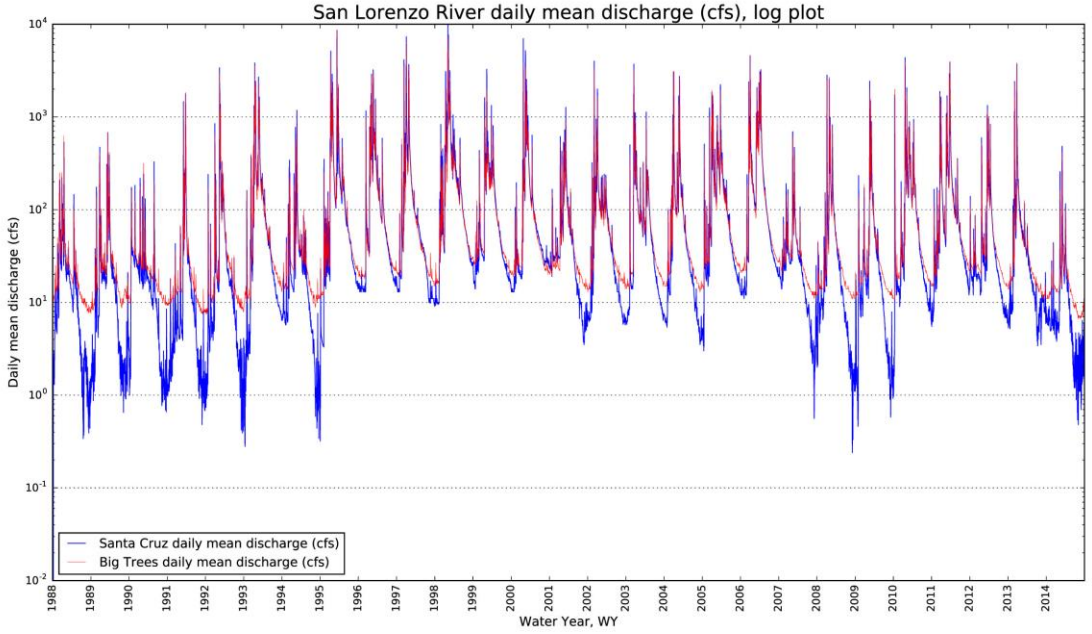

Figure III.5b

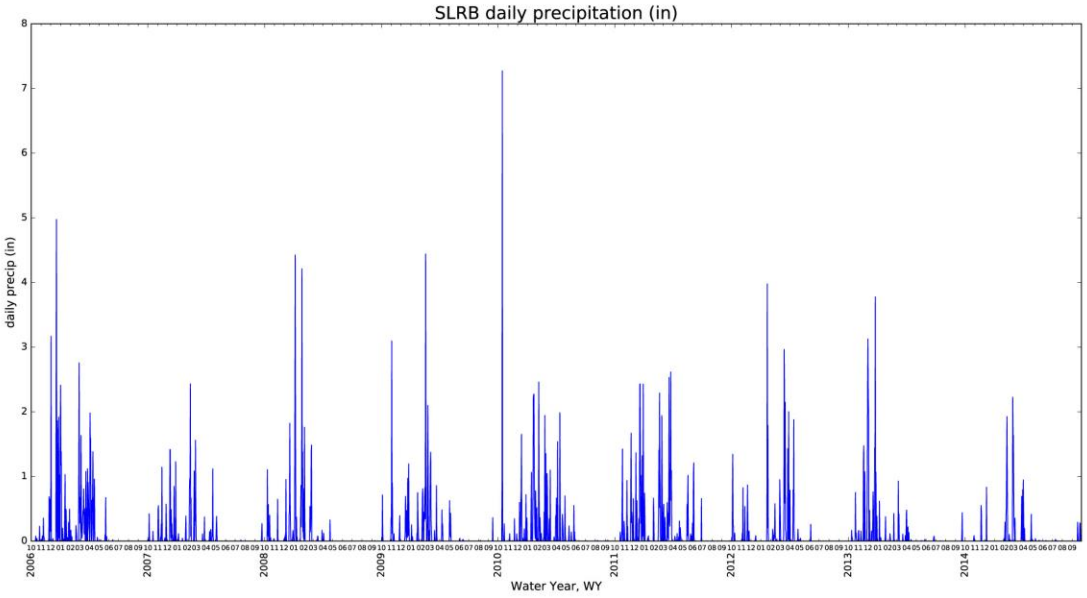

Figure III.6

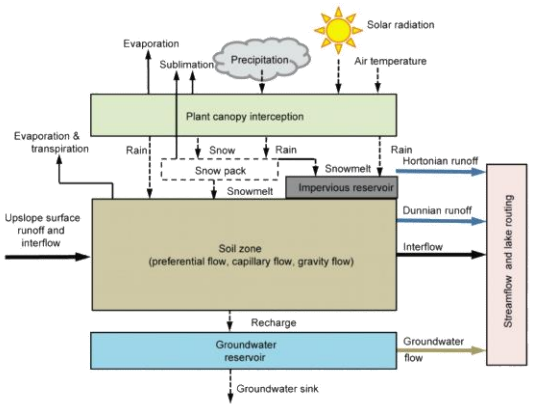

Figure IV.1a

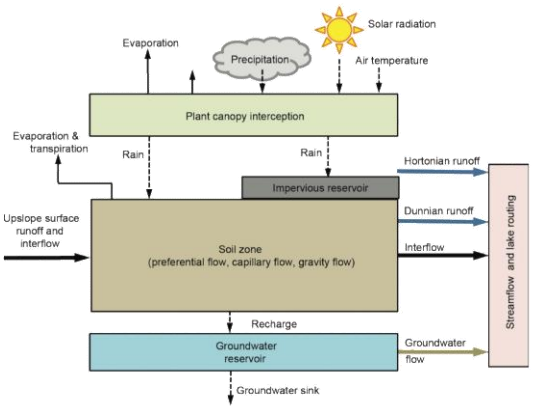

Figure IV.1b

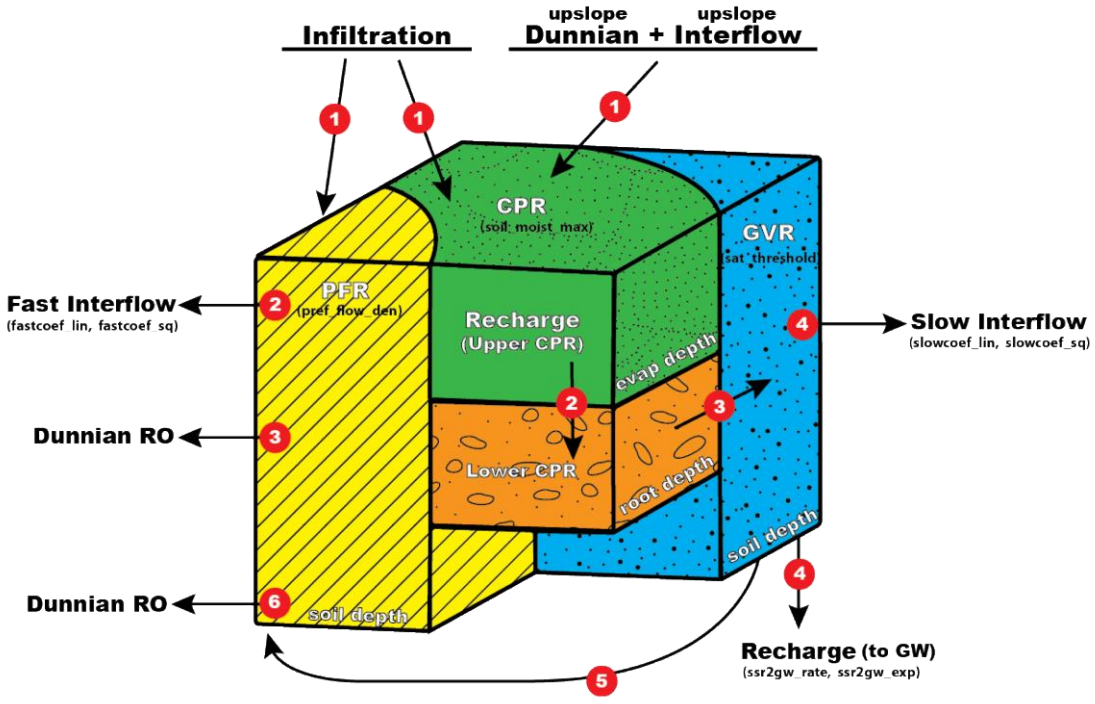

Figure IV.2

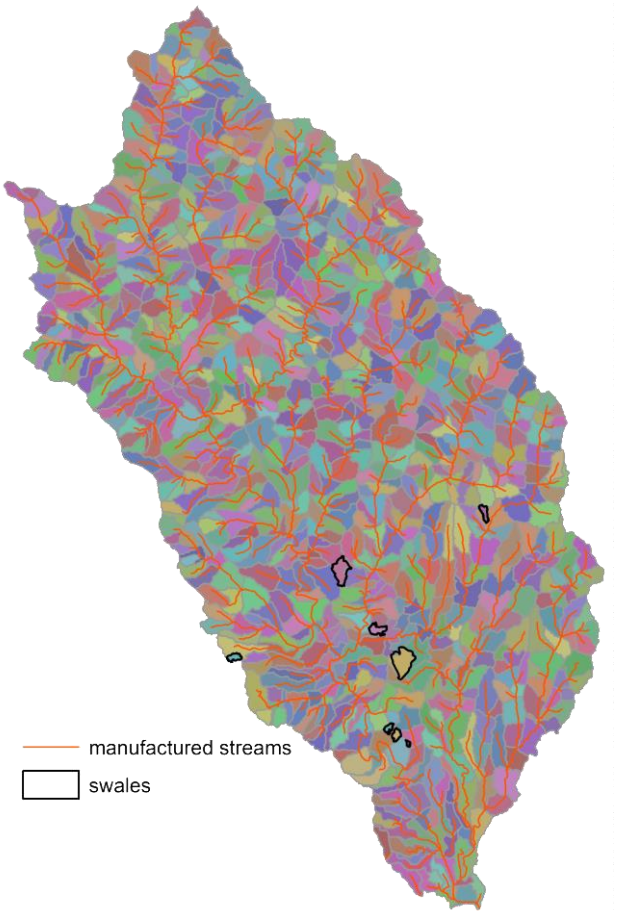

Figure IV.3

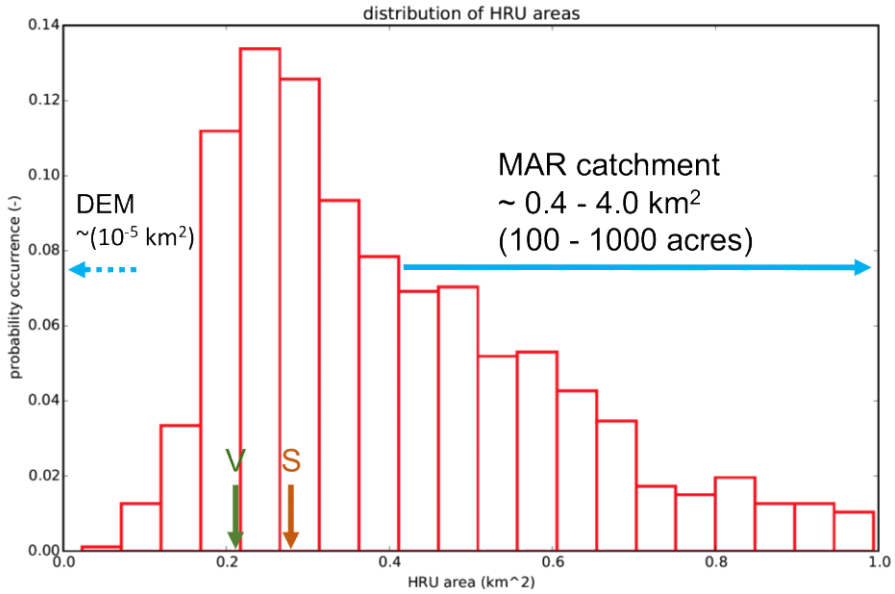

Figure IV.4

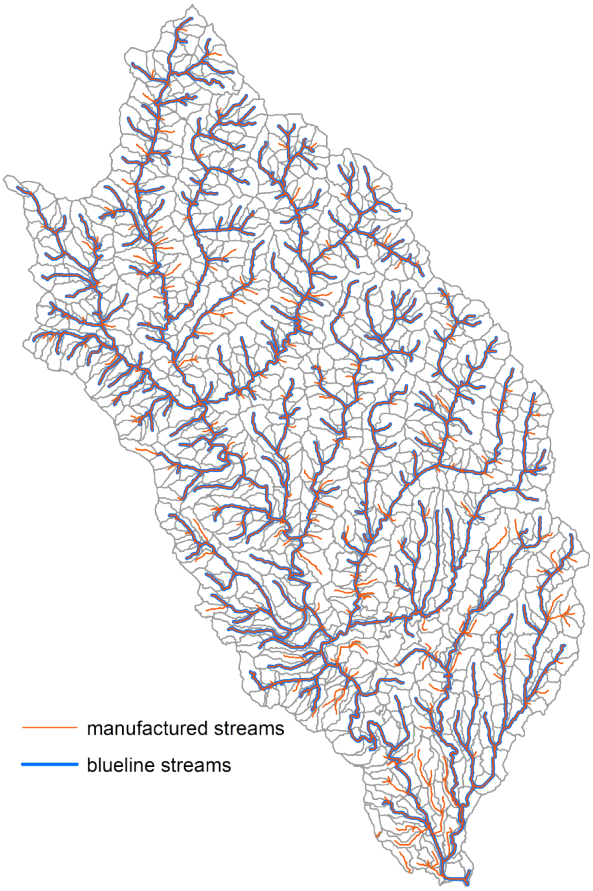

Figure IV.5

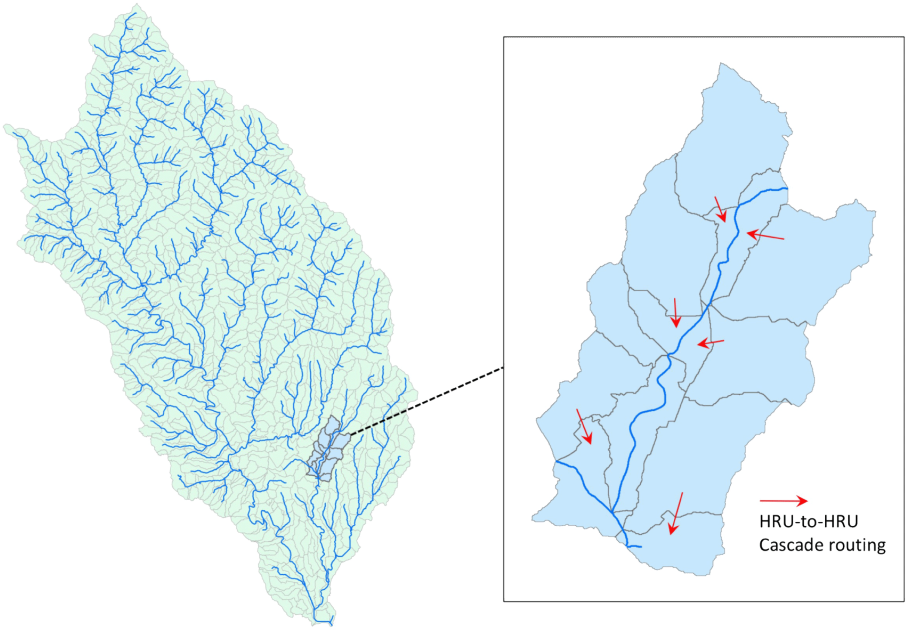

Figure IV.6

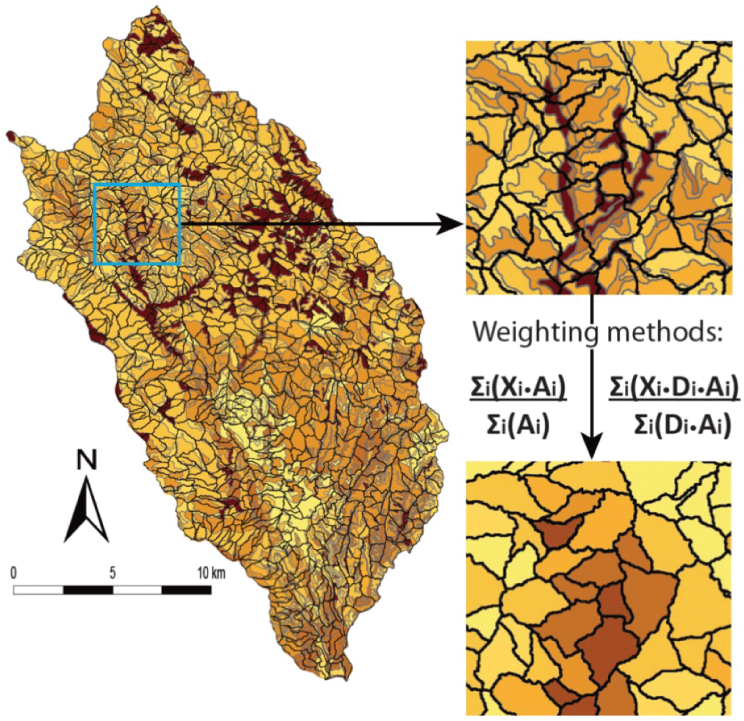

Figure IV.7a

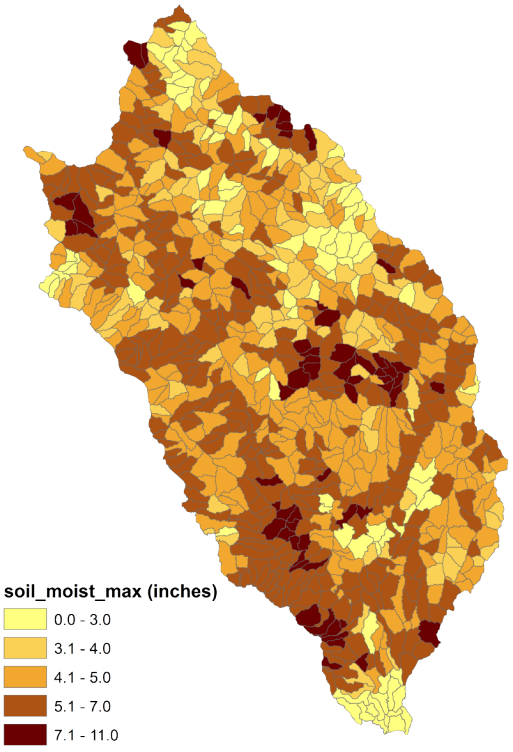

Figure IV.7b

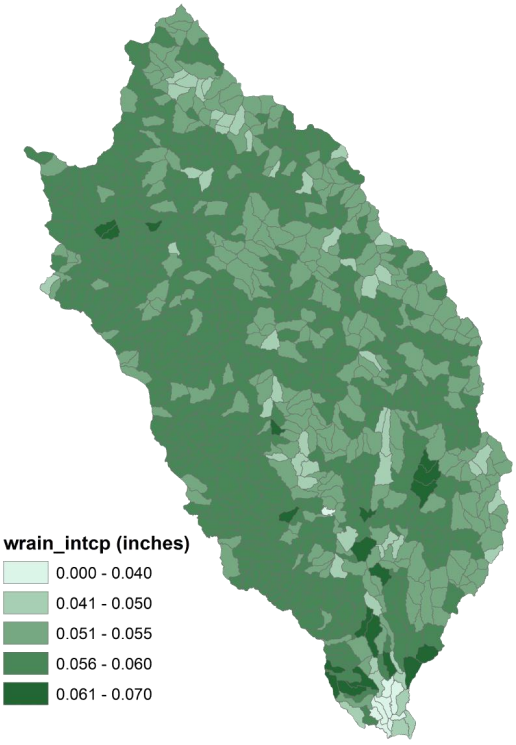

Figure IV.7c

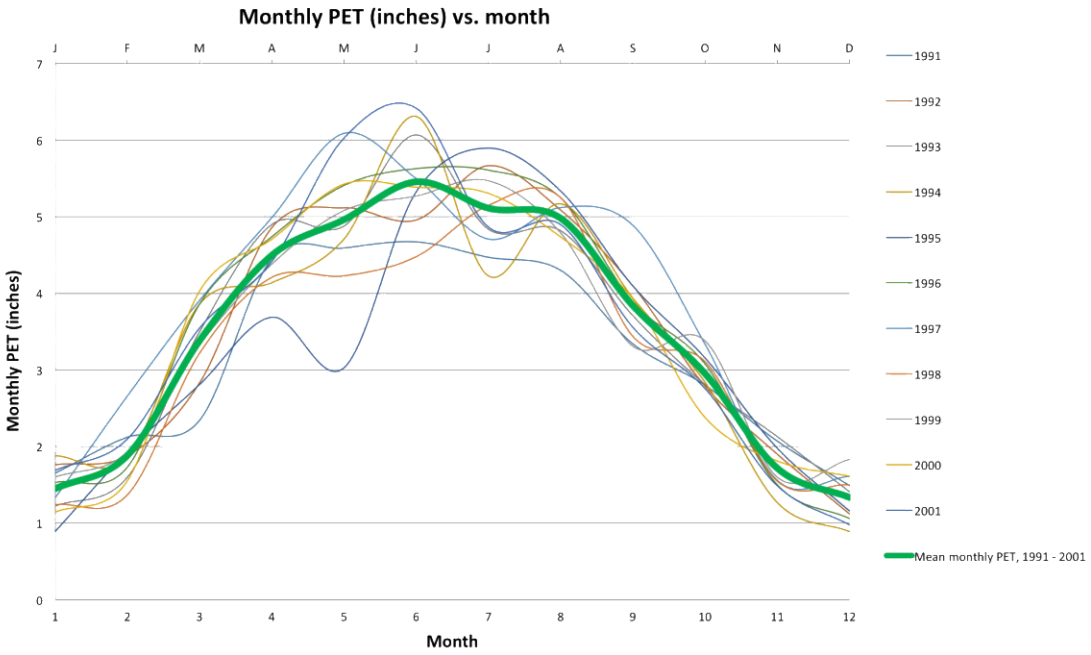

Figure IV.8a

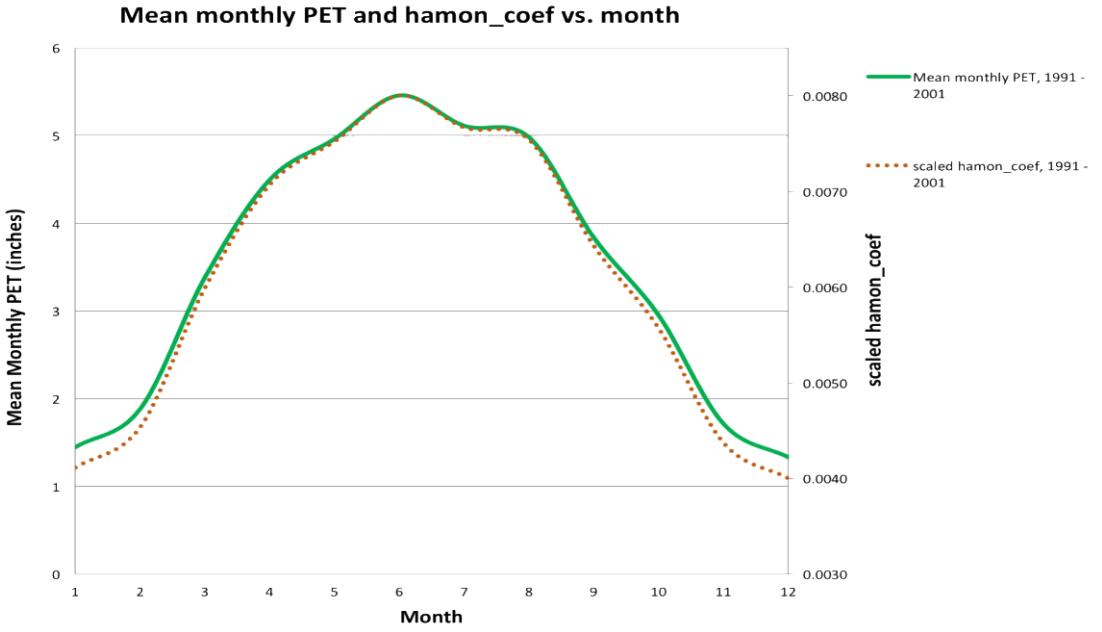

Figure IV.8b

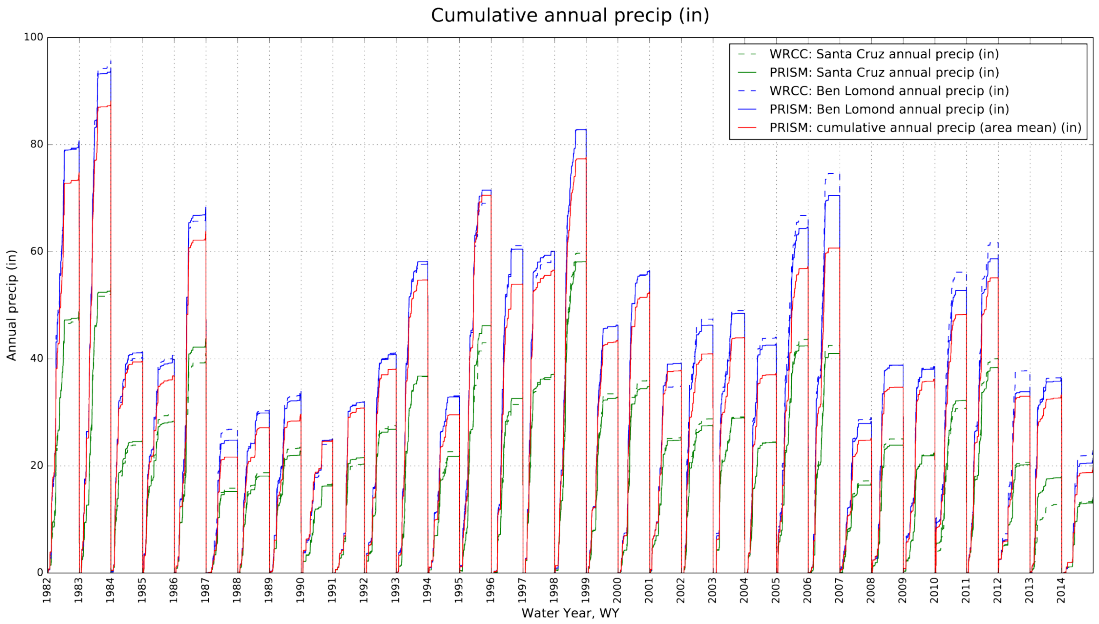

Figure IV.9a

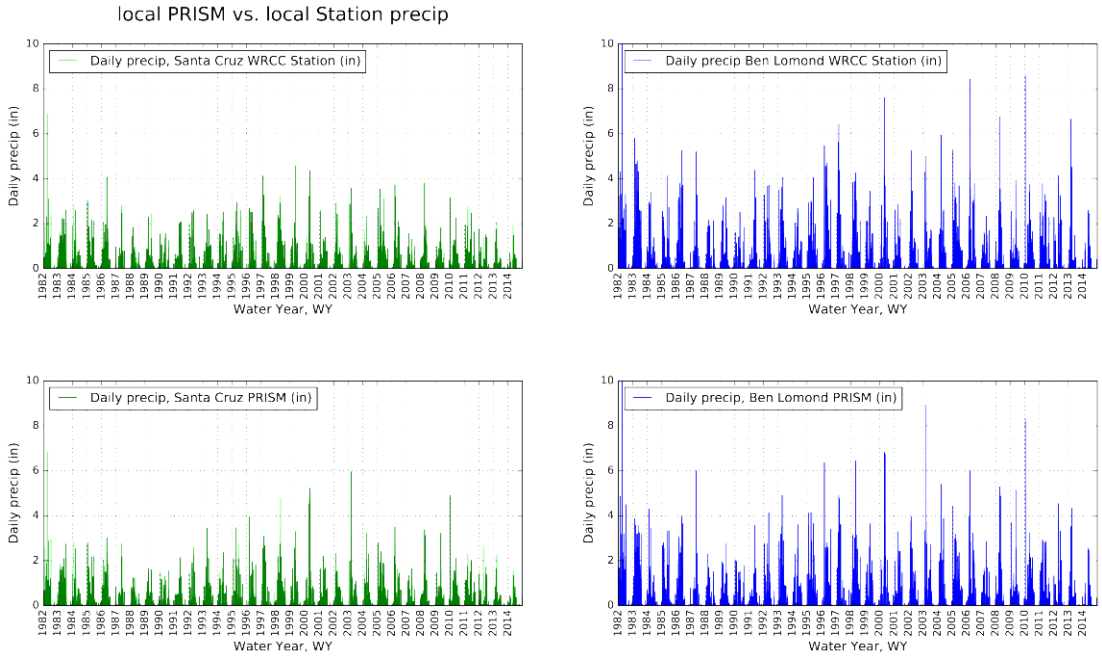

Figure IV.9b

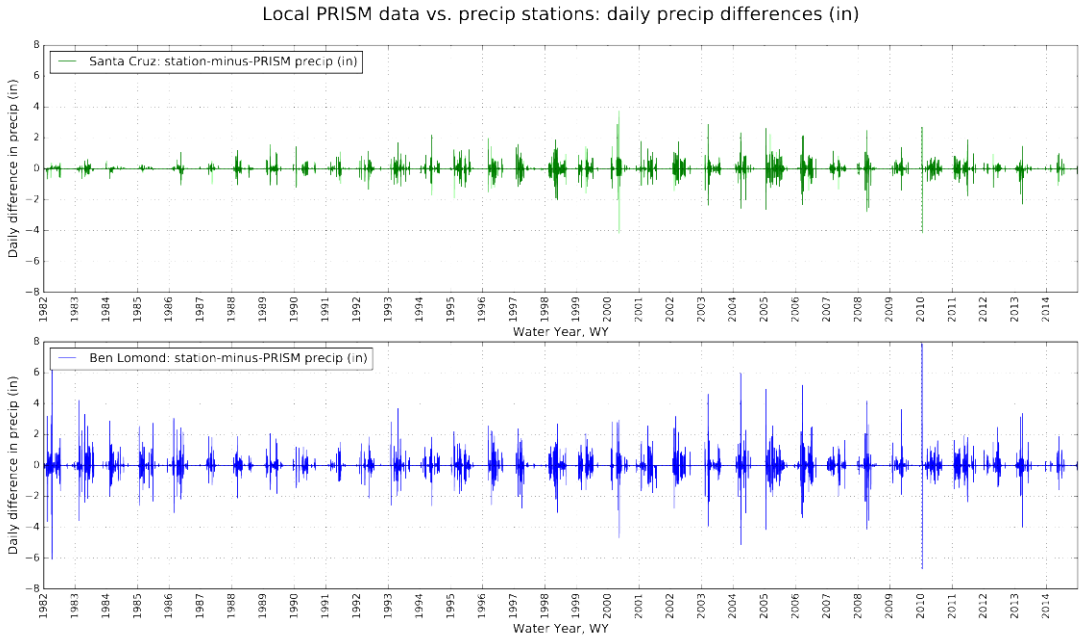

Figure IV.9c

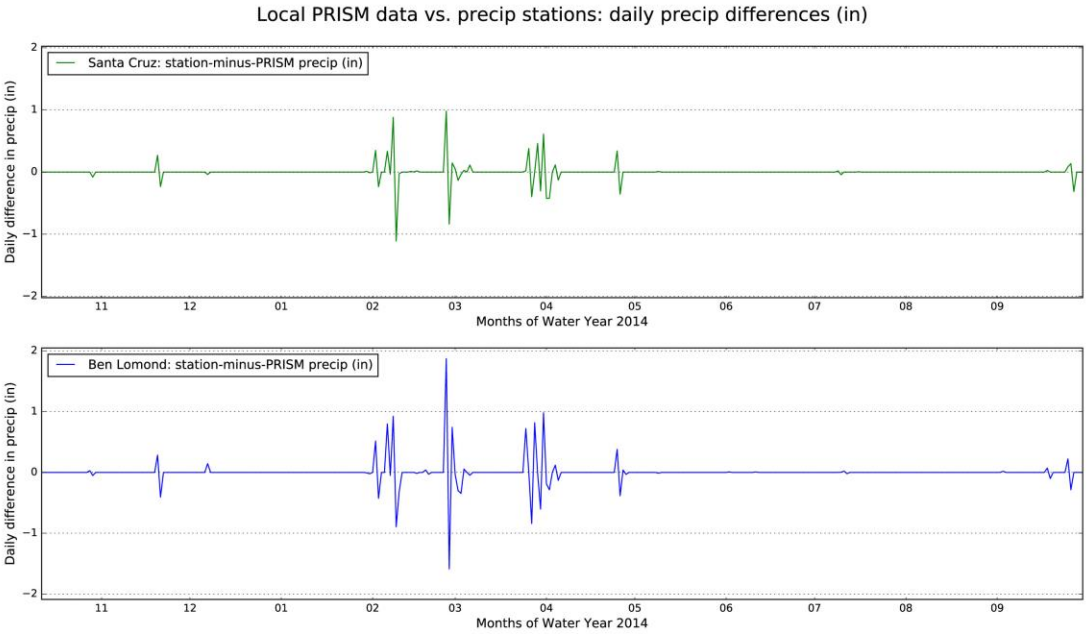

Figure IV.9d

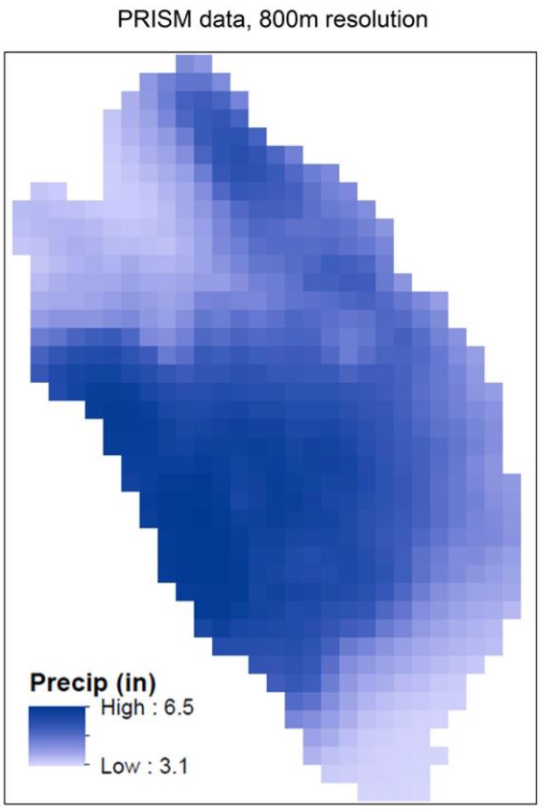

Figure IV.10a

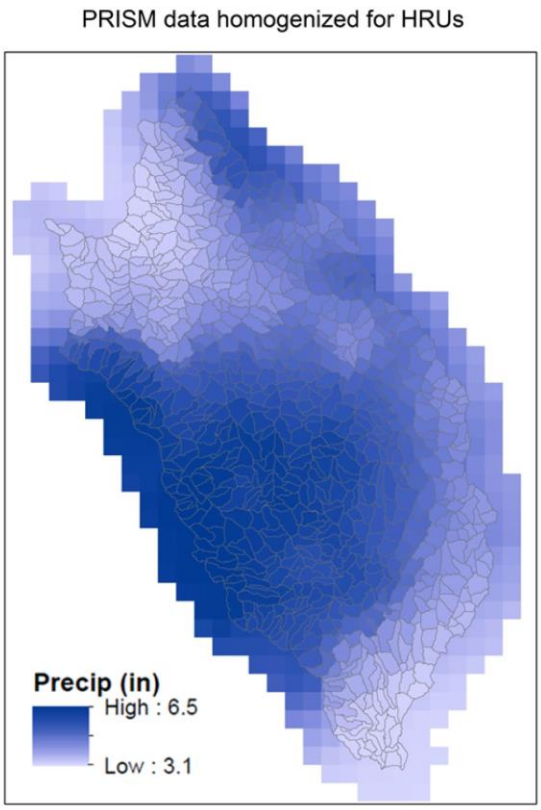

Figure IV.10b

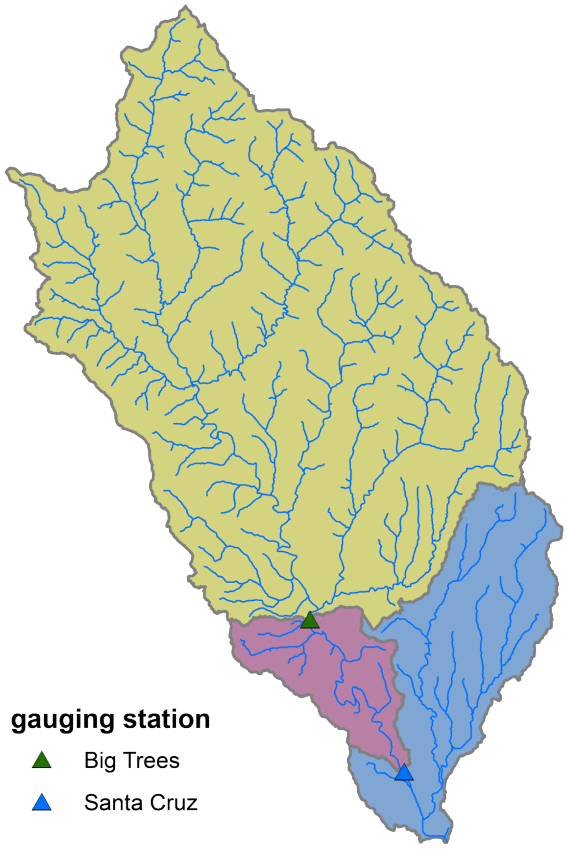

Figure IV.11

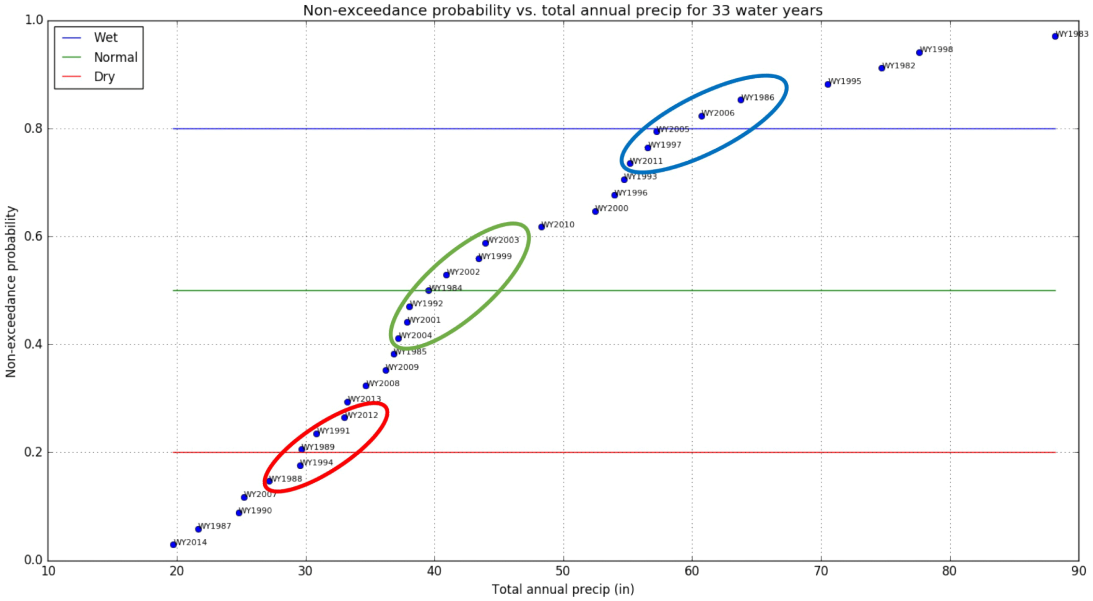

Figure IV.12

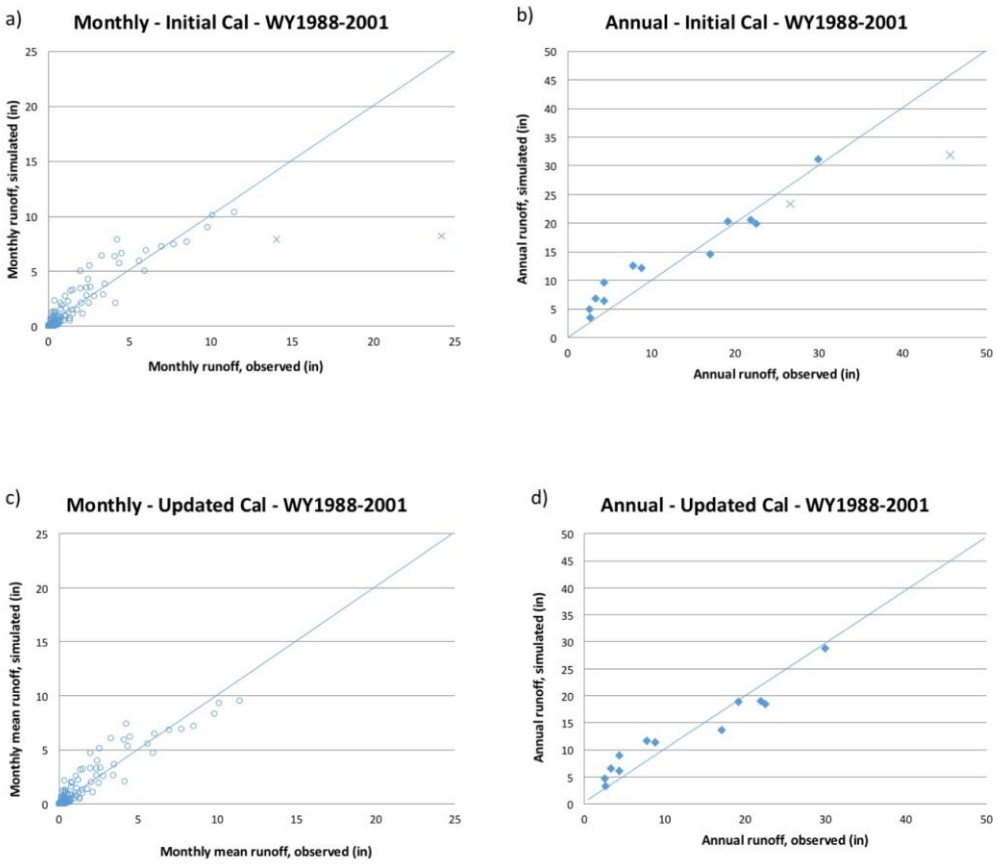

Figure V.1

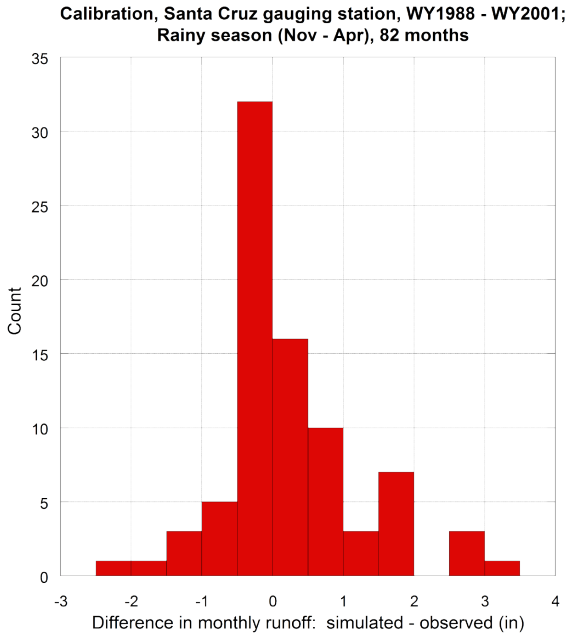

Figure V.2

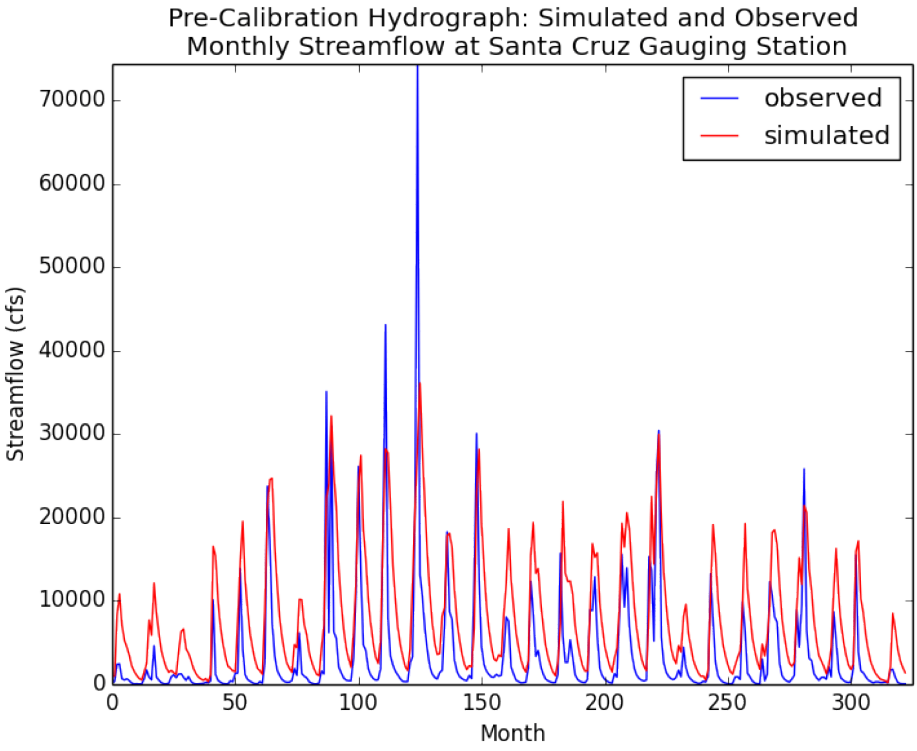

Figure V.3a

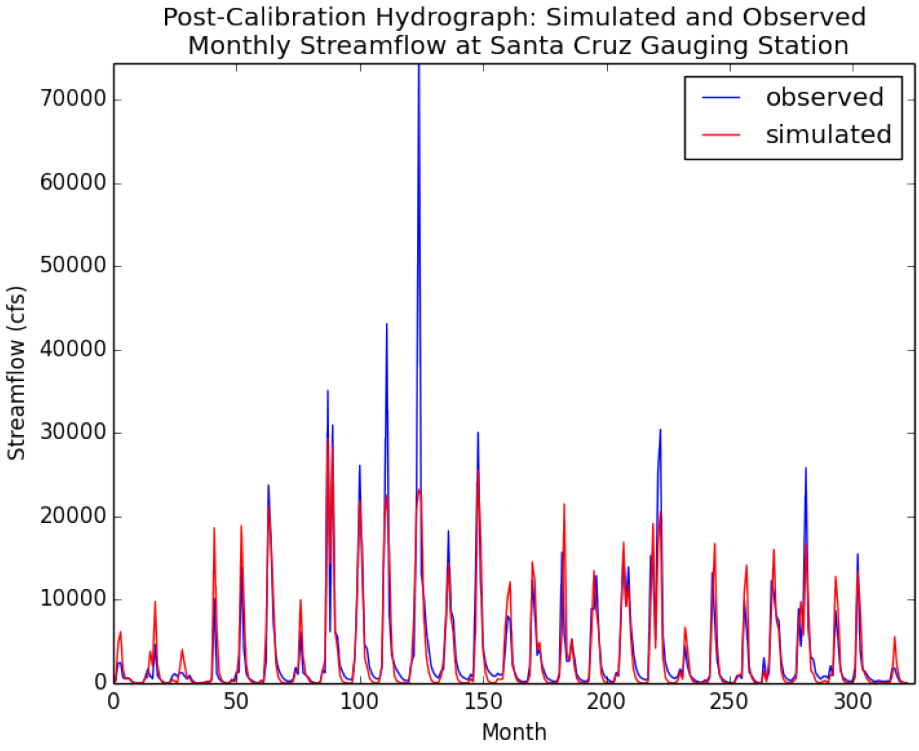

Figure V.3b

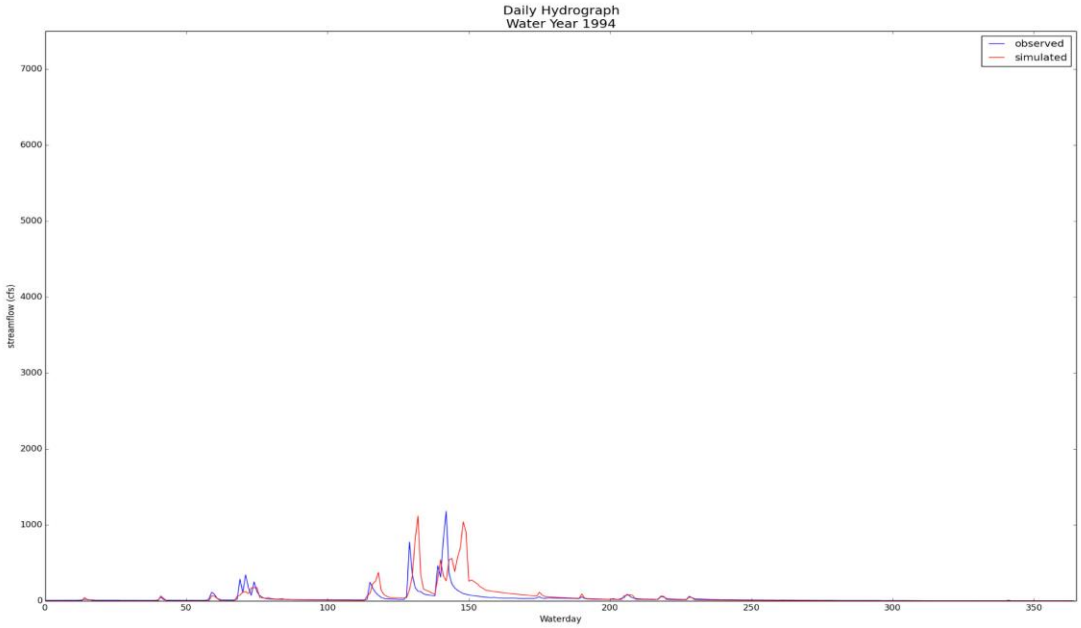

Figure V.4a

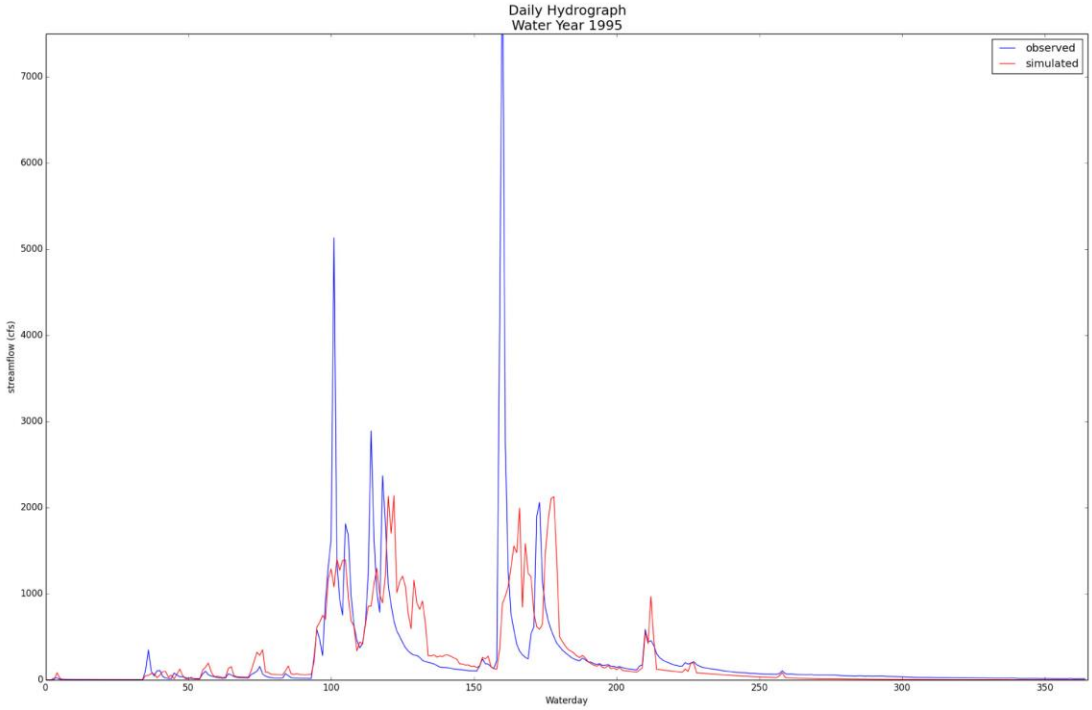

Figure V.4b

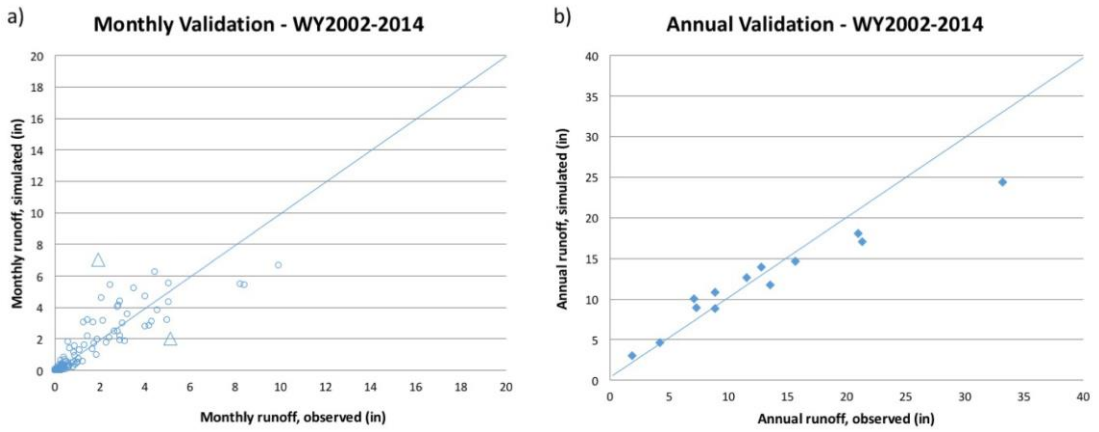

Figure V.5

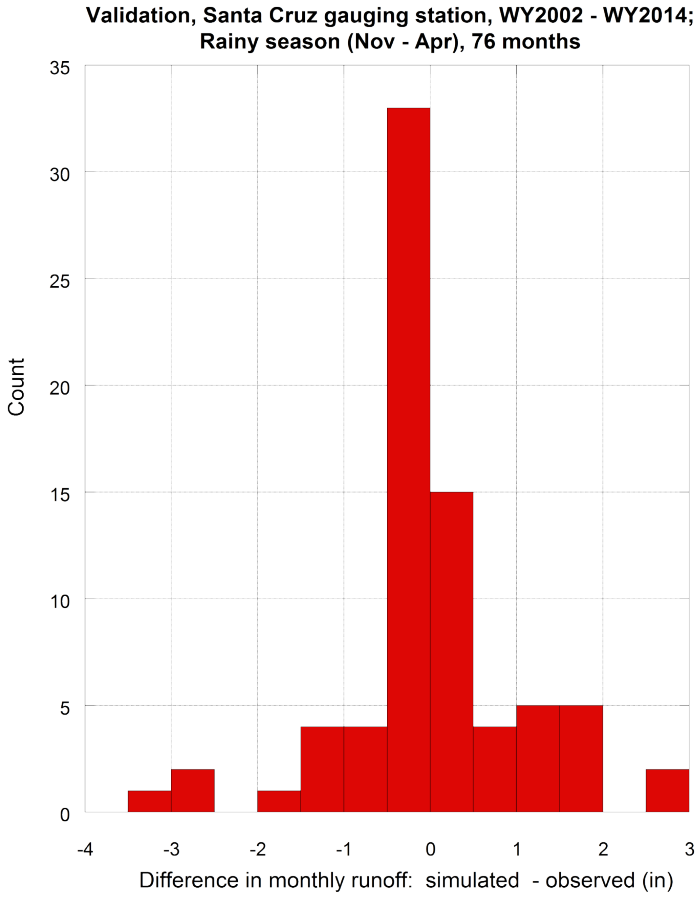

Figure V.6

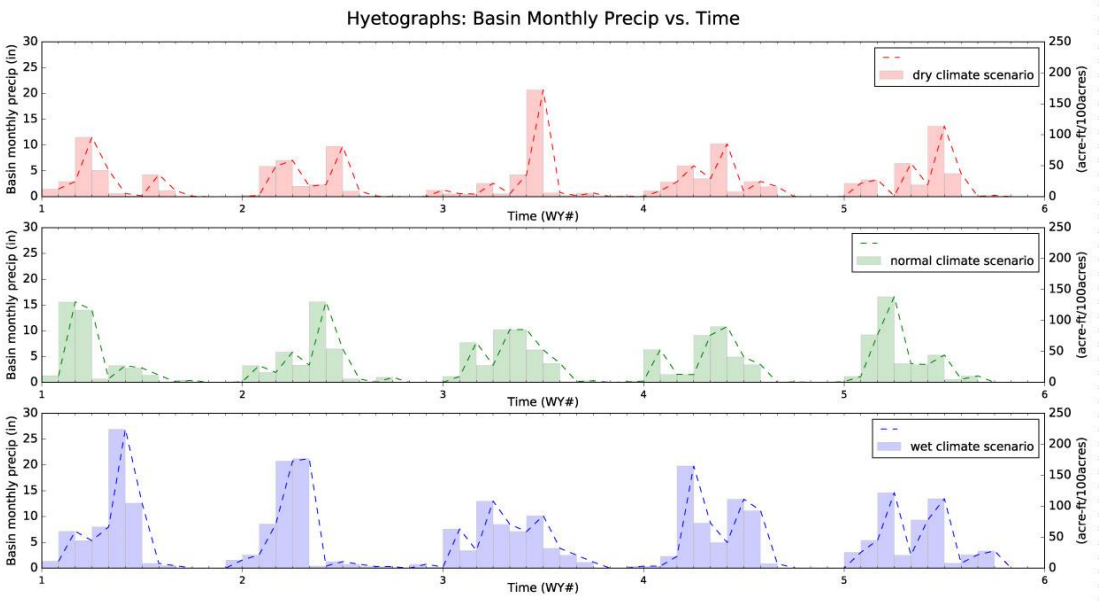

Figure V.7

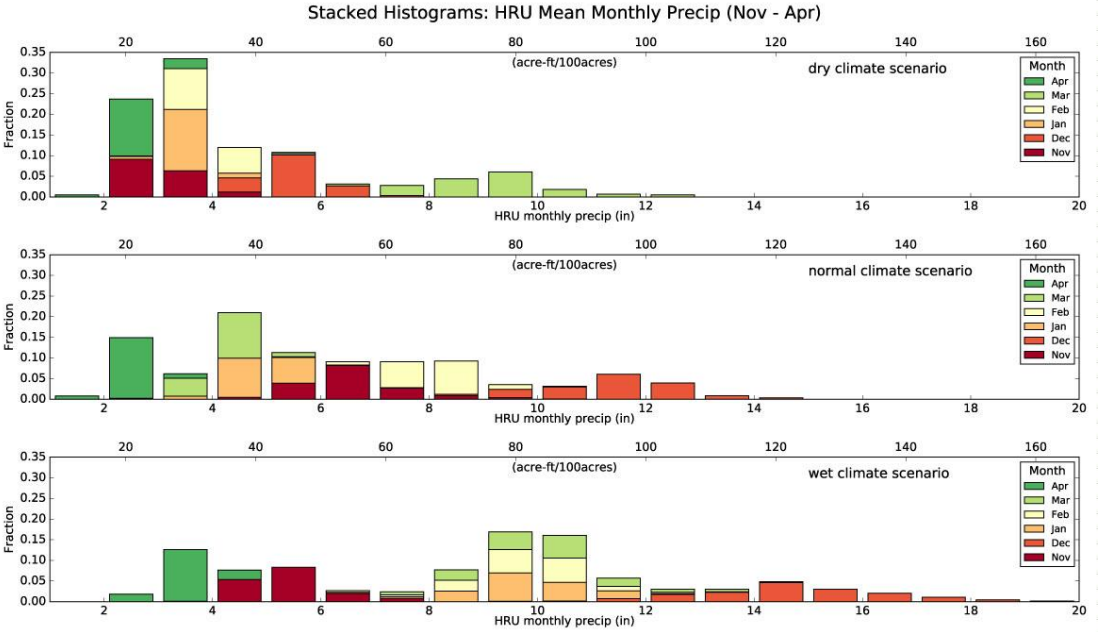

Figure V.8

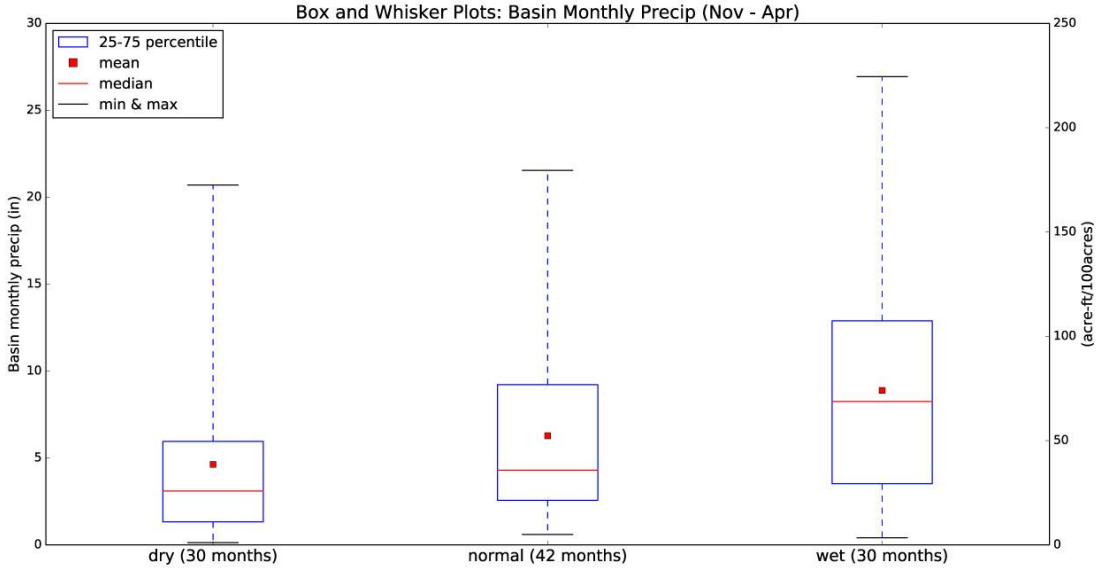

Figure V.9

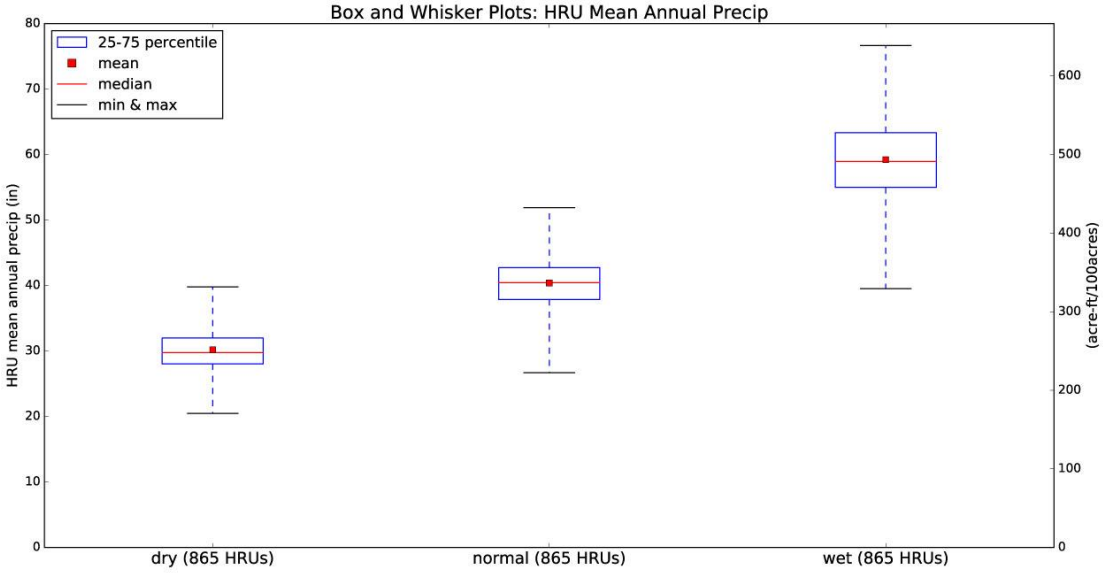

Figure V.10

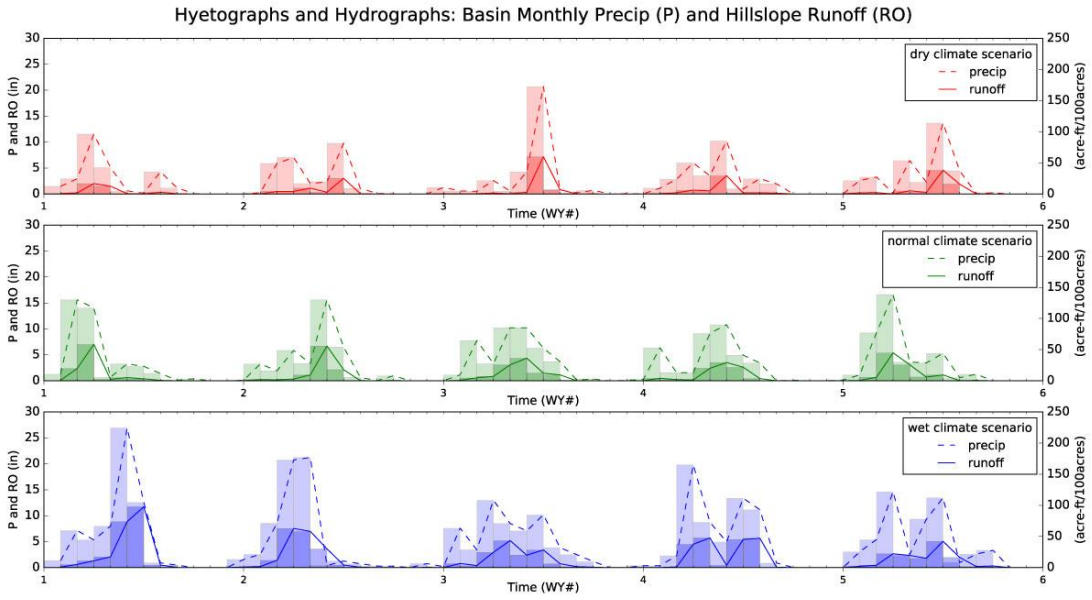

Figure V.11

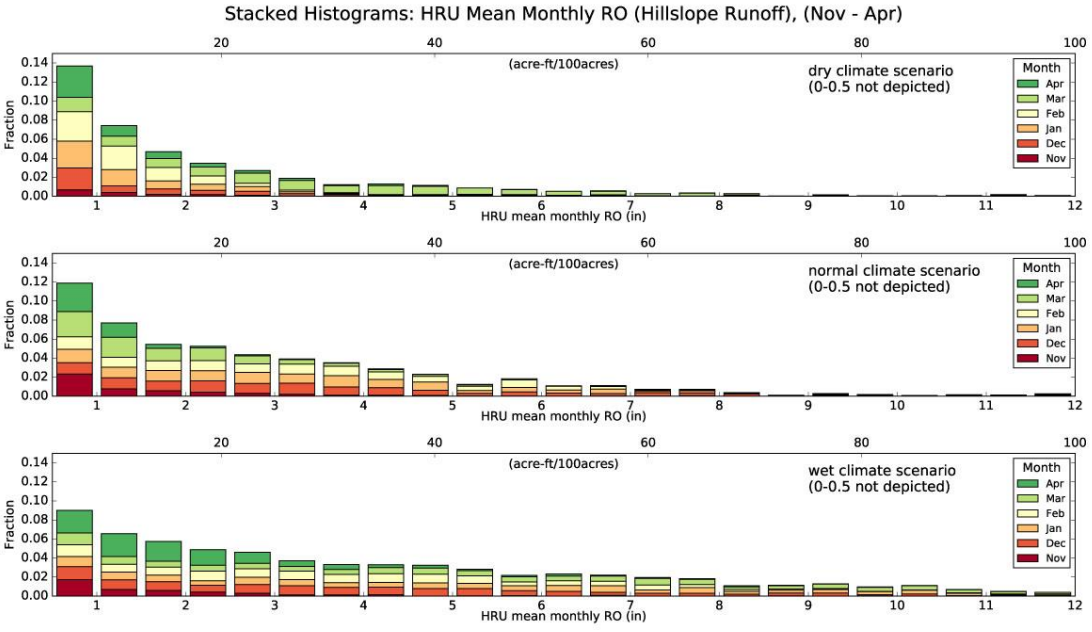

Figure V.12

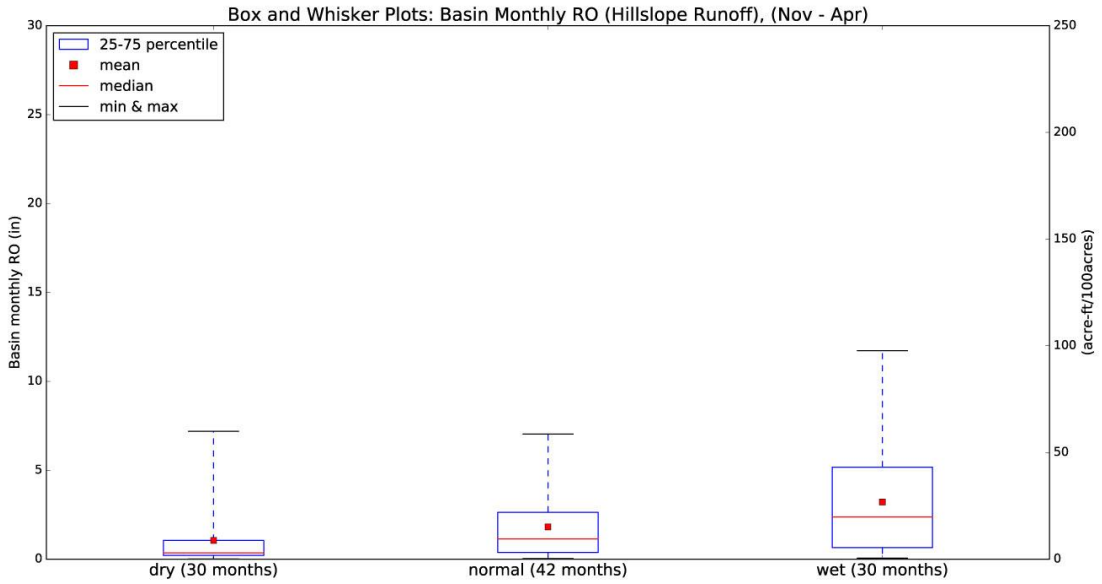

Figure V.13

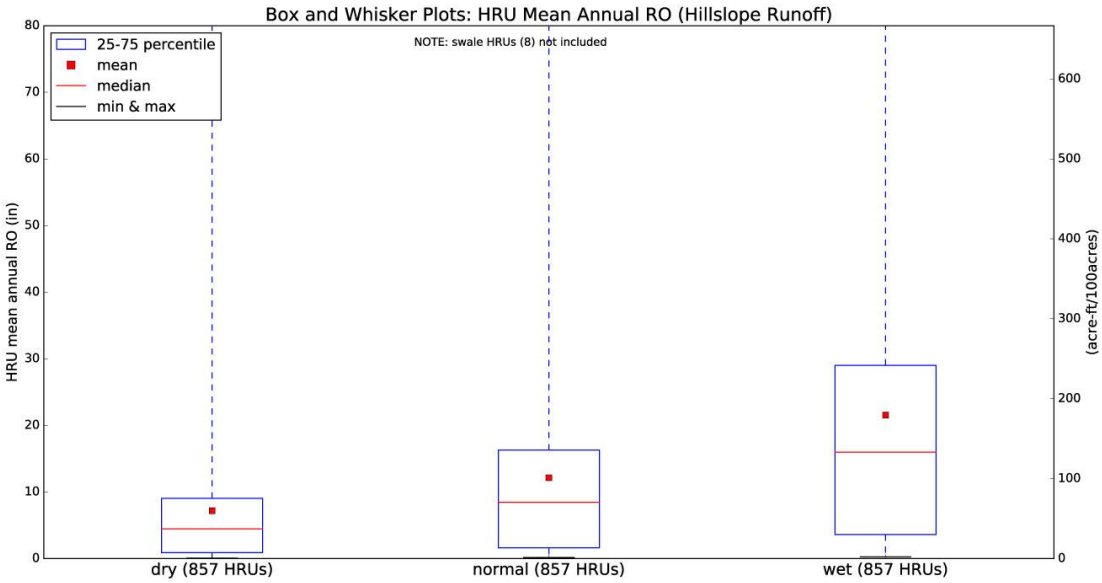

Figure V.14

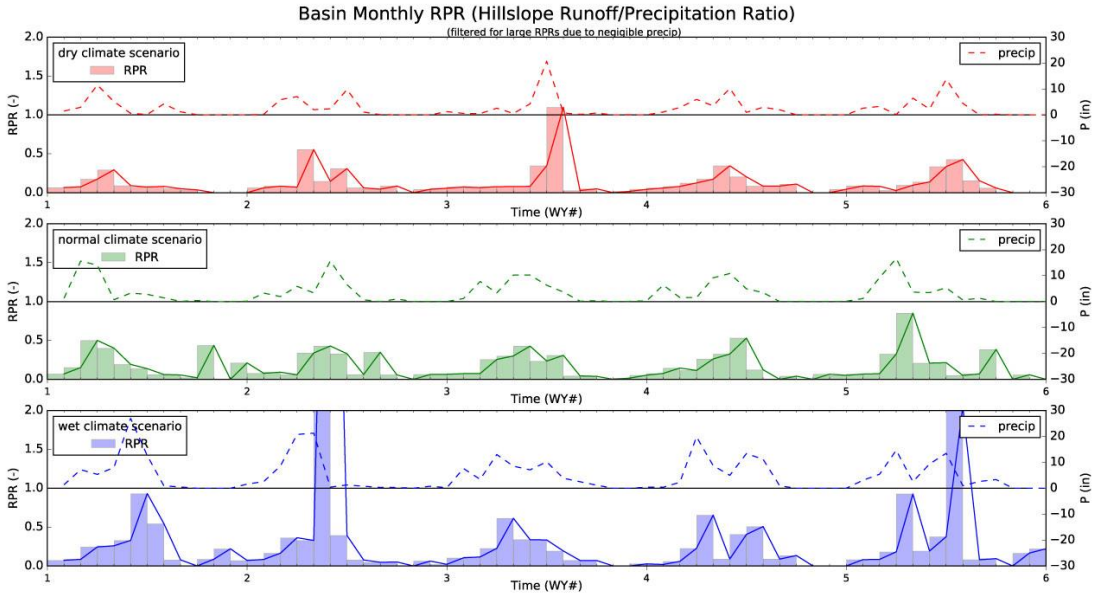

Figure V.15

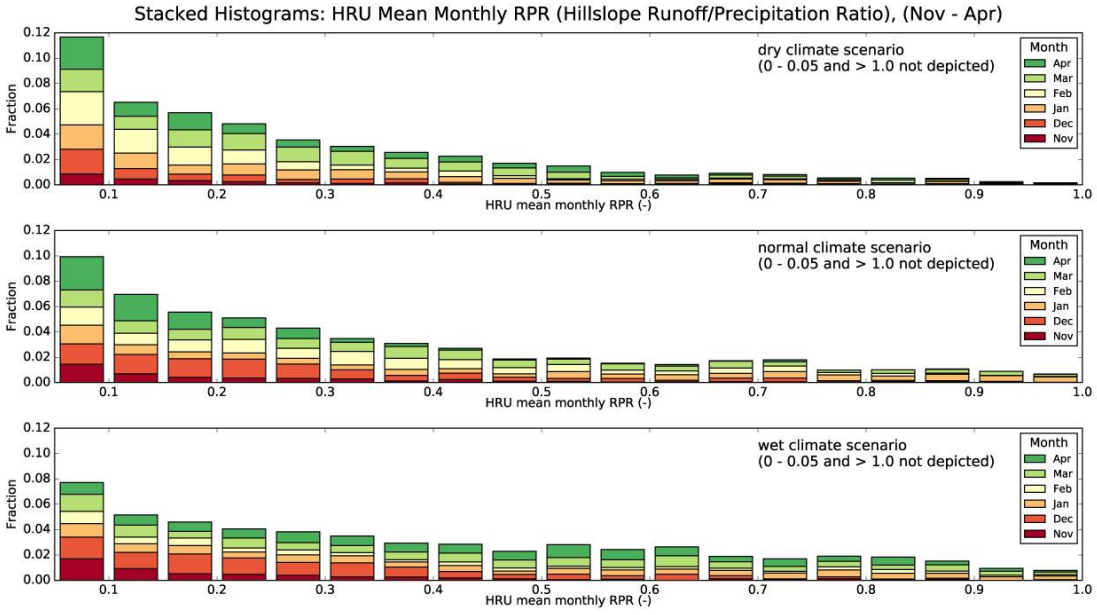

Figure V.16

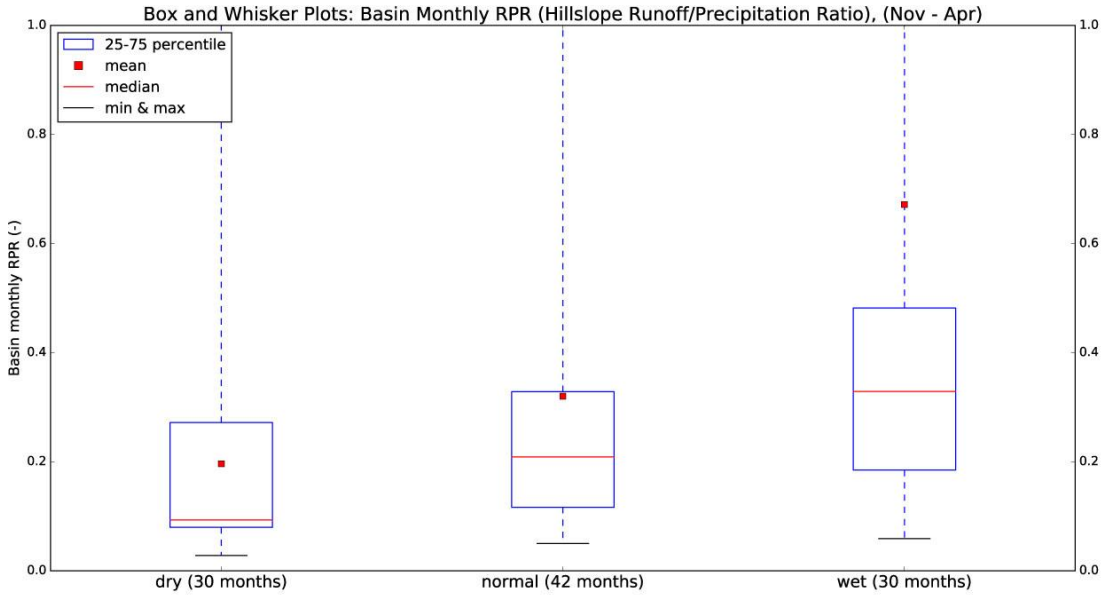

Figure V.17

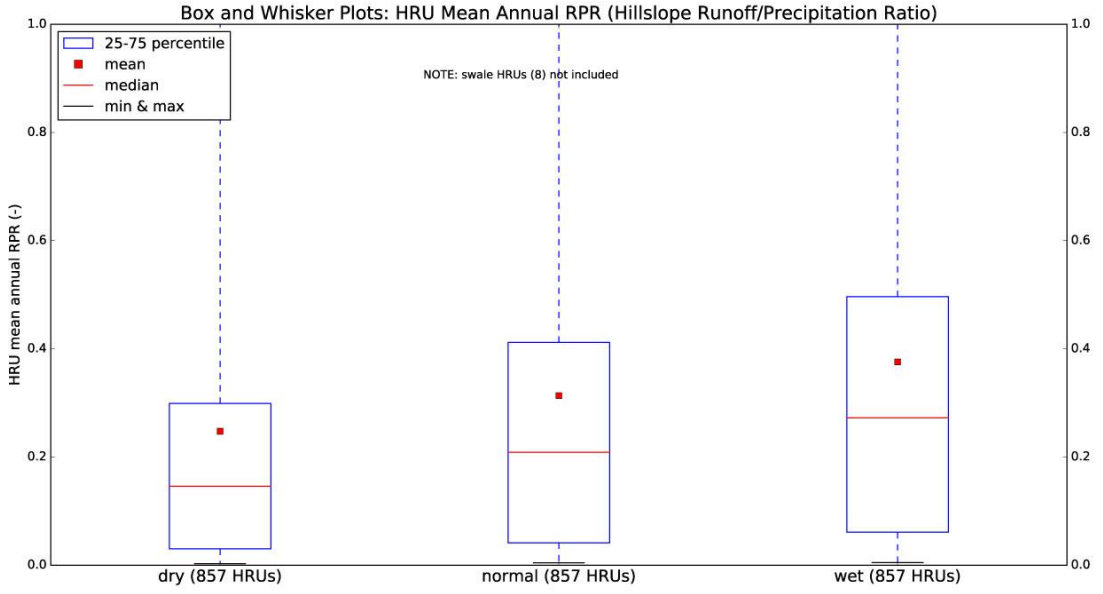

Figure V.18

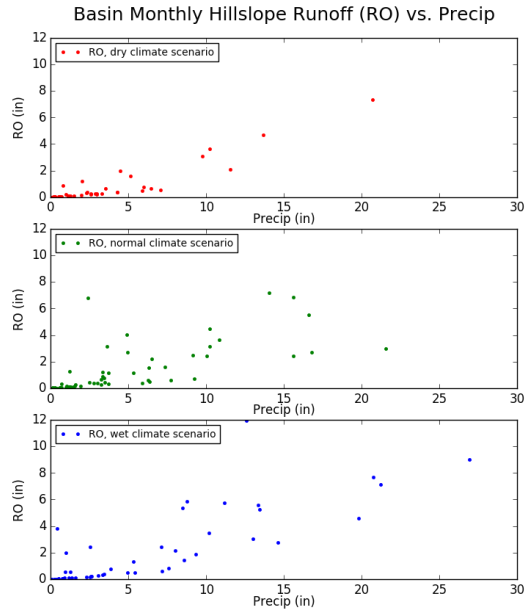

Figure V.19a

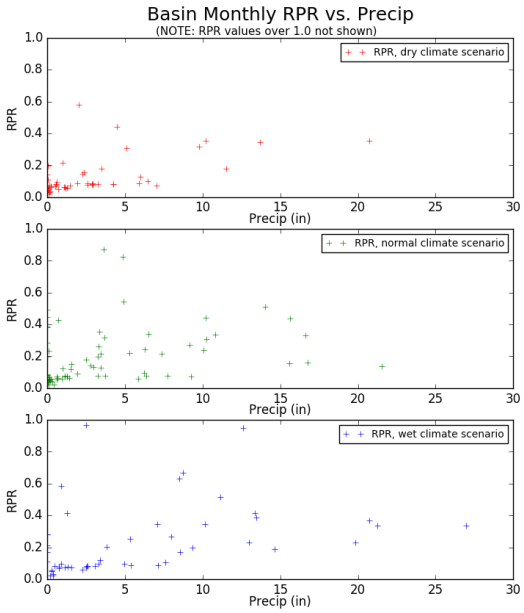

Figure V.19b

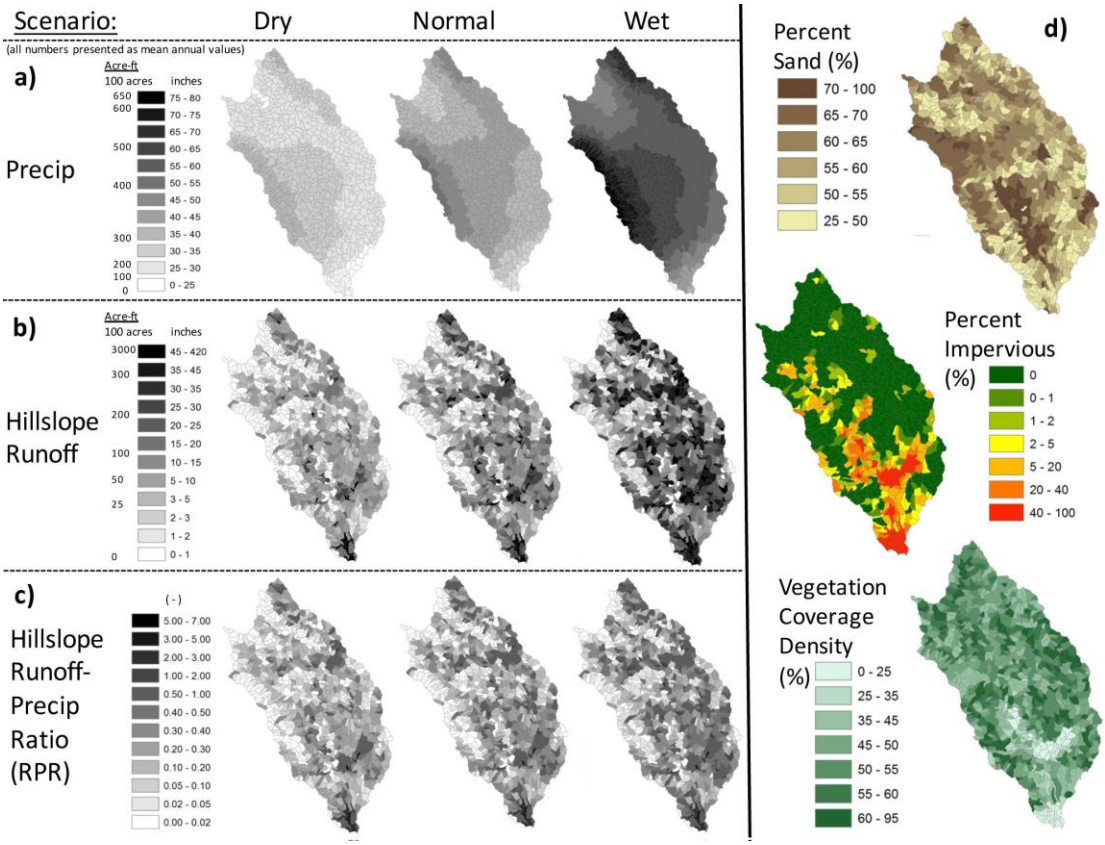

Figure V.20

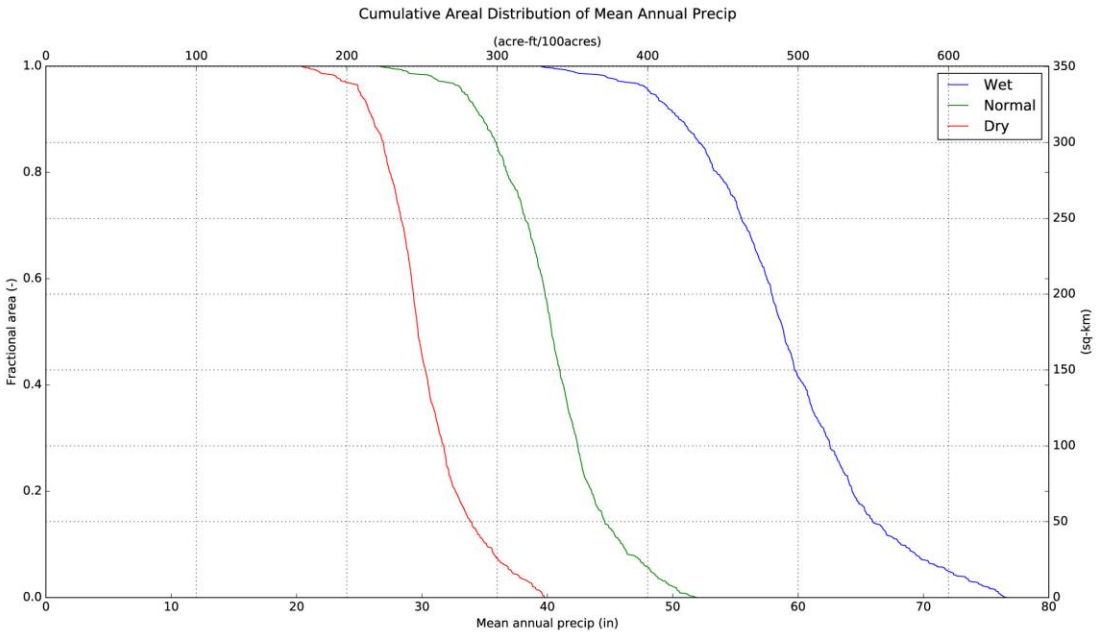

Figure VI.1

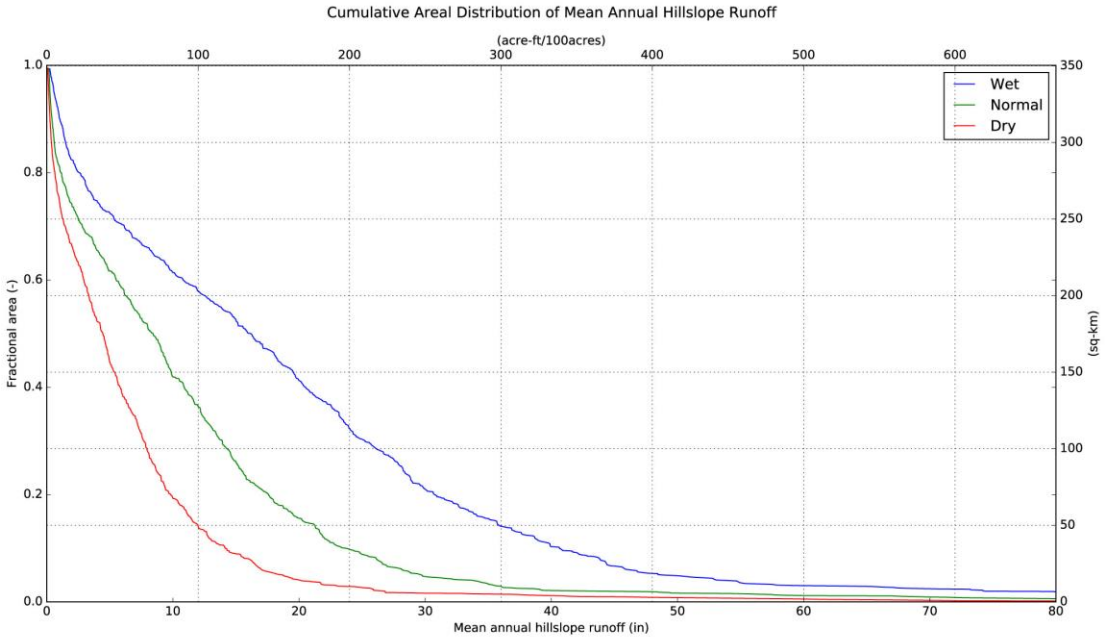

Figure VI.2

IX. Tables

Table IV.1:
PRMS Modules, Parameters and Variables:

PRMS module	*variable (in italic)* parameter (in bold)	units	value(s)
basic physical attributes (various modules)	**hru_area**	acres; (sq km)	5.7 - 245.7; (0.02 - 1.0)
	hru_aspect	degrees	49 - 262
	hru_elev	meters	4 - 839
	hru_lat	degrees North	36.97 - 37.22
	hru_slope	decimal fraction	0.03 - 0.72
	hru_type	-	0, 1, 3
strmflow - muskingum	**hru_segment**	-	0 - 859
	K_coef	hours	0.01
	obsin_segment	-	0
	segment_flow_init	-	0.0
	segment_type	-	0, 2
	tosegment	-	0 - 859
	x_coef	decimal fraction	1.0
subbasin	**hru_subbasin**	-	1 - 3
	subbasin_down	-	0 , 2, 3
cascade	**cascade_flg**	-	1
	cascade_tol	acres	0.0
	hru_down_id	-	0 - 859
	hru_pct_up	decimal fraction	1.0
	hru_strmseg_down_id	-	0 - 859
	hru_up_id	-	1 - 867
cascadegw	**gw_down_id**	-	0 - 859
	gw_pct_up	decimal fraction	1.0
	gw_strmseg_down_id	-	0 - 859
	gw_up_id	-	1 - 867
gwflow	**gwflow_coef**	fraction/day	0.015
	gwsink_coef	fraction/day	0.035
	gwstor_init	inches	10.0
	gwstor_min	inches	0.0
soilzone	**fastcoef_lin**	fraction/day	0.001
	fastcoef_sq	-	0.001
	slowcoef_lin	fraction/day	0.001
	slowcoef_sq	-	0.001
	ssr2gw_rate	fraction/day	0.01 - 0.41
	ssr2gw_exp	-	2.0
	soil2gw_max	inches	0.0
	soil_rechr_init	inches	0.0
	soil_rechr_max	inches	0.041 - 0.098
	soil_moist_init	inches	0.0
	soil_moist_max	inches	0.11 - 20.95
	pref_flow_den	decimal fraction	0.0
	sat_threshold	inches	0.41 - 33.16
	ssstor_init	inches	0.0
	soil_type	-	1 - 3
transp - tindex	**transp_beg**	month of calendar year	1
	transp_end	month of calendar year	13
	transp_tmax	degrees Celsius	0.0
	potet_sublim	decimal fraction	0.5
	rad_trncf	decimal fraction	0.5
srunoff - smidx	**smidx_coef**	decimal fraction	0.06
	smidx_exp	1/inch	0.5
	hru_percent_imperv	decimal fraction	0.0 - 1.0
	imperv_stor_max	inches	0.05
intcp	**cov_type**	-	0 - 4
	covden_sum	decimal fraction	0.0 - 0.90
	covden_win	decimal fraction	0.0 - 0.90
	srain_intcp	inches	0.0 - 0.067
	wrain_intcp	inches	0.0 - 0.067
et - potet_hamon	**hamon_coef**	-	0.004 - 0.008
soltab	(**hru_lat, hru_aspect, hru_slope**; refer to "basic physical attributes")	-	-
temp - climate_hru	*tmax*	degrees Celsius	varies
	tmin	degrees Celsius	varies
precip - climate_hru	*precip*	inches	varies
	adjmix_rain	decimal fraction	1.0
-	*runoff*	cfs	varies

Table IV.2:

Parameter Input Data by Vegetation and Soil Type

	vegetation type:					
input data:	bare	grasses	shrubs	deciduous	coniferous	reference(s):
rooting depth (in)	0	50	79	87	117	Schenk & Jackson, 2002; Canadell et al., 1996
coverage density (fraction)	0	100	55	35	35	CALVEG, 2014
binary imperviousness (fraction)	1	0	0	0.0000	0	Viger et al., 2010
interception storage (in)	0	0.0672	0.0361	0.0490	0.0573	Crouse et al., 1966; Couturier & Ripley, 1973; Garcia-Estringana et al., 2010; Fathizadeh et al., 2013; Klaasen et al., 1998; Reid & Lewis, 2009

	soil type:			
input data:	sand	loam	clay	reference(s):
n (fraction)	0.35	0.45	0.5	Fetter, 2001
FC (fraction)	0.15	0.3	0.4	Fetter, 2001
evaporation depth (in)	0.59	0.59	0.59	Heitman et al., 2008
%-sand (%)	> 50	< 50	< 50	Soil Survey Staff, 2014
%-clay (%)	< 50	< 40	> 40	Soil Survey Staff, 2014
AWC (fraction)	0.07 - 0.15	0.05 - 0.19	0.10 - 0.20	Soil Survey Staff, 2014
soil IC (in/day)	3.6 - 578	0.0 - 61.4	0.0 - 25.6	Soil Survey Staff, 2014

Table IV.3:

Calibration and Validation Summary

CALIBRATION:			Monthly Cal (6 mo, Nov - Apr)		Annual Cal:	
Location:	WaterYears:	Description:	# months:	NRMSD:	# years:	NRMSD:
Santa Cruz Gauge Sta	1988 - 2001	Calibration - Initial	84	0.158	14	0.109
	1988 - 2001	Calibration - Updated	82	0.137	12	0.106

VALIDATION:			Monthly Val (6 mo, Nov - Apr)		Annual Val:	
Location:	WaterYears:	Description:	# months:	NRMSD:	# years:	NRMSD:
Santa Cruz Gauge Sta	2002 - 2014	Validation - Initial	78	0.246	13	0.100
	2002 - 2014	Validation - Updated	76	0.212	13	0.100

Table IV.4:

Calibration Parameters:

parameter	units	description	calibration range	value(s)
gwflow_coef	fraction/day	baseflow linear routing coefficient	0 - 0.5	0.015
gwsink_coef	fraction/day	GW extraction linear routing coefficient	0 - 0.045	0.035
fastcoef_lin	fraction/day	preferential flow linear routing coefficient	0.001 - 1.0	0.001
fastcoef_sq	-	preferential flow non-linear routing coefficient	0.001 - 1.0	0.001
slowcoef_lin	fraction/day	gravity soilzone linear routing coefficient	0.001 - 0.5	0.001
slowcoef_sq	-	gravity soilzone non-linear routing coefficient	0.001 - 0.35	0.001
ssr2gw_rate	fraction/day	gravity soilzone drainage coefficient (to GW)	0.01 - 1.2	0.01 - 0.41*
ssr2gw_exp	-	gravity soilzone drainage exponent (to GW)	0.0 - 3.0	2.0
soil_moist_max	inches	max normalized water volume of capillary soilzone (AWC x rooting depth)	0.053 - 20.95	0.11 - 20.95*
pref_flow_den	decimal fraction	fraction of the total soil depth in which preferential flow occurs	0.0 - 0.5	0.0
sat_threshold	inches	max normalized water volume of gravity + preferential soilzones ((n-FC) x soil depth)	0.35 - 179.03	0.41 - 33.16*

* values vary by HRU

Table IV.5:

PRMS climate scenario organization:

Purpose	Climate Scenario:	PRMS WY:	PRMS Timeframe:	Actual WY:	Actual Timeframe:
Model Stabilization	Normal	1966	Oct 1, 1965…	1984	Oct 1, 1983…
Model Stabilization	Normal	1967		1992	
Model Stabilization	Normal	1968		1999	
Model Stabilization	Normal	1969		2001	
Model Stabilization	Normal	1970		2002	
Model Stabilization	Normal	1971		2003	
Model Stabilization	Normal	1972	…Sep 30, 1972	2004	…Sep 30, 2004
Analysis	Normal	1973	Oct 1, 1972…	1984	Oct 1, 1983…
Analysis	Normal	1974		1992	
Analysis	Normal	1975		1999	
Analysis	Normal	1976		2001	
Analysis	Normal	1977		2002	
Analysis	Normal	1978		2003	
Analysis	Normal	1979	…Sep 30, 1979	2004	…Sep 30, 2004
Analysis	Wet	1980	…Oct 1, 1979	1986	Oct 1, 1985…
Analysis	Wet	1981		1997	
Analysis	Wet	1982		2005	
Analysis	Wet	1983		2006	
Analysis	Wet	1984	…Sep 30, 1984	2011	…Sep 30, 2011
Model Stabilization	Normal	1985	Oct 1, 1984…	1984	Oct 1, 1983…
Model Stabilization	Normal	1986		1992	
Model Stabilization	Normal	1987		1999	
Model Stabilization	Normal	1988		2001	
Model Stabilization	Normal	1989		2002	
Model Stabilization	Normal	1990		2003	
Model Stabilization	Normal	1991	…Sep 30, 1991	2004	…Sep 30, 2004
Analysis	Dry	1992	Oct 1, 1991…	1988	Oct 1, 1987…
Analysis	Dry	1993		1989	
Analysis	Dry	1994		1991	
Analysis	Dry	1995		1994	
Analysis	Dry	1996	…Sep 30, 1996	2012	…Sep 30, 2012

Table VI.1:

Basin hillslope runoff (RO) response to changes in mean precip (P) (different climate scenarios)

		Climate Scenario:		
		Dry	**Normal**	**Wet**
Mean Monthly	P (in)	2.5	3.4	4.9
	% change	-	33.4	46.9
	RO (in)	0.5	0.9	1.7
	% change	-	70.8	78.4
	ΔRO/ΔP	-	**0.5**	**0.5**
	RPR	**0.12**	**0.21**	**0.37**

X. References

Anbazhagan, S., Ramasamy, S., & Gupta, S. D. (2005). Remote sensing and GIS for artificial recharge study, runoff estimation and planning in Ayyar basin, Tamil Nadu, India. *Environmental Geology, 48*(2), 158-170.

Arshad, M., Guillaume, J. H., & Ross, A. (2014). Assessing the feasibility of managed aquifer recharge for irrigation under uncertainty. *Water, 6*(9), 2748-2769.

Association of Monterey Bay Area Governments (AMBAG) (2014). LiDAR digital elevation coverage map. Available from http://www.ambag.org/programs-services/gis/lidar

Bae, D. H., Jung, I. W., & Chang, H. (2008). Long-term trend of precipitation and runoff in Korean river basins. *Hydrological Processes, 22*(14), 2644-2656.

Bartley, R., Roth, C. H., Ludwig, J., McJannet, D., Liedloff, A., Corfield, J., . . . Abbott, B. (2006). Runoff and erosion from Australia's tropical semi-arid rangelands: Influence of ground cover for differing space and time scales. *Hydrological Processes, 20*(15), 3317-3333.

Beven, K. (2004). Robert E. Horton's perceptual model of infiltration processes. *Hydrological Processes, 18*(17), 3447-3460.

Bouwer, H. (2002). Artificial recharge of groundwater: hydrogeology and engineering. *Hydrogeology Journal, 10*, 121-142.

Brauman, K. A., Daily, G. C., Duarte, T. K. e., & Mooney, H. A. (2007). The nature and value of ecosystem services: an overview highlighting hydrologic services. *Annu. Rev. Environ. Resour., 32*, 67-98.

Brunke, M., & Gonser, T. (1997). The ecological significance of exchange processes between rivers and groundwater. *Freshwater biology, 37*(1), 1-33.

California Department of Water Resources (CA DWR). (2013). *California's groundwater update 2013. A compilation of enhanced content for California's water plan update 2013.* Retrieved from www.water.ca.gov/waterplan/topics/groundwater/index.cfm

California Irrigation Management Information System (CIMIS) (2015). DeLaveaga hourly weather data, 1990-2012. Available from http://www.cimis.water.ca.gov/WSNReportCriteria.aspx

California Irrigation Management Information System (CIMIS) (2016). DeLaveaga potential evapotranspiration data, 1991-2001. Available from http://www.cimis.water.ca.gov/WSNReportCriteria.aspx

CALVEG Existing Vegetation – CALVEG, [ESRI personal geodatabase]. (2014). McClellan, CA: USDA-Forest Service, Pacific Southwest Region. ExistingVegCenCoast1997_2013_v1. [2014].

Canadell, J., Jackson, R., Ehleringer, J., Mooney, H., Sala, O., & Schulze, E.-D. (1996). Maximum rooting depth of vegetation types at the global scale. *Oecologia, 108*(4), 583-595.

Chang, H., & Jung, I.-W. (2010). Spatial and temporal changes in runoff caused by climate change in a complex large river basin in Oregon. *Journal of Hydrology, 388*(3), 186-207.

Cherkauer, D. S. (2004). Quantifying ground water recharge at multiple scales using PRMS and GIS. *Groundwater, 42*(1), 97-110.

Chorley, R. J. (1969). Water, earth, and man. A synthesis of hydrology, geomorphology, and socio-economic geography. *Water, earth, and man. A synthesis of hydrology, geomorphology, and socio-economic geography.*

Couturier, D., & Ripley, E. (1973). Rainfall interception in mixed grass prairie. *Canadian Journal of Plant Science, 53*(3), 659-663.

Crouse, R. P., Corbett, E. S., & Seegrist, D. W. (1966). Methods of measuring and analyzing rainfall interception by grass. *Hydrological Sciences Journal, 11*(2), 110-120.

Devitt, D. A., & Smith, S. D. (2002). Root channel macropores enhance downward movement of water in a Mojave Desert ecosystem. *Journal of Arid Environments, 50*(1), 99-108.

Dillon, P., Pavelic, P., Page, D., Beringen, H., & Ward, J. (2009). Managed aquifer recharge. *An Introduction Waterlines Report Series*(13).

Domingo, F., Villagarcıa, L., Boer, M., Alados-Arboledas, L., & Puigdefábregas, J. (2001). Evaluating the long-term water balance of arid zone stream bed vegetation using evapotranspiration modelling and hillslope runoff measurements. *Journal of Hydrology, 243*(1), 17-30.

Dunne, T., & Black, R. D. (1970). Partial area contributions to storm runoff in a small New England watershed. *Water Resources Research, 6*(5), 1296-1311.

Fang, L., Liu, C., Qin, G., Zhang, B., & Liu, T. (2015). Application of the PRMS model in the Zhenjiangguan watershed in the Upper Minjiang River basin. *Remote Sensing and GIS for Hydrology and Water Resources, 368*, 209-214.

Fathizadeh, O., Attarod, P., Pypker, T., Darvishsefat, A., & Zahedi Amiri, G. (2013). Seasonal variability of rainfall interception and canopy storage capacity measured under individual oak (Quercus brantii) trees in Western Iran. *Journal of Agricultural Science and Technology, 15*(1), 175-188.

Fetter, C. W. (2001). *Applied hydrogeology*. Upper Saddle River, N.J.: Prentice Hall.

Garcia-Estringana, P., Alonso-Blázquez, N., & Alegre, J. (2010). Water storage capacity, stemflow and water funneling in Mediterranean shrubs. *Journal of Hydrology, 389*(3), 363-372.

Heitman, J., Xiao, X., Horton, R., & Sauer, T. (2008). Sensible heat measurements indicating depth and magnitude of subsurface soil water evaporation. *Water Resources Research, 44*(4).

Hibbert, A., & Troendle, C. (1988). Streamflow generation by variable source area *Forest hydrology and ecology at Coweeta* (pp. 111-127): Springer.

Horton, R. E. (1933). The role of infiltration in the hydrologic cycle. *Eos, Transactions American Geophysical Union, 14*(1), 446-460.

Johnson, N. M. (2015). *San Lorenzo Valley Water District 2010 urban water management plan.* San Francisco, CA: Water Resources Consultant. Retrieved from www.slvwd.com/pdf/SLVWD%202010%20UWMP%20final%20draft.pdf

Kennedy/Jenks Consultants. (2013). *San Lorenzo Valley and North Coast Watersheds sanitary survey.* Palo Alto, CA: Kenney/Jenks Consultants. Retrieved from http://www.slvwd.com/watershed/Jan_2013_WSS_Update_report_final_W_figs+app_low_res.pdf

Kennedy/Jenks Consultants. (2015). *Annual report 2014 water year: Scotts Valley Water District groundwater management program.* San Francisco, CA: Kennedy/Jenks Consultants. Retrieved from http://sgma.water.ca.gov/basinmod/docs/download/357

Kennedy/Jenks Consultants. (2016). *Scotts Valley Water District: 2015 annual report groundwater management plan.* San Francisco, CA: Retrieved from

http://www.svwd.org/sites/default/files/documents/reports/2015_GW_Annual_Report.pdf

Kirchner, J. W. (2009). Catchments as simple dynamical systems: Catchment characterization, rainfall-runoff modeling, and doing hydrology backward. *Water Resources Research, 45*, 1-34.

Klaassen, W., Bosveld, F., & De Water, E. (1998). Water storage and evaporation as constituents of rainfall interception. *Journal of Hydrology, 212*, 36-50.

Knapp, H. V., Durgunoglu, A., & Ortel, T. W. (1991). *A review of rainfall-runoff modeling for stormwater management.* Champaign, IL: Illinois State Water Survey.

LaFontaine, J. H., Hay, L. E., Viger, R. J., Markstrom, S. L., Regan, S., Elliott, C. M., & Jones, J. W. (2013). Application of the Precipitation-Runoff Modeling System (PRMS) in the Apalachicola-Chattahoochee-Flint River Basin in the Southeastern United States: U.S. Geological Survey Scientific Investigations Report 2013-5162, 118 p., http://pubs.usgs.gov/sir/2013/5162/.

Leavesley, G. H., Lichty, R., Thoutman, B., & Saindon, L. (1983). *Precipitation-runoff modeling system: User's manual*: US Geological Survey Colorado, CO.

Loik, M. E., Breshears, D. D., Lauenroth, W. K., & Belnap, J. (2004). A multi-scale perspective of water pulses in dryland ecosystems: climatology and ecohydrology of the western USA. *Oecologia, 141*(2), 269-281.

Los Angeles County Department of Public Works (LA DPW) (2016). *Tujunga Spreading Grounds Enhancement Project*. http://dpw.lacounty.gov/wrd/Projects/TujungaSG/index.cfm

Markstrom, S. L., Niswonger, R. G., Regan, R. S., Prudic, D. E., & Barlow, P. M. (2008). GSFLOW-Coupled Ground-water and Surface-water FLOW model based on the integration of the Precipitation-Runoff Modeling System (PRMS) and the Modular Ground-Water Flow Model (MODFLOW-2005): Geological Survey (US).

Markstrom, S. L., Regan, R. S., Hay, L. E., Viger, R. J., Webb, R. M., Payn, R. A., & LaFontaine, J. H. (2015). PRMS-IV, the precipitation-runoff modeling system, version 4: US Geological Survey.

McGlynn, B. L., & McDonnell, J. J. (2003). Quantifying the relative contributions of riparian and hillslope zones to catchment runoff. *Water Resources Research, 39*(11).

Molnar, D., & Julien, P. (2000). Grid-size effects on surface runoff modeling. *Journal of Hydrologic Engineering, 5*(1), 8-16.

Mount, J. F. (1995). *California rivers and streams: The conflict between fluvial process and land use.* Berkeley, CA: University of California Press.

Newcomer, M. E., Gurdak, J. J., Sklar, L. S., & Nanus, L. (2014). Urban recharge beneath low impact development and effects of climate variability and change. *Water Resources Research, 50*(2), 1716-1734.

Nimmo, J. R. (2012). Preferential flow occurs in unsaturated conditions. *Hydrological Processes, 26*(5), 786-789.

PRISM Climate Group (2016), Oregon State University. Available from http://prism.oregonstate.edu. UC WATER [Distributor]: Merced, CA, 2016.

Pumo, D., Viola, F., La Loggia, G., & Noto, L. (2014). Annual flow duration curves assessment in ephemeral small basins. *Journal of Hydrology, 519*, 258-270.

Reid, L. M., & Lewis, J. (2009). Rates, timing, and mechanisms of rainfall interception loss in a coastal redwood forest. *Journal of Hydrology, 375*(3), 459-470.

Risley, J., Moradkhani, H., Hay, L., & Markstrom, S. (2011). Statistical Comparisons of Watershed-Scale Response to Climate Change in Selected Basins across the United States. *Earth Interactions, 15*, 1-26.

Russo, T. A., Fisher, A. T., & Winslow, D. M. (2013). Regional and local increases in storm intensity in the San Francisco Bay Area, USA, between 1890 and 2010. *Journal of Geophysical Research: Atmospheres, 118*(8), 3392-3401.

Santa Cruz Local Agency Formation Commission (LAFCO). (2005). *Countywide service review: Water services*. Retrieved from http://www.santacruzlafco.org/pages/reports/CSR%20Public%20Review%20Draft/02.Water.PublicRevwDraft.06-05.pdf

Schenk, H. J., & Jackson, R. B. (2002). Rooting depths, lateral root spreads and below-ground/above-ground allometries of plants in water-limited ecosystems. *Journal of Ecology, 90*(3), 480-494.

Schumann, A. H., Funke, R., & Schultz, G. A. (2000). Application of a geographic information system for conceptual rainfall-runoff modeling. *Journal of Hydrology, 240*(1), 45-61.

Seyfried, M., Schwinning, S., Walvoord, M., Pockman, W., Newman, B., Jackson, R., & Phillips, F. (2005). Ecohydrological control of deep drainage in arid and semiarid regions. *Ecology, 86*(2), 277-287.

Sheridan, G. J., Lane, P. N., & Noske, P. J. (2007). Quantification of hillslope runoff and erosion processes before and after wildfire in a wet Eucalyptus forest. *Journal of Hydrology, 343*(1), 12-28.

Soil Survey Staff, Natural Resources Conservation Service, United States Department of Agriculture. Web Soil Survey. Available online at http://websoilsurvey.nrcs.usda.gov/. Accessed [9/10/2014].

Stone, D. B., Moomaw, C. L., & Davis, A. (2001). Estimating recharge distribution by incorporating runoff from mountainous areas in an alluvial basin in the Great Basin region of the southwestern United States. *Groundwater, 39*(6), 807-818.

Tashie, A. M., Mirus, B. B., & Pavelsky, T. M. (2016). Identifying long-term empirical relationships between storm characteristics and episodic groundwater recharge. *Water Resources Research*.

U.S. Geological Survey (USGS) (2014a). 1/9 arc-second DEM. Available from http://viewer.nationalmap.gov/basic/?basemap=b1&category=ned,nedsrc&title=3DEP%20View

U.S. Geological Survey (USGS) (2014b). 1/3 arc-second DEM. Available from http://viewer.nationalmap.gov/basic/?basemap=b1&category=ned,nedsrc&title=3DEP%20View

U.S. Geological Survey (USGS) (2014c). *Modeling of Watershed Systems (MOWS)*. Retrieved from http://wwwbrr.cr.usgs.gov/projects/SW_MoWS/4.1%20HRU%20Map1.html

U.S. Geological Survey (USGS) (2014d). National Hydrography Database. Available from http://nhd.usgs.gov/

U.S. Geological Survey (USGS) (2015a). Stream gauge data: USGS 11160500 San Lorenzo R A Big Trees, CA. Available from http://waterdata.usgs.gov/ca/nwis/inventory/?site_no=11160500&agency_cd=USGS

U.S. Geological Survey (USGS) (2015b). Stream gauge data: USGS 11161000 San Lorenzo R A Santa Cruz, CA. Available from http://waterdata.usgs.gov/ca/nwis/inventory/?site_no=11161000&agency_cd=USGS

Viger, R. J., Hay, L. E., Jones, J. W., & Buell, G. R. (2010). Effects of including surface depressions in the application of the Precipitation-Runoff Modeling System in the Upper Flint River Basin, Georgia.

Werner, A. D., & Simmons, C. T. (2009). Impact of sea-level rise on sea water intrusion in coastal aquifers. *Ground Water, 47*(2), 197-204.

Western Regional Climate Center (WRCC) (2015a). Daily temperature and precipitation data: Ben Lomond 4, California (040673). Available from http://wrcc.dri.edu/cgi-bin/cliMAIN.pl?ca0673

Western Regional Climate Center (WRCC) (2015b). Daily temperature and precipitation data: Felton, California (043004). Available from http://wrcc.dri.edu/cgi-bin/cliMAIN.pl?ca3004

Western Regional Climate Center (WRCC) (2015c). Daily temperature and precipitation data: Santa Cruz, California (047916). Available from http://wrcc.dri.edu/cgi-bin/cliMAIN.pl?ca7916

Wilcox, B. P., Newman, B. D., Brandes, D., Davenport, D. W., & Reid, K. (1997). Runoff from a semiarid ponderosa pine hillslope in New Mexico. *Water Resources Research, 33*(10), 2301-2314.

Woolhiser, D., & Goodrich, D. (1988). Effect of storm rainfall intensity patterns on surface runoff. *Journal of Hydrology, 102*(1), 335-354.